Maintenance of mitochondrial DNA integrity in Muscle Satellite Cells

Doctoral Thesis

for

the award of the doctoral degree

of the Faculty of Mathematics and Natural Sciences

of the University of Cologne

submitted by

Ayesha Sen

Accepted in the year 2024

Tag der mündlichen Prüfung: 8th July, 2024

The dissertation has been accepted by the Faculty of Mathematics and Natural Sciences, of the University of Cologne.

Supervisors: Prof. Dr. Rudolf J. Wiesner

Prof. Dr. David Pla-Martín

“The future belongs to those who believe in the beauty of their dreams…”

-Eleanor Roosevelt

Table of Contents

Abstract

Mutations in the mitochondrial DNA (mtDNA) have been linked to skeletal muscle atrophy and sarcopenia. Muscle satellite cells (MuSCs), responsible for regenerating new muscle fibres, are generally quiescent but become activated during muscle biogenesis in the course of development and growth, exercise, or damage. The regenerative capacity of MuSCs declines with age, and this is thought to be a contributing factor to sarcopenia. With the ever-increasing age of the global population, it is essential to understand the consequences of disturbed mtDNA integrity in MuSCs in the context of sarcopenia. To explore how mtDNA mutations affect the regeneration capacity of MuSCs, we employed a mouse model expressing a dominant negative mutation of TWINKLE (K320E-Twinkle), the mtDNA helicase, under the control of tamoxifen, specifically in the MuSCs or in skeletal muscle, respectively. This mutation is known to accelerate the accumulation of mtDNA alterations. Acute activation of muscle regeneration in adult mice by cardiotoxin induced degeneration of M. tibialis anterior (TA) induced the dramatic accumulation of fibres with mitochondrial dysfunction and enhanced inflammation. Our studies using the mitoTIMER reporter, along with induction of K320E-Twinkle in MuSCs *in vitro,* pointed to an initial increase in mitochondrial biogenesis and turnover. In contrast, when K320E-Twinkle is activated upon muscle biogenesis during normal development, we do not observe mitochondrial dysfunction. However, histological analyses showed a reduced cross-sectional area and a prominent fibre type shift, from glycolytic to oxidative in the TA. Interestingly, this was observed only in the glycolytic TA muscle and not in the predominantly oxidative M. soleus. Additionally, *in vitro* analysis of MuSC differentiation showed that K320E-Twinkle impairs muscle fibre differentiation by reducing mitochondrial biogenesis. Accordingly, K320E-Twinkle-C2C12 cells also showed disturbed differentiation, along with reduced myogenic fusion, respiratory chain defects, and progressive mtDNA depletion. Proximity proteomics revealed a decrease of mitochondrial proteins in the proteome of the mutant cells. In conclusion, our results demonstrate that interfering with mtDNA replication in MuSCs impairs muscle differentiation and alters muscle architecture. Our data reveals a link between mtDNA integrity and the altered

metabolic shift from glycolytic to oxidative, similar to that observed in aged sarcopenic muscle of long-lived organisms.

Zusammenfassung

Mutationen in der mitochondrialen DNA (mtDNA) wurden mit Skelettmuskelschwund und Sarkopenie in Verbindung gebracht. Muskelsatellitenzellen (MuSC), die für die Regeneration neuer Muskelfasern zuständig sind, befinden sich in der Regel im Ruhezustand, werden aber während der Muskelbiogenese im Zuge von Entwicklung und Wachstum, körperlicher Betätigung oder Schädigung aktiviert. Die Regenerationsfähigkeit der MuSCs nimmt mit zunehmendem Alter ab, und es wird angenommen, dass dies ein Faktor ist, der zur Sarkopenie beiträgt. Angesichts des ständig steigenden Alters der Weltbevölkerung ist es von entscheidender Bedeutung, die Folgen einer gestörten mtDNA-Integrität in MuSCs im Zusammenhang mit Sarkopenie zu verstehen. Um zu erforschen, wie sich mtDNA-Mutationen auf die Regenerationsfähigkeit von MuSCs auswirken, haben wir ein Mausmodell verwendet, das eine dominant-negative Mutation von TWINKLE (K320E-Twinkle), der mtDNA-Helikase, unter der Kontrolle von Tamoxifen spezifisch in den MuSCs bzw. im Skelettmuskel exprimiert. Diese Mutation ist dafür bekannt, dass sie die Akkumulation von mtDNA-Veränderungen beschleunigt. Die akute Aktivierung der Muskelregeneration bei erwachsenen Mäusen durch Kardiotoxin-induzierte Degeneration des M. tibialis anterior (TA) führte zu einer dramatischen Anhäufung von Fasern mit mitochondrialer Dysfunktion und verstärkter Entzündung. Unsere Studien unter Verwendung des mitoTIMER-Reporters und der Induktion von K320E-Twinkle in MuSCs *in vitro* wiesen auf einen anfänglichen Anstieg der mitochondrialen Biogenese und des Umsatzes hin. Wenn K320E-Twinkle bei der Muskelbiogenese während der normalen Entwicklung aktiviert wird, können wir dagegen keine mitochondriale Dysfunktion beobachten. Histologische Analysen zeigten jedoch eine verringerte Querschnittsfläche und eine deutliche Verschiebung des Fasertyps von glykolytisch zu oxidativ im TA. Interessanterweise wurde dies nur im glykolytischen TA-Muskel und nicht im überwiegend oxidativen M. soleus beobachtet. Darüber hinaus zeigte die *in vitro*-Analyse der MuSC-Differenzierung, dass K320E-Twinkle die Muskelfaserdifferenzierung durch eine Verringerung der mitochondrialen Biogenese beeinträchtigt. Dementsprechend wiesen K320E-Twinkle-C2C12-Zellen ebenfalls eine gestörte Differenzierung auf, zusammen mit einer reduzierten myogenen Fusion,

Defekten der Atmungskette und einer fortschreitenden mtDNA-Depletion. Proximity Proteomics zeigte eine Abnahme der mitochondrialen Proteine im Proteom der mutierten Zellen. Zusammenfassend zeigen unsere Ergebnisse, dass eine Störung der mtDNA-Replikation in MuSCs die Muskeldifferenzierung beeinträchtigt und die Muskelarchitektur verändert. Unsere Daten zeigen einen Zusammenhang zwischen der Integrität der mtDNA und der veränderten Stoffwechselverschiebung von glykolytisch zu oxidativ, ähnlich der, die im gealterten sarkopenischen Muskel langlebiger Organismen beobachtet wird.

1. Introduction

1.1 Mitochondria

Mitochondria are described to have evolved from ancient endosymbiotic α-proteobacteria that were engulfed by a eukaryotic ancestor, approximately 1.5 billion years ago (Druzhyna et al., 2008; Dyall et al., 2000; Pittis & Gabaldón, 2016). They were first observed by Rudolf Albert von Kölliker in muscle, in 1857. Mitochondria are highly dynamic double-membraned organelles, vital for a variety of different and crucial cellular functions. They are pivotal in maintaining and regulating cellular metabolism and homeostasis, helping cells to respond to stress. One of the most known functions of mitochondria is to provide energy currency to eukaryotic cells, by generating metabolic energy in the form of Adenosine triphosphate (ATP). Mitochondria break down molecules, such as glucose or fatty acids, through redox-reactions to generate NADH and $FADH_2$. The electrons taken from these molecules are used by the electron transport chain (ETC), through the process of oxidative phosphorylation (OXPHOS), to generate ATP. Apart from this key role in cell bioenergetics, mitochondria modulate cellular processes such as cell-cycle progression, cell growth and differentiation. Mitochondria regulate a multitude of metabolic and signalling pathways such as cell death signalling, apoptosis, and innate immunity (Tait & Green, 2012). Mitochondria are responsible for the generation of pyrimidine nucleotides, lipids, heme-biosynthesis, synthesis of iron-sulphur clusters, calcium and iron homeostasis, but also reactive oxygen species (ROS) (Chen et al., 2023). Their plasticity and dynamic nature is evident from their ability to adjust and respond to different stressors and metabolic needs within a cell (Chen et al., 2023).

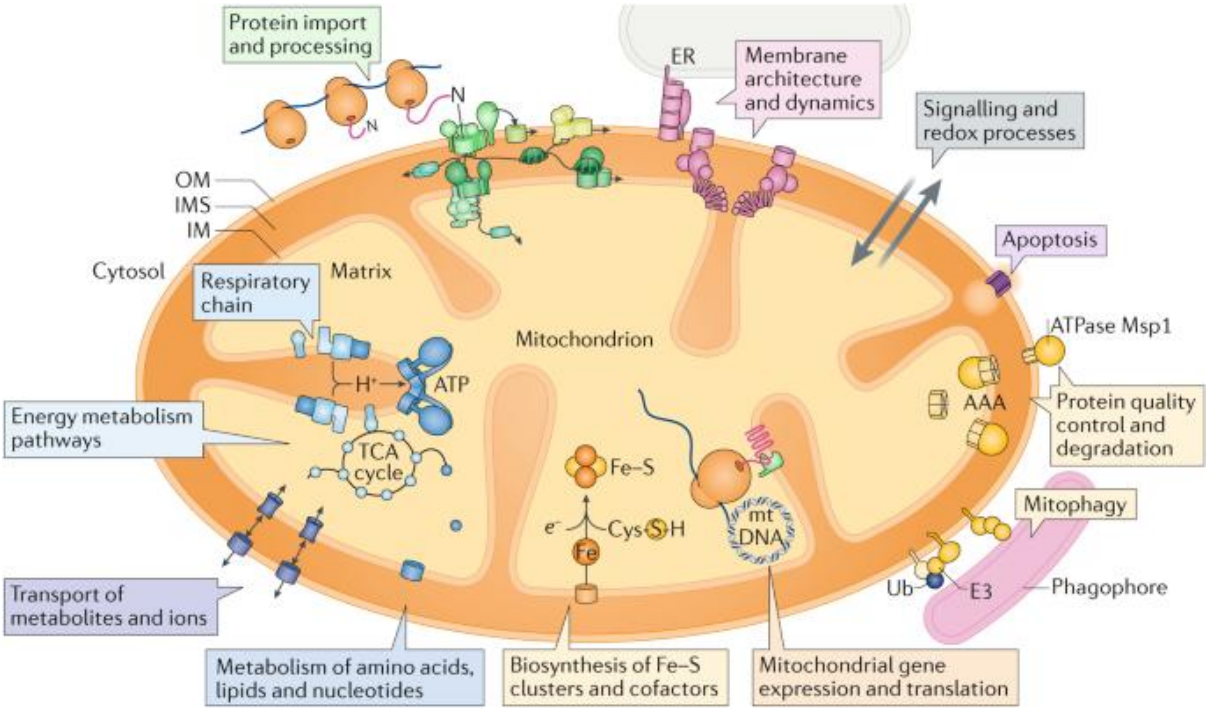

Figure 1: Schematic showing the various functions of mitochondria and mitochondrial proteins OM: Outer Membrane, IMS: Intermembrane space, IM: Inner Membrane, ER – Endoplasmic Reticulum. (Pfanner et al., 2019)

1.1.1 Mitochondrial Structure

The double-membraned mitochondria comprise of an outer membrane (OM) and an inner membrane (IM) which forms numerous folds called the cristae. The cristae extend into the mitochondrial matrix, which is the area encompassed by the inner membrane. Between the inner and the outer membrane lies the intermembrane space (IMS). Although each of the components that make up the mitochondria play distinct functional roles, the major processes occur within the mitochondrial matrix and the inner membrane (Cooper, 2000).

The outer membrane contains “porins” which are responsible for forming large aqueous channels through the lipid bilayer. The outer membrane is thus highly permeable, allowing all molecules up to 5000 Daltons to diffuse into the intermembrane space. The inner membrane, on the other hand, is made up of a lipid bilayer with a high proportion of the

phospholipid, cardiolipin, and is highly selective and impermeable to ions. The IM contains transport proteins, which make it selectively permeable to small molecules, required by mitochondrial enzymes in the mitochondrial matrix. Importantly, the inner membrane houses the components of the mitochondrial respiratory chain complexes. Finally, the matrix encompasses enzymes involved in metabolizing pyruvate and fatty acids to produce acetyl coenzyme A (acetyl CoA), along with those involved in the Tricarboxylic Acid cycle (TCA cycle). Apart from this, it also contains mitochondrial DNA (mtDNA), transfer RNAs (tRNAs), mitochondrial ribosomes, and various structural proteins.

1.1.2 Mitochondrial Respiratory Chain and Oxidative Phosphorylation

The matrix and the inner mitochondrial membrane are therefore the central hubs of oxidative metabolism. The principal source of metabolic energy is derived from the oxidative breakdown of glucose and fatty acids. While the initial step, glycolysis takes place in the cell cytosol, resulting in the conversion of glucose to pyruvate; further steps take place inside the mitochondria. First, the pyruvate is transported into the mitochondrial matrix, where it is oxidized to generate acetyl CoA. Fatty acid oxidation also generates acetyl CoA. Oxidation of acetyl CoA to CO_2 occurs via the TCA cycle.

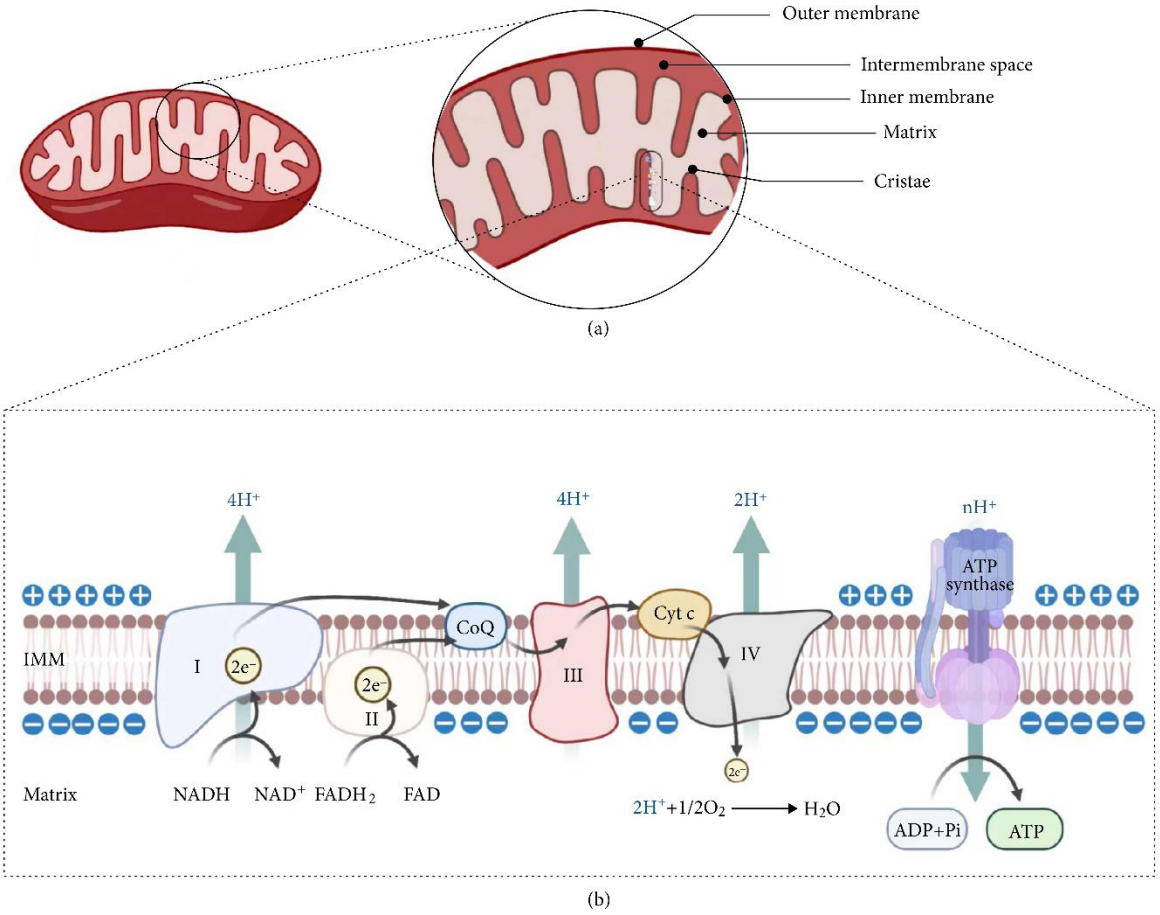

Figure 2: a. Schematic showing mitochondrial structure b. schematic of the electron transport chain and ATP synthase illustrating electron transfer and proton movement during oxidative phosphorylation. Protons are pumped into the IMS through Complex I, III and IV, generating a proton gradient to pump protons back into the matrix through ATP synthase, thereby synthesizing ATP. (Yuan et al., 2022)

Importantly, the oxidation of acetyl CoA is coupled to the reduction of NAD^+ to NADH and FAD to $FADH_2$. Energy is generated through the respiratory chain complexes, which are embedded in the inner mitochondrial membrane. The respiratory chain or the electron transport chain comprises of four multimeric complexes: Complex I (NADH- ubiquinone oxidoreductase), Complex II (Succinate dehydrogenase), Complex III (ubiquinone-cytochrome *c* oxidoreductase) and Complex IV (cytochrome *c* oxidase) (Sousa et al., 2018). NADH is oxidized by Complex I to release electrons, which enter the respiratory chain. First, they are taken up by flavin mononucleotide (FMN) and then by Coenzyme Q (ubiquinone), through an iron sulphur carrier, yielding an energy of $\Delta G°' = -16.6$ kcal/mol.

Complex II on the other hand, oxidizes $FADH_2$ to generate electrons, once again taken up by Coenzyme Q, however without any decrease in free energy. Since Coenzyme Q is lipid-soluble, it carries the electrons through the membrane, to Complex III. Here, the electrons are transferred from cytochrome b to cytochrome c, yielding an energy of $\Delta G^{\circ\prime}$ = -10.1 kcal/mol (Cooper, 2000). Then, the electrons are carried to Complex IV by cytochrome c, where they are eventually transferred to O_2, yielding $\Delta G^{\circ\prime}$ = -25.8 kcal/mol. As the three complexes transfer electrons with a decrease in free energy, they pump protons into the intermembrane space, creating a transmembrane electrochemical gradient corresponding to a ΔG of approximately -5 kcal/mol per proton. This generates a proton motive force, which is used to drive a fifth complex, ATP Synthase (Complex V), also embedded in the inner membrane. Complex V comprises of two distinct components, the F0 and the F1 subunit. The F0 subunit provides a channel through which the protons can flow back to drive the energetically favourable rotation of the F1 subunit, which can in turn catalyse the synthesis of ADP and inorganic phosphate to ATP. Synthesis of a single molecule of ATP requires the inflow of four protons (Cooper, 2000). Therefore, the electron transport chain coupled to oxidative phosphorylation is essential for cellular homeostasis. Consequently, impairment of the respiratory chain complexes or uncoupling of OXPHOS could result in altered cellular homeostasis with detrimental outcomes such as a proton leak or loss of membrane potential, which could lead to apoptosis. In case of uncoupling, the protons re-enter the mitochondrial matrix, and the electron transport chain is no longer coupled to ATP synthesis.

1.2 Mitochondrial DNA

One of the unique features of mitochondria is that they harbour their own genetic material, the mitochondrial DNA (mtDNA), in line with their endosymbiotic origin. The mtDNA is circular and double-stranded, and is therefore closer to bacterial or prokaryotic DNA. The human mtDNA is 16,569 base pair long (Anderson et al., 1981; Bibb et al., 1981) and contains 37 genes, 13 of which encode important protein subunits of the respiratory chain complexes. Of the approximately 1200 proteins of the mitochondrial proteome, only

around 1% is encoded by mtDNA, but all these 13 proteins are critical for mitochondrial function, on account of them being part of the OXPHOS complexes. Thus, seven subunits of complex I, one subunit of complex III, three subunits of complex IV and two subunits of complex V are encoded in the mtDNA. The rest of the subunits are encoded by the nuclear genome (nucDNA) and complex II is the only one that is completely nuclear encoded (Chan, 2006; Dimauro & Schon, 2003). mtDNA also contain genes for 2 ribosomal RNAs (12s and 16s rRNA), along with 22 transfer RNA molecules, all essential for mitochondrial translation. The remaining mitochondrial proteins are encoded by nucDNA and imported into the mitochondria after translation in the cytosol (Gustafsson et al., 2016; Kauppila et al., 2017).

In contrast to the nuclear DNA, the mtDNA copy number can range from hundreds to thousands in eukaryotic cells, its abundance being directly proportional to the energy requirement of the cell (Area-Gomez & Schon, 2014; Zhong et al., 2019).

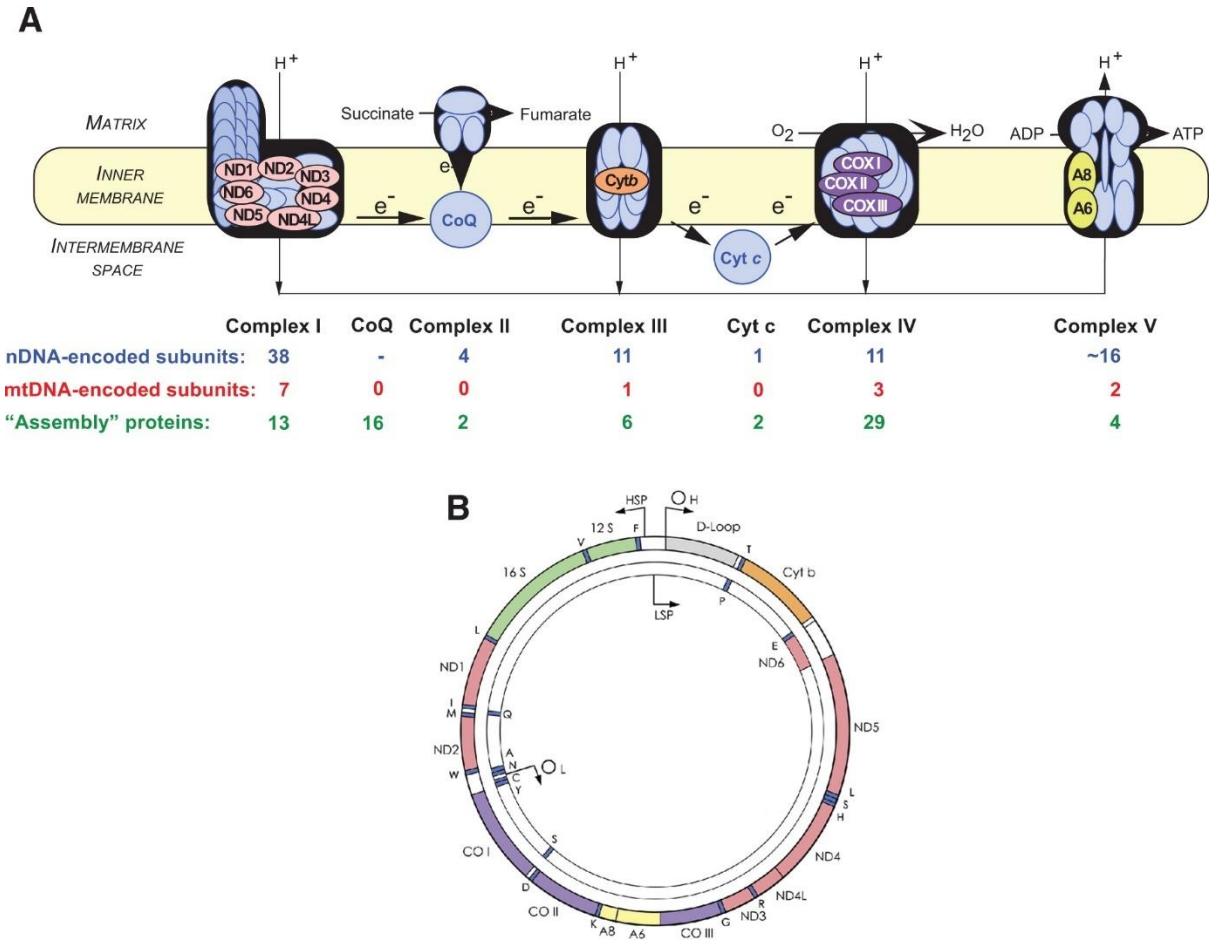

Figure 3: a. Schematic showing the different respiratory chain complex subunits and the number of complexes that are either nDNA (nucDNA) encoded or mtDNA encoded. b. The human mitochondrial DNA showing the genes encoding for the various complex subunits. OH – Origin of Heavy strand replication, OL – Origin of light strand replication, HSP: Heavy strand promoter, LSP – Light strand promoter. (Area-Gomez & Schon, 2014).

1.2.1 mtDNA Structure

The two strands of the mtDNA can be physically separated into the heavy (H) and light (L) strands based on their density (Berk & Clayton, 1974). The heavy strand is rich in the purine bases, adenine and guanine (A and G) and the light strand in the pyrimidine bases, thymine and cytosine (T and C), with most of the genetic information being present on the H strand. Unlike nuclear DNA, mtDNA is densely packed and the mtDNA genes do not have introns or intergenic sequences. The only non-coding region (NCR) is an 1118 base

pair long regulatory region, which corresponds to the displacement-loop (D Loop). The NCR contains the origin of the H-strand DNA replication (OH), along with promoters of transcription of the heavy (HSP) and light (LSP) strands (Habbane et al., 2021). A second origin for L-strand replication (OL) is located outside the NCR, within a tRNA cluster which is present around 11,000 base pairs downstream of the OH, and these two origins divide the mtDNA into a major and a minor arc (Gustafsson et al., 2016).

The mtDNA also lacks protective histone proteins that are present in nuclear DNA. They are however coated and packaged into nucleoprotein complexes called nucleoids (Alam et al., 2003; Bogenhagen et al., 2008; Farge & Falkenberg, 2019; Satoh & Kuroiwa, 1991). Of the many components of the nucleoids, the Transcription Factor A mitochondrial (TFAM), a DNA-binding protein, is the main structural component (Garrido et al., 2003; Gustafsson et al., 2016).

1.2.2 mtDNA Transcription

mtDNA transcription is not only essential for mtDNA gene expression but also for mtDNA replication, since it produces the RNA primers that are required for initiation of the replication process. Transcription originates in the NCR and is initiated by a DNA-dependent RNA polymerase called POLRMT (D'Souza & Minczuk, 2018). This initiation in turn requires association of POLRMT with TFAM and with mitochondrial transcription factor B2 (TFB2M). The TFAM, bound to DNA, thus recruits POLRMT to the HSP and LSP via its N-terminal extension. TFB2M then induces the opening of the promoter by modifying the structure of TFAM (Hillen et al., 2018; Posse & Gustafsson, 2017; Ramachandran et al., 2017). Mitochondrial transcription is thus crucial for normal cellular function, and diseases affecting the transcription machinery can have a multi-systemic and severe manifestation (Boczonadi et al., 2018).

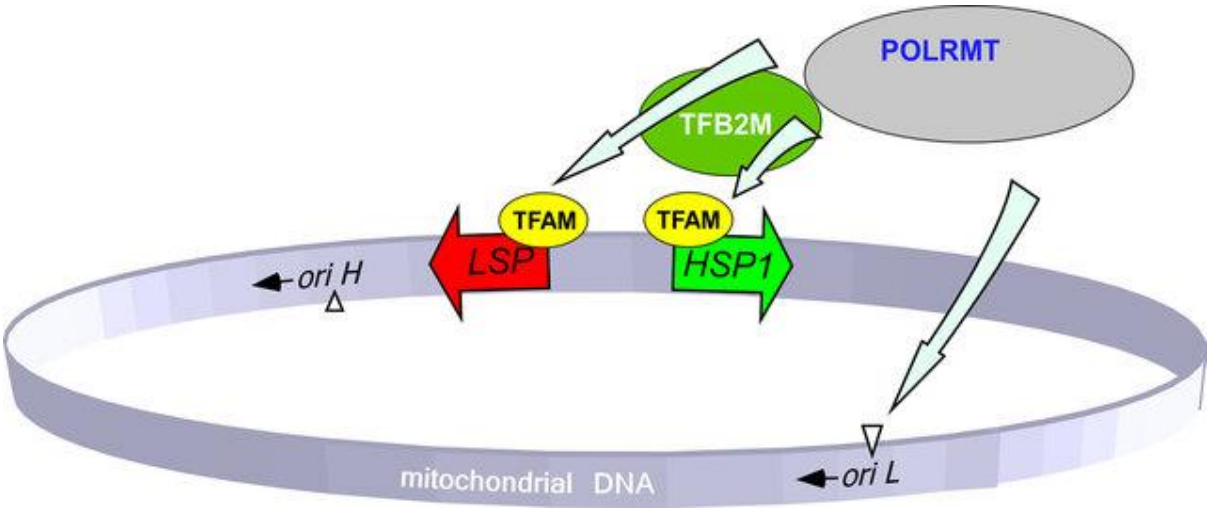

Figure 4: Schematic of mtDNA transcription initiation machinery (Litonin et al., 2010).TFAM - Transcription Factor A mitochondrial, POLRMT - DNA-dependent RNA polymerase, LSP - Light strand promoter, HSP - Heavy strand promoter, TFB2M - mitochondrial transcription factor B2, OriH / OriL - origin of the heavy strand/ light strand DNA replication.

1.2.3 mtDNA Replication

Replication of mtDNA is essential to maintain the desired, cell-type specific, mitochondrial copy number. Mitochondria have a unique enzymatic machinery for this, involving several replication factors such as the helicase Twinkle, DNA polymerase gamma (POLG) and the mitochondrial single-strand binding protein (mtSSB). These factors are distinct from those required for nuclear DNA replication. POLG is the sole polymerase that is responsible for the synthesis of both H and L strands, and is essential for mtDNA maintenance (Falkenberg & Gustafsson, 2020). POLG comprises of a main subunit POLGA and two accessory subunits POLGB. Additionally, there are some mitochondrial isoforms of DNA polymerases, which however are not involved in mitochondrial replication, but instead in different aspects of mtDNA repair (Krasich & Copeland, 2017). For the polymerase to function, it is essential that the two strands of the DNA be separated (Falkenberg, 2018). Therefore, a mitochondrial helicase, a hexameric protein known as

Twinkle, is required for strand separation at the replication fork (Korhonen et al., 2004). During mtDNA replication, Twinkle travels ahead of the polymerase to catalyse the nucleotide-triphosphate-dependent unwinding of the double stranded DNA template in the 5'to 3' direction (Falkenberg et al., 2007; Spelbrink et al., 2001). Twinkle needs a fork structure to load and initiate the unwinding (Spelbrink et al., 2001). The mtSSB binds to the newly unwound ssDNA, protects it from nucleases and prevents the formation of secondary structures. mtDNA synthesis is enhanced by mtSSB since it stimulates Twinkle's helicase activity, while also increasing the processivity of POLG. Therefore, with Twinkle and mtSSB, POLG synthesizes the mtDNA in the 5' to 3' direction and proofreads it in the 3' to 5' direction. In addition, mitochondrial topoisomerases are also essential since they allow for changes in the DNA topology (Falkenberg et al., 2007), allowing the daughter molecules to segregate correctly.

As yet, several mechanisms of mtDNA replication have been proposed. According to the strand displacement model of mtDNA replication, proposed by Vinograd and colleagues in 1972 (Robberson et al., 1972) synthesis of both H-strand and L-strand occurs simultaneously, without the formation of Okazaki fragment (short molecules of DNA acting as a feeder) like replication products (Tapper & Clayton, 1981). First, the replication starts at the OriH (OH) and after synthesis for 11kb, the replication machinery passes OriL, where the parental H-strand becomes single stranded and forms a stem-loop structure. This loop has a poly dT stretch which allows POLRMT to synthesize a short (25 nucleotide) RNA primer. This RNA primer is then required for the POLG to commence the synthesis of the L-strand. It should be noted that in this model, Twinkle is not essential for the synthesis of the L-strand, since the parental H-strand, used as the template, is already single-stranded (Falkenberg & Gustafsson, 2020). This model is also referred to as the asymmetric synthesis model (Larsson, 2010), since both daughter strands are not generated at the same time.

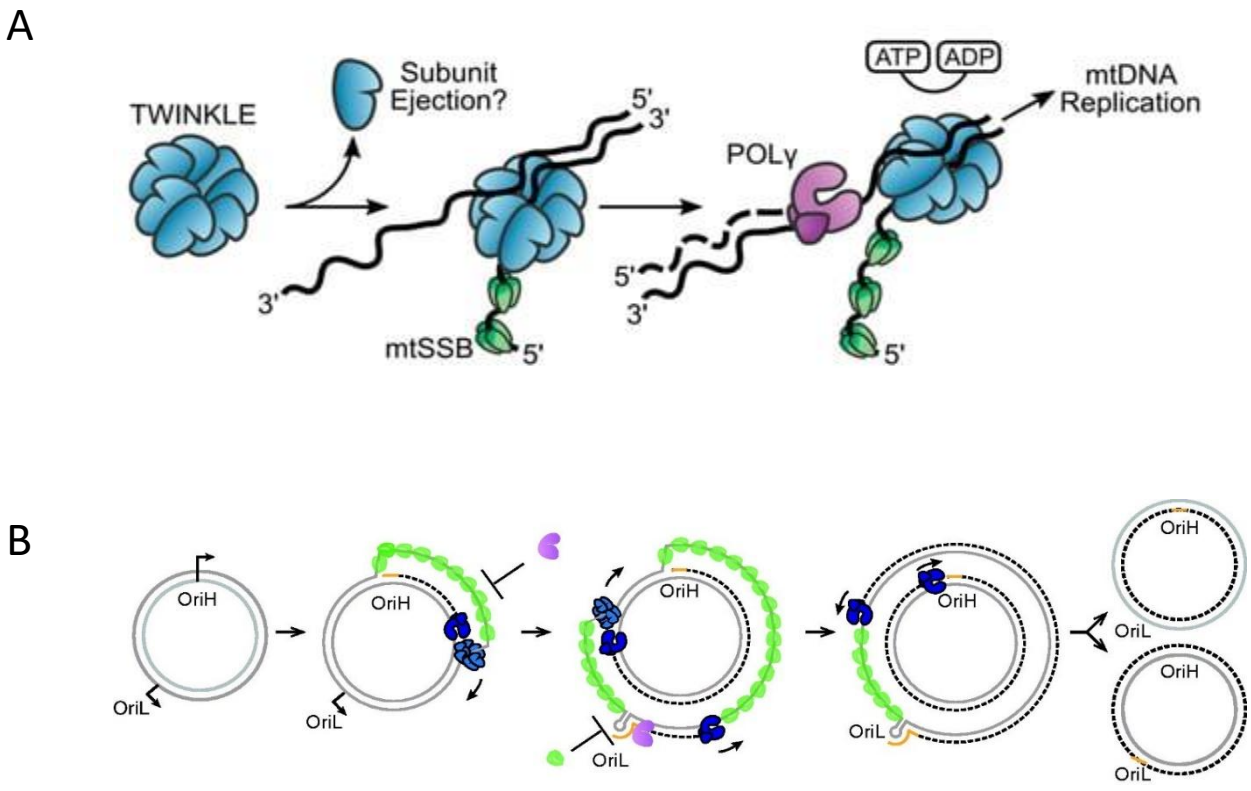

Figure 5: A. Schematic showing the helicase activity of TWINKLE at the replication fork, during mtDNA replication (Peter & Falkenberg, 2020). B. A Strand displacement model of mtDNA replication (Falkenberg & Gustafsson, 2020)

Another model is the strand-coupled model (Holt et al., 2000), according to which L-strand DNA synthesis occurs at multiple sites along the parental H-strand, with the generation of several short fragments that are ligated to form a continuous strand.

There is a third model, called the RITOLS (ribonucleotide incorporation throughout the lagging strand). This model is very similar to the strand-displacement model except that in this case the displaced parental H-strand is covered by processed RNA molecules (Falkenberg & Gustafsson, 2020).

1.3 Mitochondrial Dynamics

Mitochondria are highly plastic and dynamic organelles, undergoing continuous fission and fusion cycles, to shape their morphology, number, size, and function. Mitochondrial dynamics is essential to ensure proper mitochondrial function and for maintenance of several cellular processes such as the cell cycle, immunity, apoptosis, and mitochondrial quality control (Tilokani et al., 2018). Mitochondrial fission is characterized by the division of the mitochondrial network, in order to segregate damaged mitochondrial compartments from the intact and healthy parts of the network. Fission is mediated by the action of large GTPase proteins such as the dynamin-related protein (DRP1) and dynamin 2 (DNM2), recruited to the mitochondria by multiple adaptor proteins, such as fission 1 protein (FIS 1) (Chan, 2012), mitochondrial fission factor (MFF), mitochondrial dynamics protein (MiD) 49 and MiD51 (Chen et al., 2023). Mitochondrial fission is essential for the mitotic segregation of mitochondria to the daughter cells, for the elimination of impaired or dysfunctional mitochondria through mitophagy, and to promote apoptosis in response to severe cellular stress (Youle & Van Der Bliek, 2012). Unregulated fission could lead to mitochondrial fragmentation, mtDNA depletion, increased ROS production and reduced respiratory chain function. On the other hand, mitochondrial fusion is characterized by the union of neighbouring unhealthy/damaged mitochondrial segments to remodel the mitochondrial network. Mitochondrial fusion occurs in two parts, with the OM fusion mediated by mitofusins 1 and 2 (MFN1 and MFN2) and the IM fusion mediated by optic atrophy protein 1 (OPA1) (Pernas & Scorrano, 2016). Mitochondrial fusion is vital for maintenance of the mitochondrial membrane potential, ATP production and for maximal respiratory capacity. Unrestricted fusion can lead to formation of hyperfused mitochondria, which prevent the removal of mitochondria by starvation-induced autophagy and cause an increase in cristae number, which is associated with higher ATP synthesis activity (Gomes et al., 2011; Liesa & Shirihai, 2013).

Since mitochondrial dynamics is essential for the regulation of mitochondrial function, quality control, mtDNA stability, autophagy, mitophagy and apoptosis; altered dynamics is linked to ageing (Sebastián et al., 2016). These alterations have also been linked to various age-related disorders such as muscle atrophy and sarcopenia, cardiac and

neurodegenerative diseases. Therefore, it is essential for there to be a balance between the fusion and the fission machinery.

1.3.1 Mitophagy and Mitochondrial Biogenesis

The dedicated removal of intracellular components, which are delivered to the lysosomes for degradation and recycling, is called autophagy (Ohsumi, 2014). Also referred to as macroautophagy, the damaged or excessive organelles are removed through the formation of a double-membraned organelle called the autophagosome. The autophagosomes then fuse with lysosomes to form autophagolysosomes, where the enveloped contents get degraded (Mizushima, 2007).

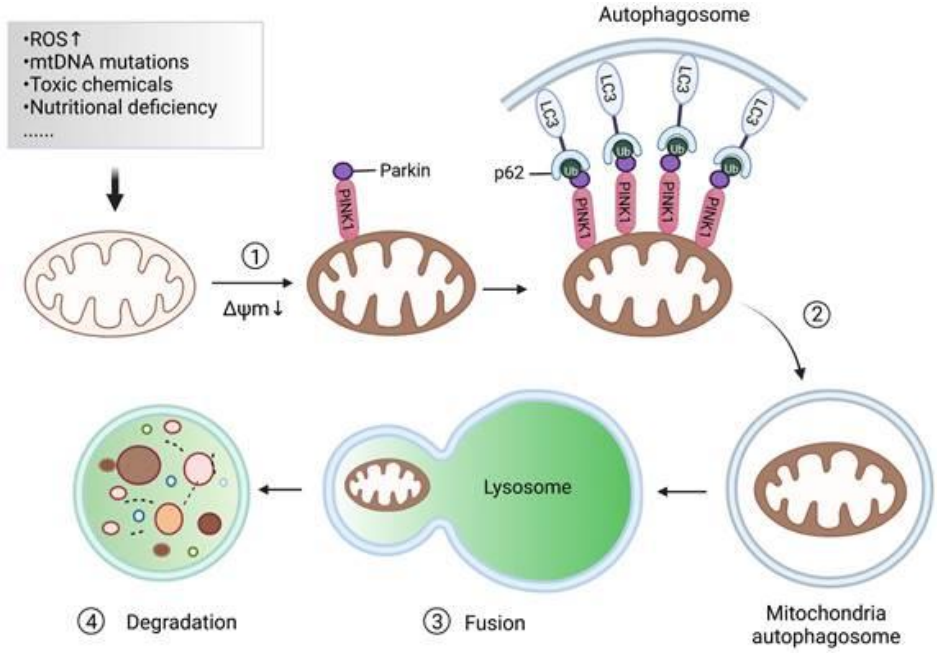

Figure 6: Schematic showing the main events of mitophagy. Mitochondrial damage due to insults causes membrane depolarization. This allows for the recruitment of Parkin and polyubiquitination of PINK1, recruiting autophagy receptors. The autophagosome envelops the damaged mitochondria and fuses with the lysosome following which the contents are selectively degraded. (Lu et al., 2023)

A specialized form of autophagy, which involves selective removal and degradation of dysfunctional mitochondria, is called mitophagy (Lemasters, 2005) . There are multiple

mitophagy pathways in mammalian cells, most of which are phosphate and tensin homolog (PTEN) - induced putative kinase (PINK)/ Parkin dependent. Here, mitochondrial dysfunction causing membrane depolarization leads to the stabilization of PINK1 on the OM, where it phosphorylates ubiquitin. This then recruits Parkin, a cytosolic E3-ubiquitin ligase to the OM (Palikaras et al., 2018), which poly-ubiquitinates mitochondrial proteins to facilitate their association with autophagy receptors. This leads to autophagosome recruitment, which eventually fuses with the lysosome and selectively degrades the dysfunctional mitochondria.

Certain mitophagy pathways, which are Parkin independent, also exist. In this case, PINK1 recruits the autophagy adaptors directly to the mitochondria to facilitate its removal (Lu et al., 2023). Additionally, we recently discovered a new non-canonical endosomal-mediated mitophagy pathway, which enables elimination of mutated mtDNA molecules (Sen et al., 2022). Mitochondrial dynamics play a vital role in mitochondrial quality control through regulation of mitophagy. Impaired mitophagy is thus associated with ageing.

Mitophagy occurs in coordination with mitochondrial biogenesis to maintain cellular function and mitochondrial homeostasis. Mitochondrial biogenesis is essential to maintain the mitochondrial mass and quality (Palikaras et al., 2015) and to compensate for the elimination of damaged mitochondria through mitophagy. Mitochondrial biogenesis is a tightly regulated process, requiring both nuclear and mitochondrial genes to synthesize new mitochondrial proteins. There exists a complex regulatory network to orchestrate mitochondrial biogenesis. Proteins involved in regulation of nuclear genes are the nuclear respiratory factors, NRF1 and NRF2; and the transcriptional coactivators of PPARgamma coactivator-1 family: PGC1a, PGC1b and PGC1 related coactivators (PRC) (Goffart & Wiesner, 2003; Lin et al., 2005). Of these, PGC1a (peroxisome proliferator-activated receptor gamma coactivator 1 alpha) is the master regulator of mitochondrial biogenesis since it coactivates multiple transcription factors enhancing transcription of nuclear encoded genes for mitochondrial proteins (Goffart & Wiesner, 2003).

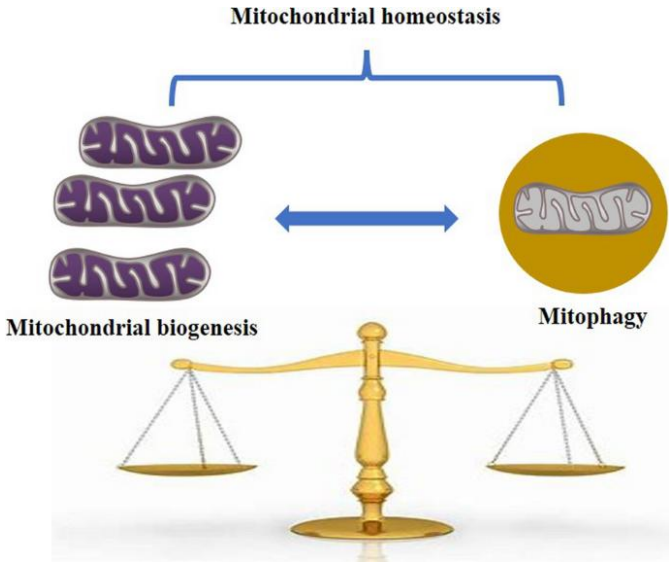

Figure 7: Balance between mitochondrial biogenesis and mitophagy, which is essential for maintaining mitochondrial homeostasis.(Liu et al., 2023)

1.4 Mitochondrial DNA defects and ageing

Since mtDNA encodes for several key respiratory chain complex subunits, defects in mtDNA maintenance and accumulation of mtDNA mutations can affect the OXPHOS pathway and in turn impair energy production. This leads to several mitochondrial and age-associated diseases in humans. While some of the mitochondrial diseases are a result of direct mutation to the mtDNA, many are caused by mutations in the nuclear genes, which are responsible for the maintenance of mtDNA replication machinery (Peter & Falkenberg, 2020). This results in generation of defective proteins responsible for mtDNA maintenance, which in turn can lead to deletions, depletion, or gene duplications. For instance, missense mutations in the Twinkle helicase gene (*PEO1*) has been implicated in Progressive external ophthalmoplegia (PEO), along with other diseases related to mtDNA instability (Copeland, 2012; Spelbrink et al., 2001). Therefore, accumulation of somatic mutations, deletions in the mtDNA, mtDNA depletion (reduction in mtDNA copy number), decrease in the quality of mitochondrial proteins, along with a dysregulation of mitochondrial dynamics can lead to an impaired OXPHOS process. This

in turn causes mitochondrial dysfunction, thereby contributing to aging, disease and eventually cell death in multiple model organism (DeBalsi et al., 2017; Srivastava, 2017).

It should be noted that due to the multi-copy nature of mtDNA, present in thousands of copies per cell, mitochondrial dysfunction arises only when the number of mutated mtDNA molecules are present beyond a certain physiological threshold. This phenomenon is described as heteroplasmy of mtDNA, that is the presence of different variants of mtDNA, wild type and those containing mutations in a cell. When the mutated mtDNA molecules in a cell are present above the physiological threshold, it leads to mitochondrial dysfunction. During ageing, mammalian tissues become mosaics, with mostly normal cells and some cells that exhibit mitochondrial dysfunction, giving rise to mosaic respiratory chain defects (Larsson, 2010).

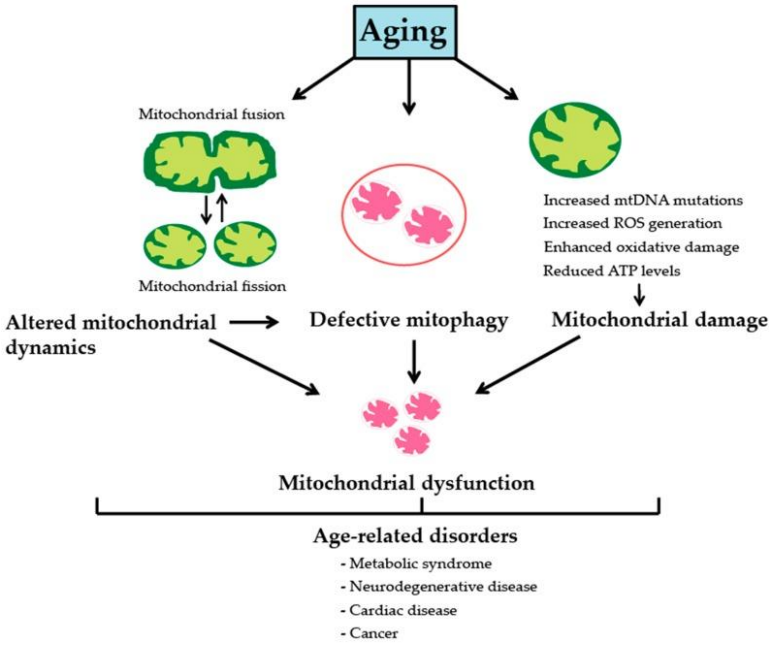

Figure 8: Depiction of mitochondrial dysfunction during ageing and age-related disorders. Ageing causes altered mitochondrial dynamics, which lead to defective mitophagy. An increase in ROS production, mtDNA mutation, oxidative damage and reduced ATP can cause mitochondrial damage. These result in mitochondrial dysfunction, which is then implicated in various age-related disorders.(Srivastava, 2017)

1.4.1 Mitochondria in ageing

It has been well established that mitochondrial function declines with ageing, concurrent with altered mitochondrial morphology (Shigenaga et al., 1994), reduced number of mitochondria (Tauchi & Sato, 1968) and a decrease in the mtDNA copy number and mitochondrial protein levels (Stocco et al., 1977). Additionally, a decline in the function of the respiratory chain is also observed (Bratic & Larsson, 2013). Recent animal models also suggest that mtDNA mutations promote an ageing phenotype. Although mitochondrial dysfunction is associated with ageing, it is unclear whether mtDNA mutations are a cause or consequence of ageing.

In humans, mtDNA deletions have been observed in ageing skeletal muscle, and mtDNA point mutations were seen in the crypt cells of the colon (Taylor et al., 2003). The mtDNA mutator mice, with a mutation in the catalytic subunit of POLG, provided the first experimental evidence for accumulation of mtDNA mutations leading to a premature ageing phenotype (Trifunovic et al., 2004). This mutation led to random point mutations and deletions. Ahlqvist and his team members (Ahlqvist et al., 2012) demonstrate that in the mutator mouse, the development of neural and haematopoietic progenitor cells already get affected during embryogenesis. They suggest that mtDNA mutagenesis affects stem cell quality and quantity and interferes with the maintenance of a quiescent state. Also, the fact that most of the mutations observed in the mutator mice are a result of replication errors during development and not due to the accumulation of damage during ageing, further confirms the stem cell hypothesis. Another mouse model, the mtDNA deletor mice, expresses a dominant mutant version of Twinkle. This model displayed low levels of mtDNA deletions, progressive RC dysfunction and a late onset of mitochondrial myopathy. However, this model did not show a progeroid phenotype, suggesting that accumulation of mtDNA deletions and progressive RC dysfunction may not be sufficient to accelerate ageing (Bratic & Larsson, 2013).

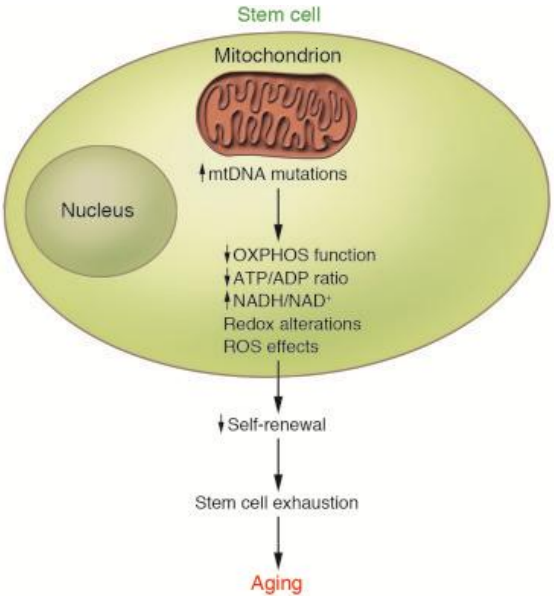

Figure 9: Model showing mtDNA mutations in the stem cell theory of ageing. This suggests that the increased mtDNA mutations that arise during development could affect ROS production, and reduce OXPHOS function, which effects cellular ATP synthesis. This contributes to deregulating stem cell homeostasis by reducing their renewal capacity, thereby giving rise to premature ageing phenotypes.(Bratic & Larsson, 2013)

Mitochondria were first implicated in ageing by Denham Harman, who postulated the free radical theory of ageing. Here, it was postulated that with increasing age, the progressive mitochondrial dysfunction increases levels of reactive oxygen species (ROS). Since ROS is responsible for the spontaneous oxidation of macromolecules such as nucleic acids, proteins and lipids, its increase consequently results in the accumulation of massive molecular damage (Harman, 1956.; Harman, 1972; Srivastava, 2017). However, recent findings show that in certain cases, an increase in ROS production in fact extends lifespan, as was seen in case of *C. elegans* and yeast (Srivastava, 2017). Therefore, it appears that increased ROS during ageing is not a cause but rather a result of ageing, and therefore questions the validity of the mitochondrial free radical theory of ageing (Wiesner et al., 2006).

Along with primary mitochondrial dysfunction that affects ageing, there are also cellular and metabolic alterations that contribute to ageing by promoting secondary changes in mitochondrial energy production or mitochondrial biogenesis.

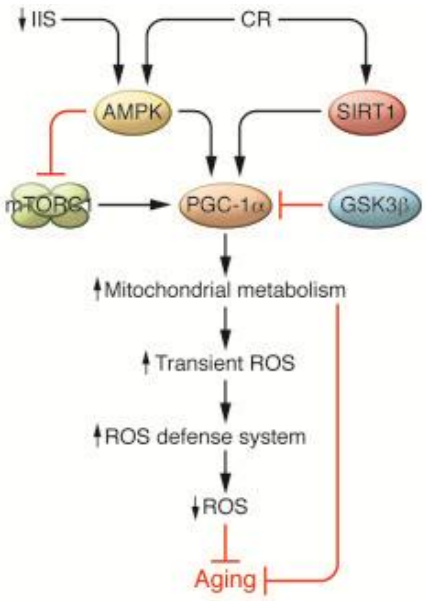

Figure 10: Schematic showing the effect of impaired insulin/IGF-1 signalling (IIS) and calorie restriction (CR) on mitochondrial function and ageing.(Bratic & Larsson, 2013)

Mitochondrial metabolism is said to be important in maintaining longevity through nutrient sensing pathways such as Insulin/IGF1 signalling (IIS) and target of Rapamycin (TOR); and through dietary restriction. Impaired IIS and inhibition of TOR activity increases mammalian lifespan (Bratic & Larsson, 2013; Holzenberger et al., 2003; Kapahi et al., 2004).

Calorie restriction, which is the reduced availability of nutrients, extends mammalian lifespan (Colman et al., 2009; Lee et al., 2002). Calorie restriction leads to an increase in mitochondrial biogenesis and respiration through activation of SIRT 1, which further activates PGC1α downstream(Cohen et al., 2004; López-Lluch et al., 2006). It should be noted that PGC1α is not involved in regulating basal mitochondrial biogenesis, but rather in increasing mitochondrial function on demand by activating the expression of certain nuclear genes in different tissues such as heart, brain, and skeletal muscle (Lee et al., 2002).

1.5 Skeletal Muscle

Skeletal muscles are the most commonly found muscles in vertebrates, typically connected to bones and ligaments and responsible for movement through contraction. In contrast to smooth muscles and cardiac muscles, which exhibit involuntary contraction, most skeletal muscle contraction is under voluntary control. Skeletal muscles are thus involved in intentional movements and postural maintenance (Frontera & Ochala, 2015). Apart from this, they serve some crucial roles such as breathing, thermal regulation, nutritional balance, glucose uptake, endocrine activity and in stabilizing joints (Shadrin et al., 2016). Around 40 percent of the human body is comprised of skeletal muscles (Alberts et al., 2002).

Each skeletal muscle is made up of various integrated tissues, such as the skeletal muscle fibres, blood vessels, nerve fibres and connective tissues. A muscle is made up of three layers of connective tissue, called the mysia. These provide structure to the muscle and aid in compartmentalizing the muscle fibres inside the muscle. The epimysium, which is the outermost layer, is a dense sheath of irregular connective tissue that wraps the muscle, allowing it to contract and move powerfully, while at the same time maintaining its structural integrity. Another function of the epimysium is to separate the muscle from other organs in the body. The second layer is called the perimysium, which surrounds a bundle of 20-80 muscle fibres, and forms distinct muscle fascicles. The fascicular organization of muscle fibres enables activation of a subset of muscle fibres to be able to trigger a specific movement. Each individual muscle fibre is enclosed in the endomysium, which is the innermost layer. It is a thin connective tissue layer of collagen and reticular fibres.

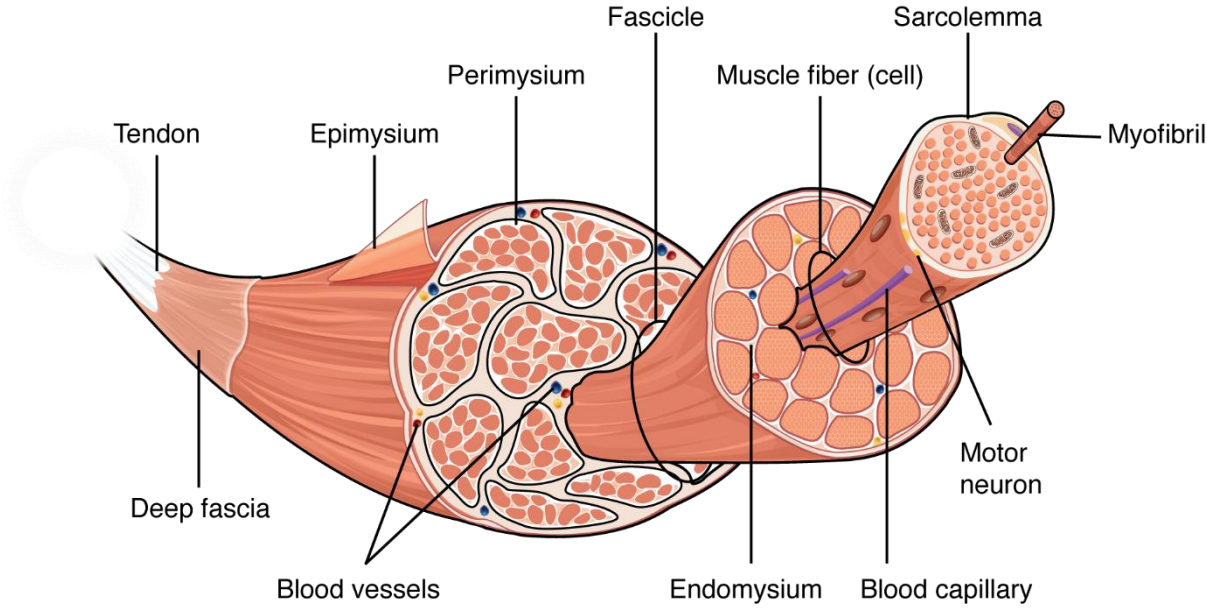

Figure 11: Skeletal muscle architecture showing the three connective tissue layers. Muscle fibres are bundled by the perimysium to form the fascicle. Multiple fascicles are enveloped by the epimysium to form a muscle. (Lindsay et al., Structure and function of the Human Body, OpenStax/Oregon State University)

Skeletal muscle is a highly organized tissue, composed of fibres called myofibres. A muscle cell is represented by a single myofibre. Unlike other cells, myofibres are long and polygonal. They are striated and multinucleated cells, with a diameter ranging from 10 to 100 micrometres, and lengths up to 30 cm. Nuclei are generally located near the periphery and are adjacent to the sarcolemma (plasma membrane), which is the sheath around each myofibre. Within the sarcoplasm (cytoplasm) of each myofibre are present numerous thin (1.2 µm diameter) myofibrils, which are composed of contractile proteins and run the length of the myofibre.

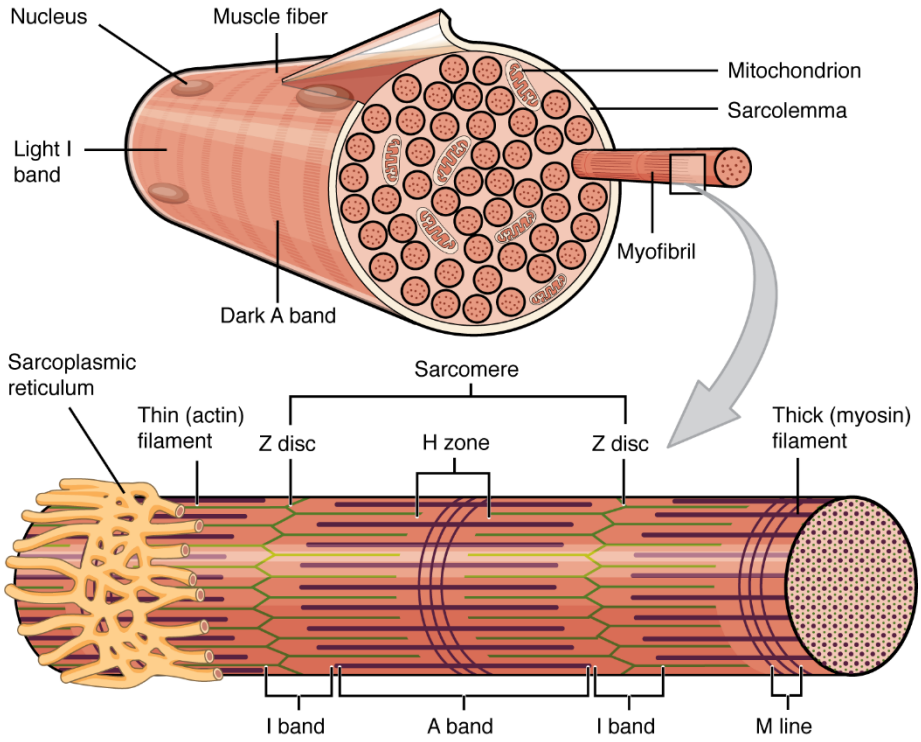

Figure 12: Diagrammatic representation of a muscle fibre (myofibre). Inset shows the organization of the thick myosin bands and the thin actin bands in the sarcomere. (Lindsay et al., Structure and function of the Human Body, OpenStax/Oregon State University)

Each myofibril is composed of several sarcomeres. The sarcomere is the smallest functional unit of a skeletal muscle fibre. It is defined as the region of the myofibril between two cytoskeletal structures called the Z-disks. The sarcomere is made up of thick and thin filaments, which give the skeletal muscle their characteristic striated appearance. The thick contractile filament is composed of a large protein called myosin, formed by one pair of heavy chain (Myosin Heavy Chain, MHC) and two pairs of light chains (Myosin Light Chain, MLC). The helical tail of myosin is formed by the two MHCs that twist around each other, whereas the two globular heads are made up by the interaction of the light chains with the heavy chains. Located within the heads are important binding sites for the main component of the thin filament, actin. They also contain an ATP binding site and serve as the enzyme, myosin ATPase (mATPase). The thin contractile filament is composed of actin, tropomyosin, and three troponins. Globular actin (G-actin) is polymerized to form filamentous actin (F-actin), the ends of which contain myosin-binding sites (McCuller et

al., 2024). Troponin I (TnI) is essential in countering the interaction of actin to myosin, thus preventing muscle contraction when the muscle is at rest. Tropomyosin is a multiprotein complex, with some components facilitating its binding to troponin T (TnT). Troponin C (TnC) binds to calcium, facilitating muscle contraction. Additionally, another protein called Titin is also present within a sarcomere and is required because of the elastic properties it confers. The thick filaments span the centre of the sarcomere and extend towards the Z disks to form the A band. The thin filaments are anchored at the Z-disks and extend inwards, overlapping with the thick filaments, forming the I band. Titin spans from Z disk to Z disk, end to end. The centre of the A band, called the H band, is the region with only thick filaments (Pham & Puckett, 2024).

Muscle contraction occurs when the myofilaments slide across each other, reducing the distance between two Z disks and consequently shortening the sarcomere. mATPase hydrolyses ATP into ADP and inorganic phosphate, providing the energy required for muscle contraction (Scott et al., 2001). The rate at which mATPase hydrolyses ATP to produce the cross-bridge action, influences the speed of muscle contraction.

1.5.1 Muscle Fibre Types

Skeletal muscle is a heterogeneous tissue and is composed of different fibre types. This heterogeneity in muscle fibres is essential in allowing the wide variety of different functions that skeletal muscles can perform. The different fibre types can be differentiated based on biochemical, morphological, or physiological characteristics. The main criteria for classification of muscle fibre types are their contractile function and the rate of ATP regeneration. They can thus be broadly classified as oxidative or glycolytic fibres. The contractile function determined by mATPase activity is in turn determined by the MHC isoform present in the fibre. Each MHC isoform has its characteristic ATPase activity, with different myosins being derived from different genes. Further classification based on these isoforms gives rise to four main fibre types, Type I, Type IIa, Type IIb and Type IIx.

Gene	Protein	Expression Pattern
MYH1	MyHC IIx/d	Type 2B
MYH2	MyHC IIa	Type 2A Extraocular muscle
MYH3	Embryonic MyHC	Fetal development Muscle regeneration
MYH6	α-cardiac MyHC	Heart atria
MYH7	MyHC I β-Cardiac MyHC	Type 1 Heart ventricles
MYH8	Fetal MyHC	Fetal development Muscle regeneration
MYH11	Smooth muscle MyHC	Smooth muscle
MYH13	Extraocular MyHC	Extraocular muscle

Figure 13: Different isoforms of myosin heavy chain of skeletal origin, and their expression patterns (adapted from Tajsharghi & Oldfors, 2013).

Type I fibres are slow-twitching oxidative fibres, with the smallest cross-sectional area. Since they produce ATP through aerobic respiration (oxidative), they have a high number of mitochondria, meaning more ATP can be produced during each metabolic cycle. This confers Type I fibres with a higher resistance to fatigue, allowing for longer contractile periods. Furthermore, these fibres are extensively supplied with blood capillaries and possess myoglobin, which stores oxygen within the fibres and is responsible for the dark red colour of the fibres. The fibres have low glycogen levels and low mATPase activity. Type 1 fibres are therefore best suited for endurance types of muscle contraction such as running a marathon, maintaining posture or producing isometric contractions.

Type IIa fibres are fast-twitching oxidative fibres (Korthuis, 2011). They mostly produce ATP through respiration, and contain a much lower number of mitochondria compared to Type I fibres. They do however have a higher mATPase activity, responsible for faster

contraction. They can thus produce relatively high amounts of tension, but do not fatigue quickly due to their oxidative metabolism. Type IIa fibres also appear red in colour. Since these fibres possess characteristics that are intermediate between slow oxidative and fast glycolytic, they are often referred to as intermediate fibres. Type IIa fibres are best suited for medium duration and moderate movements such as walking or biking (McCuller et al., 2024).

Type IIb fibres are fast-twitching glycolytic fibres and have a high mATPase activity. These fibres use glycolysis to produce ATP, thus they have a large diameter with large stores of glycogen, for quick ATP production. Therefore, they do not possess a large number of mitochondria and have a limited capillary supply with very low amounts of myoglobin. Consequently, these fibres fatigue very easily and can only be used for short periods. This confers a white colour to the Type IIb fibres. Type IIb fibres produce rapid, forceful contractions during quick and powerful movements, and are best suited for short-duration intense movements such as sprinting or weight lifting. Type IIX fibres are also fast glycolytic fibres, with properties intermediate to Type I and Type IIb fibres.

Fiber type	MyHC-I	MyHC-IIa	MyHC-IIx	MyHC-IIb
Activity used for	Aerobic	Long-term aerobic	Short-term anaerobic	Short-term anaerobic
Power produced	Low	Medium	High	Very high
Contraction time	Slow	Moderately fast	Fast	Very fast
Resistance to fatigue	High	Fairly high	Intermediate	Low
Maximum endurance	Hours	< 30 min	< 5 min	< 1 min
Oxidative capacity	High	High	Intermediate	Low
Glycolytic capacity	Low	High	High	High
Mitochondrial density	High	High	Intermediate	Low
Capillary density	High	Medium	Low	Low
Size of motor neuron	Small	Medium	Large	Very Large
Major storage fuel	Triglycerides	Creatine Phosphate, glycogen	Creatine phosphate, glycogen	Creatine phosphate, glycogen
Fasting tolerance	Long	Medium	Short	Short
Denervation induction atrophy sensitivity	High	Medium	Low	Low
Senescence	Slow	Very fast	Fast	Fast

Figure 14: Tabular representation of the different characteristics of fibre types I, IIa, IIx and IIb (Yang & Chan, 2022)

Depending on their function, the proportions of fibre types vary from muscle to muscle. They also vary between species. In most skeletal muscles, individual fascicles are

composed of two or more of these fibre types, however with one fibre type usually predominating (Korthuis, 2011). For instance, the TA and the quadriceps, involved in quick powerful movements, have a high proportion of type IIb or type IIx fibres. On the other hand, the soleus, involved in maintenance of posture, is mostly composed of type I and type IIa fibres (Schiaffino & Reggiani, 2011). Interestingly, type IIb fibres which are present in smaller animals such as rodents are absent in larger mammals such as humans. Of note, muscle fibres are highly plastic and can adapt to changing demands by altering fibre type composition (Scott et al., 2001).

1.5.2 Mitochondria in skeletal muscles

In skeletal muscle, mitochondria are primarily distributed within the subsarcolemmal (SS) and the intermyofibrillar area (IMF). The SS mitochondria are grouped beneath the sarcolemma and the IMF mitochondria are nested between parallel myofibres. Additionally, the IMF mitochondria are distributed into two subpopulations, with one population residing at the I band and the other at the A band. The SS and the IMF mitochondria differ in their functional characteristics, kinetics and metabolism of mitochondrial proteins (Palmer et al., 1977; Wahwah et al., 2020). They are also morphologically different. The SS mitochondria play a role in gene expression and resistance to ROS. On the other hand, IMF mitochondria are involved in processes such as OXPHOS and modulation of calcium flux (Ferri et al., 2020).

Mitochondria are associated with the sarcomere I band in anaerobic glycolytic fibres, but accumulate in the I band and A band in oxidative fibres (Franzini-Armstrong & Boncompagni, 2011).

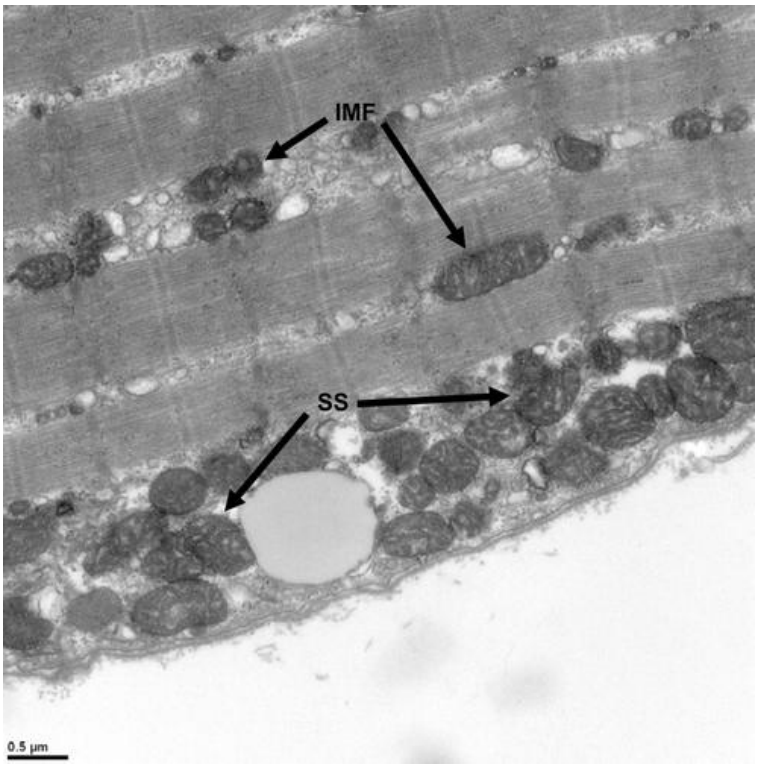

Figure 15: Transmission electron micrograph of a human skeletal muscle showing the mitochondrial localization in a muscle fibre. The subsarcolemmal (SS) mitochondria are localized beneath the basal lamina, i.e the sarcolemma. The intermyofibrillar (IMF) mitochondria are nested between parallel myofibres. (Wahwah et al., 2020)

Since the muscle is a highly plastic tissue, it can alter its size, metabolic properties, fibre type proportions and other such parameters. Moreover, skeletal muscle is heavily involved in different functions that require a lot of energy. Therefore, the mitochondria generate ATP for various skeletal muscle functions, and their calcium uptake capacity plays a key role in muscle contraction.

Mitochondria behave in a dynamic manner within the myofibre, with changes in metabolic demand inducing modifications in shape (Hood et al., 2019). The metabolic plasticity is regulated by mitophagy, maintaining a constant balance between the amount of short and elongated mitochondria (Twig & Shirihai, 2011).

1.6 Muscle Satellite Cells

Skeletal muscles have a robust regenerative capacity to maintain their normal physiology. Skeletal muscles have their own pool of stem cells, located at the periphery of muscle fibres. They are called muscle satellite cells (MuSCs) due to their unique anatomical position between the sarcolemma and the basal lamina of the muscle fibre. Unlike skeletal muscle fibres, MuSCs are mononucleated and unipotent. They were first identified by Alexander Mauro in 1961 (Mauro, 1961).

Myofibre turnover is a process that occurs throughout the lifetime of an individual to maintain the viability of muscle tissues. This is essential during ageing, in diseases and with disuse, where skeletal muscle fibres get either damaged or atrophied frequently (Dumont et al., 2015). Skeletal muscle regeneration occurs in four stages (Carosio et al., 2011a). First, necrosis occurs following muscle fibre injury or damage, where the MuSC niche is altered. Necrosis is accompanied by an inflammatory response during which two subpopulations of macrophages are recruited. The early population of macrophages (M1) secrete pro-inflammatory markers, such as interleukin 1 (IL1) and tumour necrosis factor alpha (TNFα). In contrast, the second population of macrophages (M2) secrete anti-inflammatory markers such as interleukin 10 (IL 10), lasting until inflammation persists. The third stage involves the activation, differentiation, and fusion of MuSCs, with the second macrophage population facilitating proliferation and differentiation. Finally, the maturation and remodelling of newly formed fibres take place (Carosio et al., 2011a).

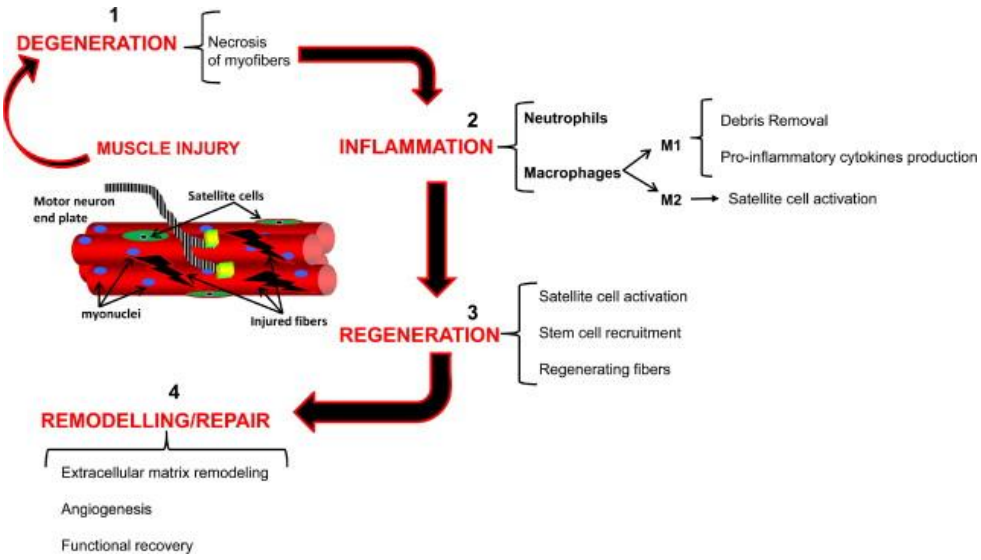

Figure 16: Schematic representation of the four interrelated phases of skeletal muscle regeneration (Carosio et al., 2011b).

Histologically, a hallmark of regenerated muscle fibres are their reduced diameter and the presence of centrally located nuclei (Clark, 1946; Hall-Craggs & Singh Seyan, 1975). Following the fusion of a myoblast with a myotube, the new nucleus migrates towards the centre of the myotubes (centration), where it spreads along the longest axis, after which they are finally dispersed towards the periphery and get anchored there after complete regeneration (Cadot et al., 2015; Roman & Gomes, 2018).

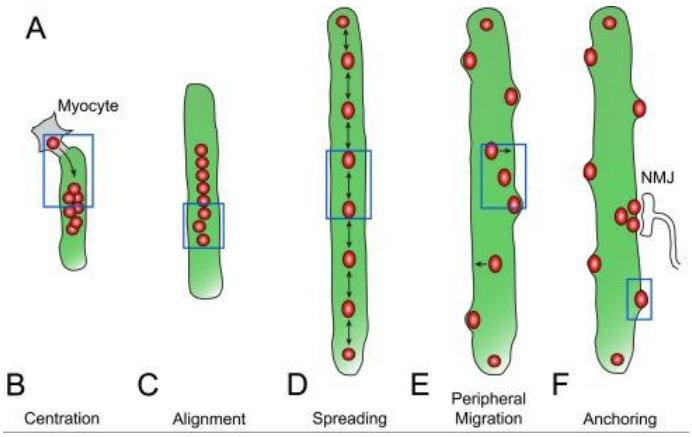

Figure 17: Representation of nuclear repositioning during muscle regeneration. (Roman & Gomes, 2018)

MuSCs are the primary taskforce responsible for regeneration of skeletal muscle and for maintenance of muscle tissue integrity (Fu et al., 2022). MuSCs generally exist in a quiescent state. However, during muscle biogenesis, or upon muscle injury, MuSCs are activated. Upon activation, the MuSCs either self-renew to maintain the stem cell pool, or undergo several proliferation steps and then differentiate to form new muscle fibres, which either fuse to existing fibres or generate new ones. MuSCs can be identified through the expression of certain markers for and regulators of the quiescent state, as well as of activation and progression through the myogenic lineage. The Paired homeo Box7 (Pax7) transcription factor is one such factor, along with Paired homeo box 3 (Pax3) (Wang et al., 2014). Apart from these, there exist a set of myogenic regulatory factors (MRFs) responsible for the specification, commitment, and progression of MuSCs through the various stages of regeneration (Relaix & Zammit, 2012). These include Myogenic Factor 5 (Myf5), Myogenic determinant 1 (MyoD), Myogenic regulatory factor 4 (Mrf 4) and Myogenin. Pax7 is the most commonly used marker to identify MuSCs. Expression of markers such as muscle (m)-Cadherin and CD34 can also be used for the identification of MuSCs (Fukada et al., 2007; Gnocchi et al., 2009).

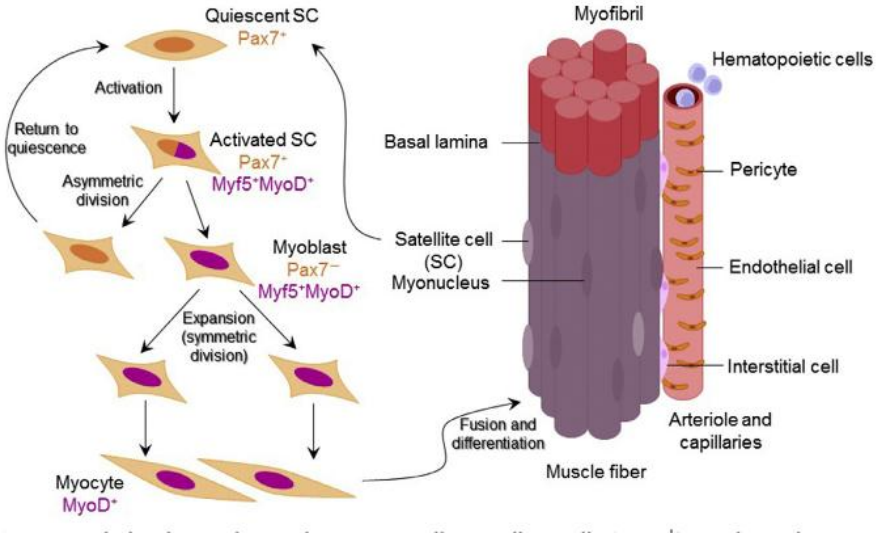

Figure 18: Skeletal muscle satellite cells in skeletal muscle regeneration. Upon injury and during biogenesis, quiescent MuSCs are activated to form muscle precursor cells. They undergo several proliferation steps to expand, and finally differentiate to form myofibres.

These myofibres either fuse to existing muscle fibres or form new fibres. (Boppart et al., 2015)

1.6.1 MuSC Quiescence

During healthy resting periods, MuSCs remain in a quiescent state, by staying in the G_0 stage of the cell cycle. They must remain quiescent to adapt to the slow turnover rate of skeletal muscles, and for the long-term maintenance of themselves (Wang et al., 2014). Quiescent MuSCs are described to possess high stemness. They have several characteristic features such as small cell size, high nucleo- cytoplasmic ratio and low RNA and protein synthesis levels. Compared to activated MuSCs, quiescent MuSCs have a unique gene expression profile, with high expression of genes such as M-Cadherin, Integrin B (ITGB1), CD34, Calcitonin Receptor (CalcR), Alpha 7 – Integrin and Notch receptor, amongst others. MuSCs quiescence is tightly regulated by a complex cell intrinsic network of transcription factors, translation factors, extra cellular matrix, metabolites, and mechano-sensors (Fu et al., 2022). Several signalling cascades are involved in maintaining quiescence in MuSCs. Of these, Notch signalling is one of the key pathways. Activation of Notch by its ligands represses the expression of the myoblast determination protein MyoD and therefore prevents re-entry into the cell cycle (Bjornson et al., 2012). At the same time, Notch activation also increases the expression of Pax7 and improves the homing of MuSCs (Evano & Tajbakhsh, 2018). The extra cellular matrix (ECM) is required to maintain MuSC quiescence. Forkhead Box O (FoxO) transcription factors are also critical for maintaining quiescence, with inhibition of FoxO activity deteriorating the genuine quiescent stage of MuSCs (García-Prat et al., 2020). Consequently, failure to stay in quiescence causes loss of stemness, precocious differentiation, senescence, and apoptosis of MuSCs, resulting in a loss of stem cell number and function. Ageing has a key role in disrupting MuSCs quiescence, thus resulting in a decline in muscle regeneration capacity in aged muscle (Chen et al., 2020).

1.6.2 MuSCs Heterogeneity, Maintenance and Self-Renewal

Along with being key in muscle regeneration, MuSCs are also important in maintenance of the MuSC population through self-renewal. MuSCs can divide either symmetrically or asymmetrically. During symmetric division, MuSCs undergo planar division, with the orientation of division parallel to the basal lamina. Symmetric division results in two identical daughter stem cells and is thus essential for expansion of MuSCs. Symmetric division is required to replenish the stem cell pool and to maintain homeostatic numbers of MuSCs through repeated rounds of injury and regeneration (Wang et al., 2014). During asymmetric division, the MuSCs undergoes an apical-basal division, with the orientation of division perpendicular to the basal lamina. Asymmetric division results in the generation of two cells, one daughter stem cell at the apical position, required for maintenance of stem cell numbers and a second daughter progenitor cell at the basal position (Kuang et al., 2007). Additionally, asymmetric division is characterized by asymmetric distribution of the template DNA, with the daughter stem cell inheriting the template DNA and the daughter progenitor cell containing the newly synthesized DNA. It has been hypothesized that the high fidelity of DNA information is preserved since the daughter stem cells keep the original copy (Cairns, 1975; Shinin et al., 2006). It is the differences in the environmental cues generated by the muscle fibre and the basal lamina that shape the fate of the two daughter cells (Fu et al., 2022).

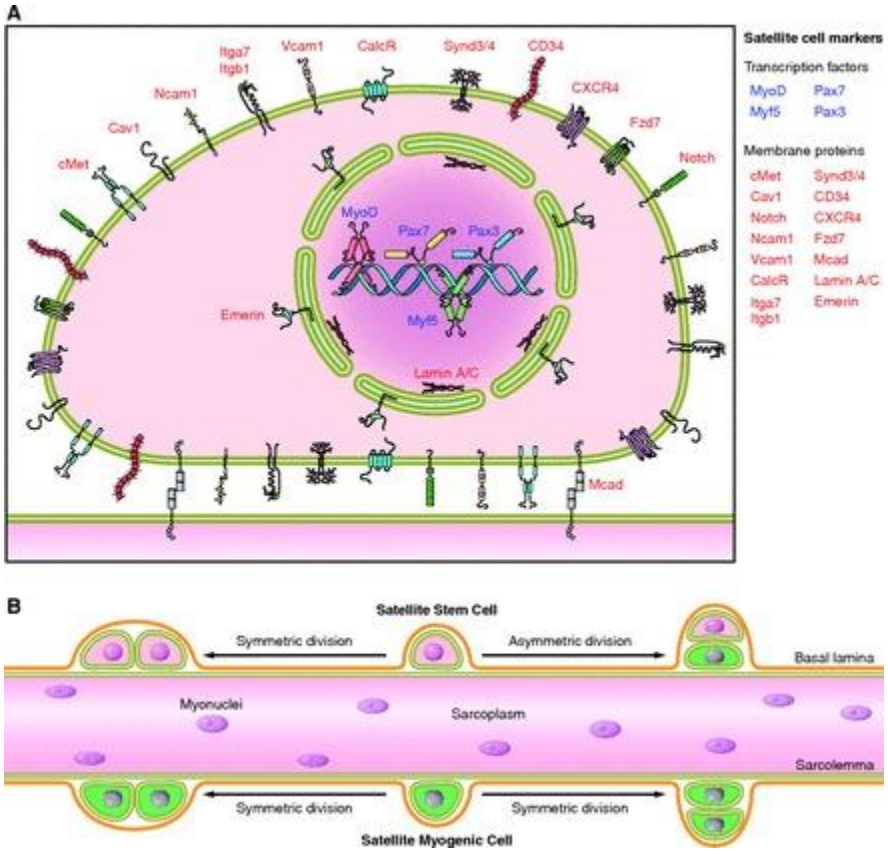

Figure 19: A. Transcription factors and proteins expressed in MuSCs. B. Schematic showing symmetric and asymmetric division of satellite cells.(Yin et al., 2013)

The majority of MuSCs undergo symmetric division, with 10-30 percent of division being asymmetric. Nonetheless, asymmetric division is essential for muscle regeneration and maintenance of muscle homeostasis. During ageing, there is a reduction in symmetric division, resulting in reduced number of daughter stem cells and increased numbers of daughter progenitor cells (Fu et al., 2022). This loss of balance between symmetric and asymmetric division is one of the primary reasons for a decline in muscle regeneration capacity during ageing.

MuSCs also exhibit heterogeneity with some cells expressing higher levels of Pax7 compared to others. MuSCs with high Pax7 show a greater tendency towards asymmetric division and take longer to enter the cell cycle. In contrast, MuSCs with lower levels of Pax7 have a higher tendency to differentiate (Rocheteau et al., 2012).

1.6.3 MuSCs Activation, Expansion, Proliferation and Differentiation

Upon injury, the MuSC quiescence niche is disrupted by exposure to external signals from the environment. This causes MuSCs activation, where they enter the cell cycle in order to proliferate. MuSC activation occurs across the entire length of the myofibre, and not only in the damaged site. The proliferating MuSCs and their progeny are referred to as myogenic precursor cells (MPCs) or myoblasts (Yin et al., 2013). The activation is governed by several niche factors and signalling pathways and accompanied by changes in the morphological characteristics, such as increased size of MuSCs and expansion of the cytoplasm. An increase in the number of mitochondria and other organelles is also observed (Fu et al., 2022).

Following activation, MuSCs expand very quickly over a short period. The MPCs are characterized by initial expression of phosphorylated p38 (Fu et al., 2022), followed by expression of Myf5 and MyoD. Myf5 has a distinct role in the proliferation of the adult myoblasts, whereas MyoD is a determinant of myogenic differentiation (Yin et al., 2013). Consequently, early expression of MyoD leads to precocious differentiation without proliferation, whereas low MyoD levels results in myoblasts with increased proliferation and self-renewal capacity. Furthermore, the entry of the MuSCs into different stages of the myogenic program is dependent on whether Myf5 or MyoD expression prevails (Rudnicki et al., 2008).

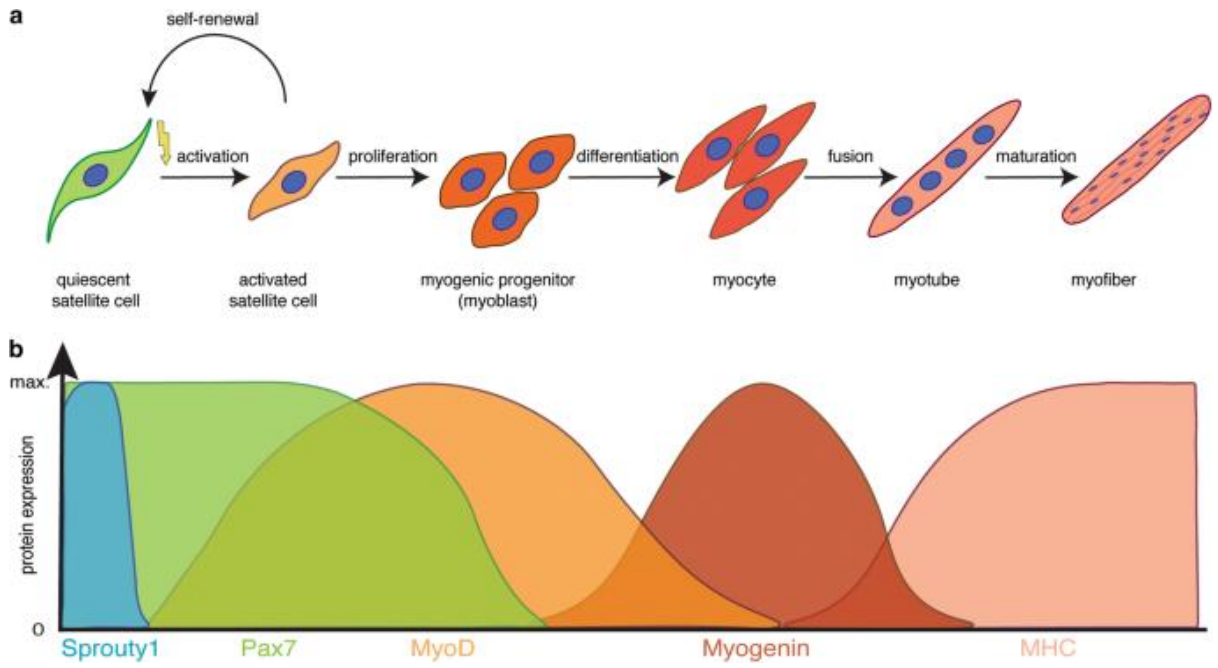

Figure 20: Expression profile of key myogenic regulators during myogenic lineage progression. (Schmidt et al., 2019)

After some rounds of proliferation, most of the MPCs start differentiating, and fuse either to existing myofibres or to each other to generate nascent myofibres. MyoD and Myf5 are still expressed; however, Pax7 is no longer expressed. Expression of Myogenin initiates the terminal differentiation program. The expression of the MRFs are crucial for proper skeletal muscle formation, morphology and function. Along with the MRFs, there also exists a collection of myogenic microRNAs (Williams et al., 2009) involved in myogenic regeneration.

Additionally, there exist various circulating factors in the MuSC niche with myogenic potential (Relaix & Zammit, 2012).

1.6.4 MuSC metabolism – Mitochondria in MuSCs

MuSCs undergo metabolic reprogramming during the different stages of the myogenic program. Quiescent MuSCs have a very low metabolic rate. Similar to other adult stem populations, quiescent MuSCs have few mitochondria with low levels of mtDNA

(Bhattacharya & Scimè, 2020).They are dependent on mitochondrial fatty acid oxidation (FAO, beta-oxidation of fatty acids), and OXPHOS, and do not rely on glycolysis for their metabolic needs. Quiescent MuSCs with low Pax7 expression, which are more myogenically committed, have more mitochondria and mtDNA with increased ATP generation. In contrast, satellite cells with high stemness have reduced mitochondrial density and lower mitochondrial activity (Rocheteau et al., 2012). Dependence on FAO contributes to the maintenance of quiescent state, and its inhibition has been associated with premature MuSC differentiation and impaired muscle regeneration. Furthermore, FAO is linked to a low metabolic rate with minimized ROS production, therefore preserving MuSC regenerative capacity (Relaix et al., 2021). As a result, they can preserve their function for many years, even surviving 30 days post mortem in humans (Latil et al., 2012).

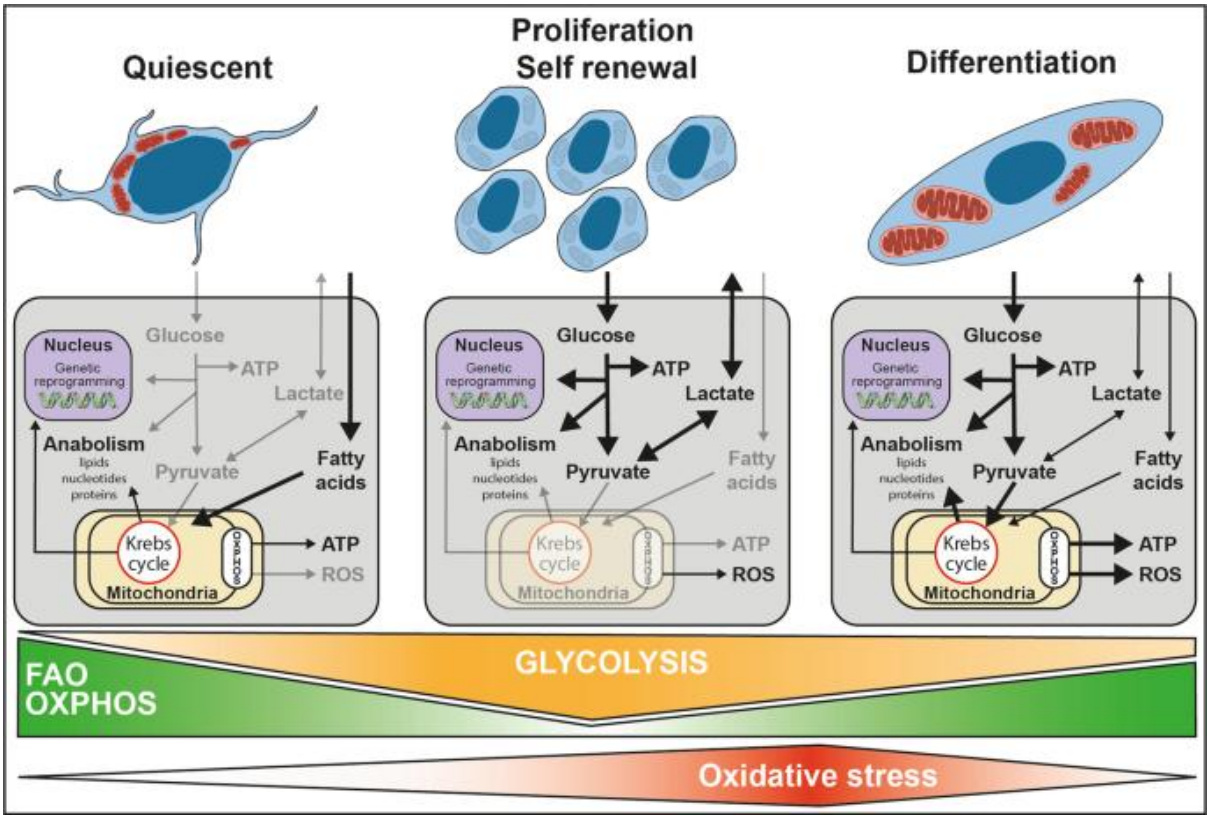

Figure 21: Metabolic pathways that regulate quiescence, self-renewal, proliferation, and differentiation during myogenesis.(Relaix et al., 2021)

Upon MuSC activation, the myogenic precursor cells, called myoblasts, need to proliferate. Hence, there is a constant energy demand, due to which the myoblasts are in a highly glycolytic state. Glycolysis is useful in providing the proliferating MuSCs with the necessary macromolecules to meet their anabolic demands (*Figure* 21). Committed MuSCs have devised several methods to suppress OXPHOS, thus increasing their proliferative rate. For instance, proliferation is associated with hypoxia-inducible factor 1-alpha (HIF1α) activation, which promotes glycolysis and attenuates OXPHOS, thus inhibiting differentiation (Yang et al., 2017). Proliferating MuSCs have low levels of the respiratory chain complex subunits; mitochondrial proteins and enzymes, compared to differentiating cells (Bhattacharya & Scimè, 2020; Hoffmann et al., 2018).

Once the MuSCs start differentiating, there is increased metabolic activity. Due to this, glycolysis subsides and the MuSCs metabolism is associated with increased OXPHOS (Relaix et al., 2021). This is essential for terminal differentiation. Expression of genes involved in both OXPHOS and in FAO is increased. Differentiated myofibres have higher mitochondria with pronounced levels of mtDNA, ETC complex proteins and the enzymes of the TCA cycle (Franko et al., 2008; Remels et al., 2010).

1.7 Sarcopenia

Sarcopenia refers to the loss of skeletal muscle mass and strength, associated with ageing, and was first described by Rosenberg in 1989 (Rosenberg, 1989). The term sarcopenia comes from the Greek “sarx” meaning flesh and “penia” meaning loss. Studies show that the decline in muscle mass and strength begin as early as the 4th decade of life, occurring in a linear fashion, with up to 50% of muscle mass being lost by the 8th decade (Metter et al., 1997). Since muscle accounts for around 60 percent of the body’s protein, its loss is responsible for structural and molecular modifications that lead to functional impairment. Sarcopenia can thus have profound consequences in older adults, with severe and adverse health outcomes such as loss of function, disability, frailty and death (Walston, 2012). As a result, sarcopenia is strongly associated with several comorbidities such as a high risk of falls, followed by hospitalization leading frequently to

lung infection and sometimes death, as well as increased prevalence of metabolic diseases such as diabetes mellitus (type 2) and obesity (Pacifico et al., 2020).

There is a lack of standardized measurements for sarcopenia, since muscle functionality is not measured under the current scope of muscle mass and strength. Therefore, there is no consensus on a clinical definition for sarcopenia. Thus far, sarcopenia still does not have a broadly accepted clinical definition, nor does it have consensus diagnostic criteria along with a lack of treatment guidelines. There are three methods accepted at present, by which sarcopenia can be defined and diagnosed. The first is by the European Working Group on Sarcopenia in Older People (EWGSOP), which defines sarcopenia as the presence of low skeletal mass and either low muscle strength (based on grip strength) or low muscle performance (based on walking performance). If all three conditions are met, severe sarcopenia is diagnosed (Cruz-Jentoft et al., 2010). They also define a presarcopenia stage, described as only the loss of muscle mass. The second, given by the European Society for Clinical Nutrition and Metabolism Special Interest Groups (ESPEN-SIG), defines sarcopenia as the presence of low muscle mass and muscle strength (Muscaritoli et al., 2010). The third, given by the International Working Group on Sarcopenia (IWGS), defines sarcopenia in a similar fashion as ESPEN-SIG, however they also state that sarcopenia is associated with “muscle mass alone or in conjunction with increased fat mass” (Fielding et al., 2011). However, the fact that there is no universal consensus for an operation definition of sarcopenia is cause for concern and important in the scope of public health. This is especially true in a world where the proportions of older adults are increasing the world over.

The pathophysiology of sarcopenia includes an impairment in myofibre metabolism and alteration in MuSCs, resulting in poor or defective myogenesis and consequently upsetting skeletal muscle homeostasis (Riuzzi et al., 2018). Sarcopenia is associated with neurological deficiencies, with motor neuron denervation, reduced number of neuromuscular junctions and a loss of motor units. This leads to muscle fibre denervation, causing fibre atrophy and thereby affecting muscle quality and strength furthermore (Kwon & Yoon, 2017; Wilkinson et al., 2018).

Decrease in muscle mass is due to both a decrease in muscle fibre size, i.e. muscle atrophy, and due to decrease in the number of muscle fibres, i.e. hypoplasia. Interestingly, it has been shown that upon ageing, type II muscle fibres are more prone to atrophy than type I fibres (L. Larsson et al., 1978; Lexell et al., 1983). Sarcopenia is associated with changes in muscle architecture, such as a reduction in cross-sectional area CSA, fascicle length (affecting muscle shortening velocity) and pennation angle (involved in muscle strength) (Narici & Maffulli, 2010).

Another key pathophysiologic event is the presence of chronic, low-grade inflammation in skeletal muscles, called inflammaging. It has also been shown that sarcopenia is accompanied by infiltration of fat (steatosis) and connective tissue (fibrosis) (Taaffe et al., 2009). The accumulation of fat within aged muscle can impair muscle strength and metabolism (Marcus et al., 2010.). This is of particular concern in older individuals, where sarcopenia is combined with obesity and gives rise to a condition called sarcopenic obesity (Baumgartner, 2000). Additionally, fat infiltration is thought to sustain sarcopenia through the release of pro-inflammatory cytokines such as TNF-α, lL-6, IL-1 mediated by macrophage infiltration. This chronic inflammation is thought to be a mechanism for insulin resistance (Narici & Maffulli, 2010). Therefore, the loss of muscle mass during sarcopenia promotes insulin resistance, resulting in further progression of sarcopenia and increasing the risk of development of metabolic syndromes.

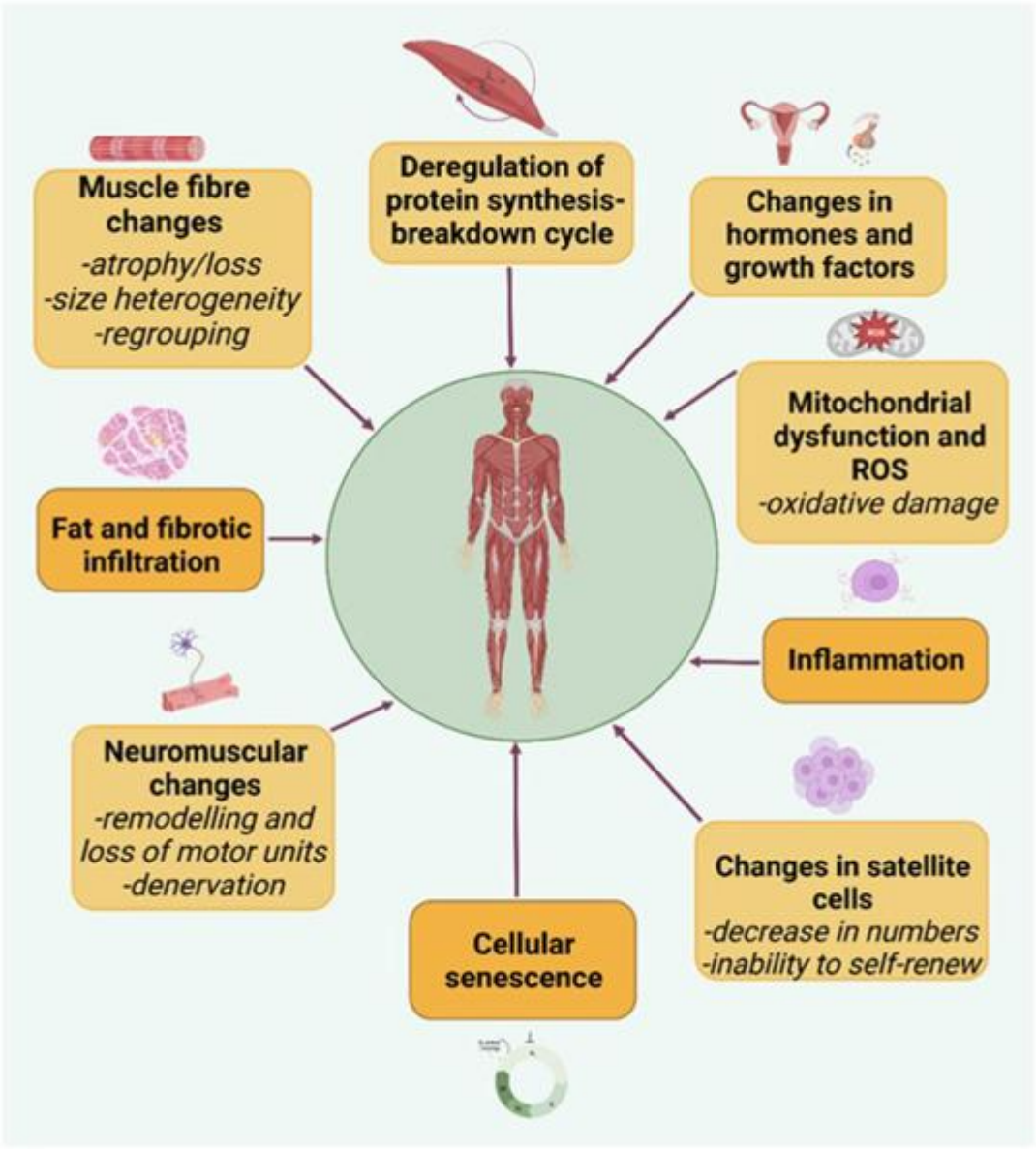

Figure 22: Mechanisms that have been implicated in the pathogenesis of sarcopenia. (Robinson et al., 2023)

While the exact cause of sarcopenia is not understood, several factors are thought to play a role in its pathogenesis. Some of the primary factors are decreased nutritional intake (malnutrition), decreased physical activity and obesity. Chronic inflammation and dysfunction of the neuromuscular junction and alterations in muscle metabolism are

additional major factors, however a decline in the regenerative capacity of MuSCs is thought to be one of the major contributing factors to sarcopenia (Tournadre et al., 2019).

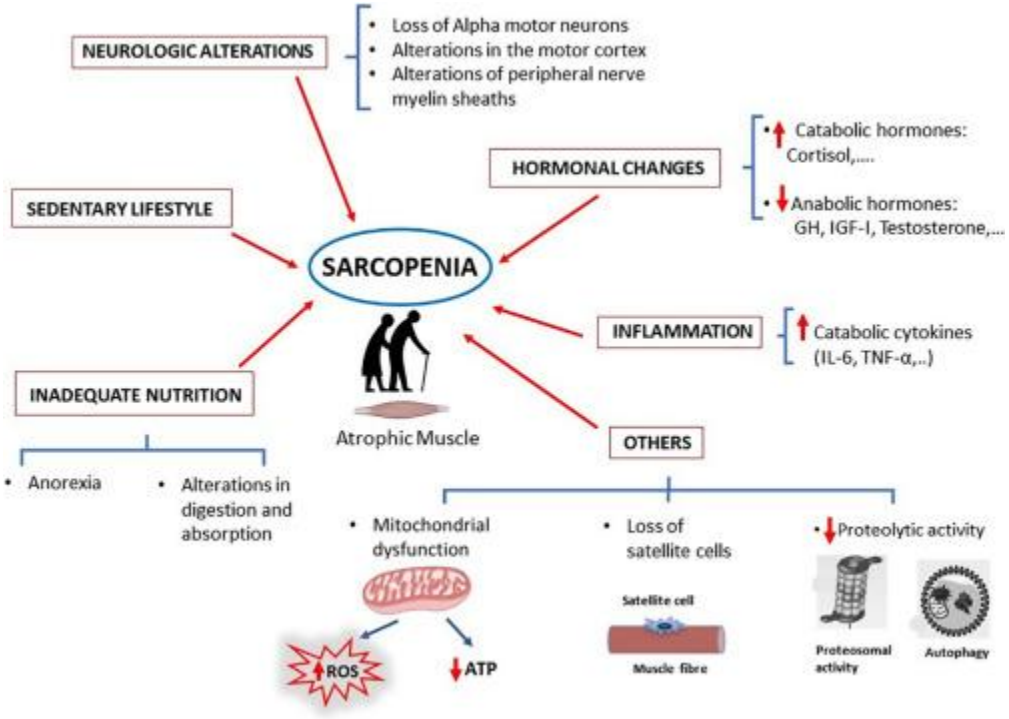

Figure 23: The major causes of sarcopenia.(Priego et al., 2021)

Alterations and impairment in mitochondrial function have been heavily implicated in sarcopenia (Calvani et al., 2013; Ferri et al., 2020). Given that mitochondria play a key role in cellular bioenergetics, this is not surprising. Mitochondrial dysfunction is associated with low levels of ATP and increased generation of ROS and Reactive Nitrogen Species (RNS), which activate several harmful cellular pathways. Ageing skeletal muscle is associated with decreased mitochondrial mass, reduced ATP synthesis and activity of TCA cycle enzymes (Marzetti et al., 2024). This can be explained by altered mitochondrial dynamics and changes in mitochondrial biogenesis and mitophagy. Respiratory chain defects also contribute to fibre denervation, which generate excess ROS/RNS affecting nearby healthy fibres as well, cementing their role in the pathogenesis of sarcopenia (Pollock et al., 2017).

Transcriptomic data shows reduced mitochondrial gene expression in geriatric populations. Notably, genes involved in mitochondrial structure and function are downregulated more in aged women compared to men, indicating increased predisposition of aged females to skeletal muscle impairment (Bellanti et al., 2021; Liu et al., 2013). Moreover, mitochondrial dysfunction also impairs skeletal muscle quality by inducing apoptosis.

Interestingly, reduced expression of PGC1alpha gene and protein levels could play a role in the reduced mitochondrial content observed, since PGC1alpha regulates mitochondrial biogenesis and OXPHOS (Bellanti et al., 2021). Importantly, increased mtDNA mutations, alterations and reduced mtDNA copy number could be responsible for the decline in mitochondrial mass and function (Herbst et al., 2021).

Finally, a reduced ability to remove damaged and dysfunction organelles from skeletal muscles during ageing could cause accumulation of mitochondrial alterations, in turn contributing to sarcopenia.

1.8 Aim of the Thesis

The main objective of this thesis was to study the effects of disturbed mtDNA integrity in MuSCs during differentiation, *in vivo* and *in vitro*.

2. Materials and Methods

2.1 Materials

Table 1: List of Reagents

Reagent	Source	Identifier
Ketaset 100mg/ml Ketaminhydrochloride	Zoetis	402082.00.00
Rompun 2% - Xylazinehydrochloride	Bayer	6293841.00.00
ECL – Western Lighting ® Plus	PerkinElmer	NEL104001EA
Sodium Chloride –Solution (0.9%), sterile	PanReac, AppliChem	A1671,0100
PowerUp™ SYBR™ Green	Applied biosystems.	A25742
Miglyol – Mittelkettige Triglyceride	Caelo	Ch.B.: 211102-28
ROTI®Liquid Barrier Marker für di Mikroscopie	Carl Roth	AN92.1
Dulbecco's Phosphate Buffered Saline. Sterile	Gibco	14190-198
TRIzol® Reagent	Ambion – by Life Technologies	15596018
TRI Reagent	Zymo Research	R2050-1-50
cOmplete Mini, EDTA-free – Protease inhibitor cocktail	Roche	11836170001
Dispase II – neutral protease	Roche	04 942 078 001
Paraformaldehyde	Roth	0335.1
BSA – Albumin, IgG-free	Roth	3737.2
Goat Serum (Normal)	Dako	X0907
Nitro Blue Tetrazolium	Sigma Aldrich	N5514-25TAB
Tamoxifen	Sigma	T5648-1G
EDTA,	PanReac, AppliChem	A5097,0250
3,3' – Diaminobenzidine tetrahydrochloride hydrate	Sigma	D5637-1G
UltraPure™ Agarose	Invitrogen by Life technologies	16500 – 500
Sodium Hydroxide	Carl Roth	6771.1
Sodium Chloride	Carl Roth	3957.1
Bromophenol Blue Na-Salz,	Carl Roth	A512.1
TRIS Buffer	Carl Roth	4855.2
Tween® 20	Carl Roth	9127.2
Paraformaldehyde	Merck	1.04005.1000

Triton X-100	Ultrapure, Union Carbide Chemicals and Plastics	9002-93-1
Glycine, Blotting grade	Carl Roth	0079.4
SDS Ultra pure	Carl Roth	2326.3
Ponceau S	Carl Roth	5938.1
Sodium deoxychlate	Sigma Aldrich	D6750-10G
Sucrose – D(+)-Sacharose	Sigma	4621.1
Magnesium Chloride	Carl Roth	KK36.1
Entellan™	Sigma Aldrich	1.07961.0100
1-Bromo-3-chloropropane	Sigma Life Sciences	B9673-200ML
Mayer's Haematoxylin	Carl Roth GmbH	T865.1
Eosin Y Solution, 0.5% in water	Carl Roth GmbH	X883.2
Acetic Acid	Roth	3738.2
Ethanol	Roth	9065.4
Xylol – Xylene (isomere)	Carl Roth	CN80.2
HCl – Hydrochloric acid 32%	VWR, BDH Chemicals	7647-01-0
0.05% Trypsin-EDTA	Gibco, Thermo Fischer	25300-054
F-10 (1X), Nutrient Mixture (Ham), [+] L-Glutamine	Gibco	11550-043
Dulbeccos's Modified Eagle Medium, [+] 4.5g/L D-Glucose, [-] Pyruvate	Gibco	61965-059
Opti-MEM® I (1X), Reduced Serum Medium, [+] L.Glutamine, HEPES, [-] Phenol Red	Gibco	11058-021
Sodium Pyruvate 100mM	Gibco	11360-039
Red Blood Lysis Solution 10X	Milteny Biotec	130-094-183
Satellite Cell Isolation Kit, mouse	Milteny Biotec	130-104-268
Collagen G, Type 1 from calf skin	Sigma Aldrich	L7213-100ml
Plasmocin prophylactic	InvivoGen	ant-mpp
Chick Embryo Extract – Lyophilised	Life Science Production	MDL-004E-UK
Penicillin Streptomycin	Gibco, Thermo Fischer,	15140-122
Dimethyl sulphoxide (DMSO)	Carl Roth	4720.4
Methanol	Carl Roth	4627.5
Nonfat dried milk powder	PanReac, AppliChem	A0830,0500
TEMED	Carl Roth GmbH	2367.1
Glycerol gelatine	Sigma Life Sciences	GG1-15ML
Ethidium Bromide Solution	Carl Roth	2218.2
ROTIPHORESER Gel 40 (37, 5:1) Acrylamide Gel	Carl Roth	T802.1

40% ready to use		
λ DNA/HindIII Marker	Fermentas	SM0101
DreamTaq™ Green PCR Master Mix	Thermo Scientific	K1082
Long Range DNA Polymerase, 2.5 U/µl	biotech rabbit GmbH	BR0300302

Table 2: List of materials

Material	Source	Identifier
Cuvettes for Spectophotometer	Carl Roth	D76185
Deckgläser, 24 x 40 mm	Roth	1871
SuperfrostPlus™ Gold Adhesion Microscope Slides	Epredia,	K5800AMNZ72
20G x 1 ½ TW, (0.9mm x 40mm), BD Eclipse Needle	Becton, Dickinson and Company	305888
1ml Syringe – BD Plastipak™, Sterile	Becton, Dickinson and Company	303172
Scalp Vein Set – ECOFLO – Dispomed. 18G, 30cm		
BD Microlance™ 3 – 27G x ¾ - Nr 20, 0.4 x 19mm. Sterile	Becton, Dickinson and Company	302200
Sterican® 23G x 1”, 06x 25mm BL/LB. Gr.16	Braun	
Feather Disposable Scalpel	Feather Safety Razor	5205052
Glass Pasteur pipette, L 150mm	Carl Roth	22026041
Plastic Pasteur Pipette 3ml Graduated.	Pastette Alpha Laboratories	LW4111
MicroAmp® Optical 96-well Reaction Plate	applied biosystems®, by Life technologies™	N8010560
MicroAmp™ Optical Adhesive Film	applied biosystems, by Thermo Fischer Scientific	4311971
Embedding Molds	Polysciences Europe GmbH	686601
Perfusion Set – Intrafix® SafeSet, Type Back Check Valve	Braun	4063001
150ml Bottle Top Filter	Corning	430624
Sapphire Filter Tip 1250ul	Greiner	778353
PCR SoftTubes 0.2ml, transparent	Biozym	711080
gentleMACS™ C Tubes	Milteny Biotech	130-096-334

Magnetic columns – LS Columns	Milteny Biotech	130-042-401
Cell Strainer – 70µm (Sterile)	starlab	CC8111-0072
Cell Strainer – 40µm (Sterile)	Greiner bio-one	542040
Tissue Cuture Testplate 6 – 4ocs	TPP	92406
VACUUM FILTRATION 250 “rapi”- FILTERMAX	TPP	99250
Tissue Culture Dish 100	TPP	93100
Tissue Culture Flask 75	TPP	90075
Cell counting slide – EVE TM	NanoEntek	EVS-050
Cryo Tube 20	TPP	89020
quadroMACS . Multi Stand	Milteny Biotec	130-042-303
gentleMACS Dissociator	Milteny Biotec	130-093-235
Glass Plates with spacer – 1.5mm	Bio-Rad	63386
15ml Tubes	Sarstedt	62.554.502
50ml Tubes	Sarstedt	62-547.254

Table 3: List of Instruments

Instrument	Source
Gel Logic 200 Imaging System	Kodak
Eppendorf Biophotometer OD 600.	Eppendorf
iCycler	BioRad
LAS 500 – CCD camera	GE Healthcare
T3000 Thermocycler	biometra
Heating Block - Thermo Shaker	Eppendorf
QuantStudio1	applied biosystems – by Thermo Fischer Scientific
Scan LAf MARS - Air flow hood	Babogene – Scandinavian by Design
Hera Cell - Cell culture Incubator	Thermo Scientific
Function Line – Cell Culture incubator – Kendro	Heraeus Instruments
EVE – Automatic cell counter	NanoEntek
Rotina 380R Centrifuge	Hettich centrifuges
Mini Protean Tetra System	Bio-Rad
Precision Weighing balance	Sartorius
Weighing Balance – BP2100	Sartorius

Table 4: List of Primers

Gene	Forward Primer (5' – 3')	Reverse Primer (5'- 3')
K320E-Twinkle	AAAGTCGCTCTGAGTTGTTATC	GATATGAAGTACTGGGCTCTT
Mlc1f-Cre	CACGACCAAGTGACAGCAAT	AGAGACGGAAATCCATCGCT
Pax7-Cre	ACTAGGCTCCACTCTGTCCTTC	GCAGATGTAGGGACATTCCAGTG
mitoTIMER	GGACGGCTGCTTCATCTACA	TAGTCCTCGTTGTGGGAGGT
Long Range	GTTCAACGATTAAAGTCCTACGTG	GTTGTTTGATCCTGTTTCGTG
mtDNA	CCTATCACCCTTGCCATCAT	GAGGCTGTTGCTTGTGTGAC
Nuclear DNA	ATGGAAAGCCTGCCATCATG	TCCTTGTTGTTCAGCATCAC

2.2 Transgenic Mouse Models

Several transgenic mice were used for the completion of the thesis, namely K320E-Twinkle^{Skm} (Skeletal muscle), K320E-Twinkle^{MuSC} (Muscle Satellite Cells), mitoTIMER K320E-Twinkle^{Skm} and mitoTIMER K320E-Twinkle^{MuSC}. K320E-Twinkle^{Skm} mice were generated by crossing C57BL/6J mice with a dominant-negative mutation of the mitochondrial helicase Twinkle (point mutation K320E; Rosa26-Stop-construct; downstream EGPF) with C57BL/6J mice expressing Cre recombinase under the control of the MLC1f promoter (MLC1f-Cre). K320E-Twinkle^{MuSC} mice were generated by crossing K320E mice with C57BL/6J mice expressing a tamoxifen inducible Cre recombinase under the control of the Pax7 promoter (Pax7-Cre^{ERT}). mitoTIMER K320E-Twinkle^{Skm} and mitoTIMER K320E-Twinkle^{MuSC} were generated by crossing mice C57BL/6J expressing mitoTIMER with either K320E-Twinkle^{Skm} mice or K320E-Twinkle^{MuSC} mice respectively.

All mice used for experiments were housed in a standard animal house, maintained at 23°C with a 12:12h light-dark cycle. They were kept in individually ventilated cages that had a specified pathogen-free hygiene level, with free access to water and standard rodent chow. All animals were regularly monitored for potentials signs of pain and suffering. All breedings, procedures and experiments were carried out in accordance with the protocols approved by the local authority (LANUV, Landesamt für Natur, Umwelt und

Verbraucherschutz NRW, breeding approval number: 2021-A256 and experimental approval number: 2019-A090).

2.3 Genotyping

Genotyping of different transgenic mouse lines was done by standard PCR amplification, using genotype specific primers, with DNA isolated from ear-punch biopsies or tail biopsies. DNA was isolated by lysing the tissue in lysis buffer (10mM NaOH, 0.2mM EDTA) at 96°C for 45 minutes. Then, samples were quickly placed on ice for 5 seconds, to which was added an equal volume of neutralization buffer (40mM Tris-HCl, pH 7.6) and they were then centrifuged at 1000 g for 1 minute. Standard PCR reactions were set up using 2X Dream Taq, 4µM of primers (listed in *Table* 4) for K320E-Twinkle, Mlc1f-Cre, Pax7-Cre or mitoTIMER, and 1.5 µl of template DNA in a final reaction volume made up to 25µl.

The following are the cycling conditions for the PCR setups.

Table 5: PCR Setup for Mlc1f-Cre

Step	Temperature	Time	No. of cycles
Lid Temp	95		
Initial Denaturation	95	3 min	
Denaturation	95	30 sec	
Annealing	53	30 sec	
Extension	72	45 sec	30
Final Extension	72	5 min	
Hold	8	Infinite	

Table 6: PCR Setup for Pax7-Cre

Step	Temperature	Time	No. of cycles
Lid Temp	95		
Initial Denaturation	94	3 min	
Denaturation	94	15 sec	
Annealing	65	20 sec	
Extension	72	45 sec	34
Final Extension	72	5 min	
Hold	8	Infinite	

Table 7: PCR Setup for K320E-Twinkle

Step	Temperature	Time	No. of cycles
Lid Temp	95		
Initial Denaturation	94	3 min	
Denaturation	94	30 sec	
Annealing	56	45 sec	
Extension	72	1m 30 sec	44
Final Extension	72	5 min	
Hold	8	Infinite	

Table 8: PCR Setup for mitoTIMER

Step	Temperature	Time	No. of cycles
Lid Temp	95		
Initial Denaturation	95	5 min	
Denaturation	95	30 sec	
Annealing	58	30 sec	
Extension	72	30 sec	35
Final Extension	72	10 min	
Hold	8	Infinite	

Amplified PCR products were resolved on a 2% agarose gel (stained with 0.8µg/ml EtBr), in TAE Buffer (40mM Tris base, 20mM Acetic Acid, 1mM EDTA, pH 8), and visualized under UV transillumination and imaged using a Gel documentation system (Gel Logic 200 Imaging System, Kodak). Positive controls were always used to confirm the genotype. All mice used were genotyped twice, once after they were weaned, and once after use in an experiment.

2.4 Regeneration Experiments

K320E expression, through activation of the Pax7-Cre^{ERT} promoter, was induced in the muscle satellite cells of K320E-Twinkle MuSCs mice when they were 3 to 4 months old. Activation was done by daily injections of 750 mg/kg Tamoxifen intraperitoneally, for 5

consecutive days. Two days after the last tamoxifen treatment, mice were anesthetized with 0.1ml/10g of Ketamine and Xylazine solution. Once the mice had reached surgical tolerance, their right leg was shaved and 50µl (10µM in 0.9% NaCl) of cardiotoxin (CTX) from *Nasa mossambica mossambica* (C9759, Sigma,) was injected into the tibialis anterior (TA) muscle, using a 29-gauge needle. Mice were sacrificed 1 week, 4 weeks and 8 weeks post CTX injury.

2.5 Histological Analysis

2.5.1 Sample Collection and Preservation

2.5.1.1 Fresh frozen samples

Animals were sacrificed by cervical dislocation. The Tibialis anterior (TA) muscle and the soleus (Sol) muscle, were dissected, rapidly isolated from the hind limbs, mounted on cork with OCT and snap frozen in isopentane, pre-chilled in liquid nitrogen. The snap frozen muscles were stored at -80°C until use. For all further staining protocols, muscles were cut into 10µm sections using a cryostat which was maintained at -20°C. These sections were transferred to special charged slides (SuperfrostPlus™ Gold Adhesion Microscope Slides, Epredia) which were stored in slide boxes at -80°C until further use.

2.5.1.2 Fixed samples

For histological analyses of tissues from mitoTIMER animals, mice were previously fixed by intra-cardial perfusion. In such cases, mice were anesthetized with 0.1ml/10g of Ketamine and Xylazine solution. Once mice reached surgical tolerance, they were fixed on a special dissection board made with Styrofoam and covered with aluminium foil. Mice were gently cut open from the abdomen, upwards towards the chest cavity to expose the heart. A blunt scalp vein set with an 18-gauge cannula was inserted into the left ventricle of the heart, followed by a cut in the right atrium to ensure venous drainage. Mice were

perfused with 1X PBS for 2 minutes, using a gravitational flow perfusion apparatus, followed by 4% PFA/PBS for 15 minutes.

After perfusion, the TA and soleus muscle were collected and placed in properly labelled microcentrifuge tubes containing pre-cooled 4% PFA. The tissues were stored in 4% PFA at 4°C for 24-48 hours. Tissues were then cryo-protected by placing them in successive gradient of 15% Sucrose solution in PBS at 4°C (with gentle nutation) for 6 hours, then transferred to a 30% sucrose solution in PBS at 4°C (with gentle nutation), overnight. Finally, tissue was frozen on dry ice in labelled cryo-moulds containing OCT Compound (Tissue-Tek**,** Sakura). Tissues were cut into 10um sections, in the dark, to avoid photo bleaching.

2.5.2 Haematoxylin and Eosin (H & E) Staining

H & E staining was performed on both frozen sections. Slides with 10µm thick sections were first air dried at RT for 10 minutes, stained with Mayer's Haematoxylin (Carl Roth) for 3 minutes, washed in tap water for 1 minute, and finally washed under running tap water for 10 minutes. Following this, the sections were stained with Eosin Y (Carl Roth) solution, containing 0.01% HCl for 2 minutes, washed in MQ water for 2 minutes, dehydrated in ascending concentrations of ethanol for 1 min each (50%, 70%, 96% and 100%), and cleared twice in xylene, 2 minutes each. The sections were mounted in Entellan (Sigma Aldrich) and left to dry overnight under the fume food before being imaged on the NanoZoomer S360 Digital slide scanner (Hamamatsu).

2.5.3 Cytochrome c oxidase (COX) and Succinate dehydrogenase (SDH) histochemical staining/analysis

COX/SDH histochemical analysis was performed in order to assess the functional integrity of the respiratory chain complexes of the OXPHOS pathway. fresh frozen sections were air dried at RT for 10 minutes, then circled with ROTI® Liquid Barrier Marker (Carl Roth)incubated in COX reactive solution (20mg/ml catalase, 0.07% sucrose

(Sigma), 0.02% cytochrome c (reduced form, Sigma) and 0.01% DAB tetra hydrochloride (Sigma) in 50mM Na_2HPO_4, final pH 7.4) for 20 minutes at 37°C. Samples were then washed in 1X PBS (Gibco) for 2 minutes and incubated in SDH reactive solution (0.2% w/v NBT (Sigma), 0.2M sodium succinate, 50mM MgCl2, 50mM Tris-HCl in 1X PBS, final pH 7.4) for 40-60 minutes, at 37°C, in the dark, following a final wash with MQ water twice, 2 minutes each. The sections were then mounted in pre-warmed glycerol-gelatine (Sigma), in a 65°C oven, for 5 minutes. All sections were imaged within 2-3 hours of staining, on the NanoZoomer S360 Digital slide scanner (Hamamatsu).

2.5.4 Fibre Type Staining – Immunofluorescence

In order to assess the fibre type composition of muscle sections, 10µm thick frozen sections were collected from the muscle mid-belly and stained with MyHC (myosin Heavy chain) fluorescence. The frozen sections were air dried for 10 minutes at RT, circled with ROTI® Liquid Barrier Marker (Carl Roth), fixed in 4% PFA for 30 minutes, RT, and washed thrice in 1X PBS, 2-3 minutes per wash. Samples were incubated with 0.1M glycine (in 1X PBS), to reduce cross-reactivity of antibodies with PFA, washed twice in 1X PBS for 2-3 minutes, and blocked in blocking buffer (5% NGS, 1% BSA, and 0.3% TritonX-100 in PBS) for 1 hour at RT. The sections were incubated in three primary antibodies: anti-MyHC-I (BA-D5s, Ms-IgG2b, 1:100 dilution, DHSB), anti-MyHC-IIA (SC-71s, Ms-IgG, 1:100 dilution, DHSB) and anti-MyHC-IIB (BF-3-s, Ms-IgM, 1:100 dilution, DHSB) overnight, at 4°C. After washing the sections thrice in 1X PBS, 10 minutes per wash, samples were incubated in three secondary antibodies: goat anti-mouse IgG1 conjugated with Alexa 647 fluorophore (1:500 dilution, Invitrogen), rabbit anti-mouse IgG2b conjugated with Alexa 488 fluorophore (1:500 dilution, Invitrogen), and goat anti-mouse IgM conjugated with Alexa 546 fluorophore (1:500 dilution, Invitrogen). Sections were finally mounted in Fluoromount G + DAPI (Invitrogen), after being washed thrice in 1X PBS, 5 minutes each time. Primary and secondary antibodies were diluted in the above-mentioned blocking buffer. Mounted sections were left to air dry overnight (in the dark) at RT, then stored at 4°C in slide boxes, till they were imaged with the EVOS Fl Auto 2 Imaging System (Thermo Fischer Scientific).

2.5.5 F4/80 Immunofluorescence

In order to assess inflammatory phenotype after muscle regeneration, sections were stained with F4/80 to check macrophage infiltration. 10µm thick frozen sections were collected from the regenerated region of the TA muscle, air dried for 10 minutes at RT, circled with ROTI® Liquid Barrier Marker (Carl Roth), and fixed with 4% PFA for 30 minutes. After three washes, 2-3 minutes each, with 1X PBS, samples were incubated in 0.1M glycine (in 1X PBS), followed by three more washes of 2-3 minutes each with 1X PBS. Sections were blocked for 1 hour at RT in blocking buffer (5% NGS, 1% BSA, and 0.3% TritonX-100 in 1X PBS), and incubated overnight in primary antibody anti F4/80 (1:500, Proteintech,), at 4°C. The following day, after three washes with 1X PBS, sections were incubated in the secondary antibody: goat anti-rabbit conjugated with Alexa 647 fluorophore (1:1000 dilution, Invitrogen) and mounted in Fluoromount + DAPI. Both primary and secondary antibodies were diluted in the blocking buffer. Sections were left to dry overnight, and stored at 4°C, till they were imaged with the EVOS Fl Auto 2 Imaging System (Thermo Fischer Scientific).

2.6 DNA Isolation from cells and Tissues

Total genomic DNA (gDNA) was isolated from both cells and from tissues, using the DNeasy Blood and Tissue Kit (69504, Qiagen), following the manufacturer's instructions. For samples that were to be used for molecular biology analysis, such as isolation of DNA, RNA or protein, muscles were rapidly isolated, placed in properly labelled microcentrifuge tubes, flash frozen in liquid nitrogen and stored at -80°C until further use. Briefly, tissues were first minced, lysed in the tissue lysis buffer and digested with Proteinase K, overnight at 56°C. For cells, lysis was done in lysis buffer with Proteinase K digestion, for 10 minutes at 56°C. Following this, lysed solution was applied to a spin column which binds gDNA, and the remaining contents of the solution were washed away. After two washing steps, the DNA was finally eluted with either elution buffer or with nuclease free water. The volume of the elution buffer was adjusted depending on

the initial amount of cells or tissues that was taken, with lower volume resulting in higher yields and vice-versa. DNA concentration was determined, and DNA purity was assessed by measuring the optical density at 260nm and 280nm, using an Epoch™ Microplate Spectrophotometer (BioTek). DNA was then used to check mtDNA deletions and depletion using a long-range PCR and qPCR for mtDNA copy number respectively.

2.7 Analysis of mtDNA alterations by Long Range PCR (LR PCR)

In order to screen for the presence of deletions or alterations in mtDNA, long range PCR was performed on DNA isolated from skeletal muscle tissues and MuSCs. DNA was isolated as described in section 4.6. 75 ng of DNA was amplified using the LR KIT (BR0300302, Biotech Rabbit), according to manufacturer´s instruction. Briefly, 75 ng of DNA was taken, and amplified using 0.25U/µl of LR enzyme, with the aid of 1X LR Buffer, 1X LR PCR enhancer and dNTPs (200µM final concentration). The primers for long range PCR are listed in *Table* 4. The PCR cycling conditions are described in the following table.

Table 9: PCR Setup for Long Range PCR

Step	Temperature	Time	No. of cycles
Lid Temp	110		
Initial Denaturation	95	2 min	
Denaturation	95	30 sec	
Annealing	55	30 sec	
Extension	68	14 min	35
Final Extension	68	10 min	
Hold	8	Infinite	

After PCR amplification, 20µl of the product, following addition of a glycerol-based DNA loading dye (TriTrack, Thermo Fischer Scientific), was run on a 1% agarose (Invitrogen) gel, dissolved in TAE Buffer (40mM Tris Base, 20mM acetate, 1mM EDTA, pH ~ 8.6). The gel was stained with Ethidium Bromide (0.8 ug/ml, Carl Roth), and run at 110V for 2 hours, or till the bands were well separated. Images were acquired using a transilluminator, and Gel documentation system (Gel Logic 200 Imaging System, Kodak).

2.8 Analysis of mtDNA copy number by delta CT method using Real Time-PCR

To screen for mtDNA depletion, mtDNA copy number was determined using Real Time PCR /qPCR with 20ng of total DNA per reaction. Analysis was done by thresholding the amplification differences between mtDNA and nuclear DNA, using the delta CT method. Primers specific for mtDNA and nuclear DNA, listed in *Table* 4, were used.

2.9 RNA Isolation, cDNA synthesis and RT-PCR

Total RNA was isolated either from cells or from tissues, using TRIzol® reagent (Ambion, Life Technologies), according to manufacturer's instruction. In case of tissues, an additional step was required, wherein the tissue was homogenized in TRIzol® reagent, using a 1ml glass homogenizer. Cells were directly collected in TRIzol® and lysed by gentle pipetting. 1-Bromo-3-Chloro Propane was used for phase separation. The RNA, present in the upper phase of the tri-phasic solution was precipitated using Isopropanol, followed by washing steps using 75% Ethanol in Diethly Pyrocarbonate (DEPC) water to remove unwanted salts. Reconstitution of the RNA pellet was done in warmed nuclease-free water, with the volume of water used depending on the size of the RNA pellet. RNA concentration was determined, and RNA purity was assessed by measuring the optical density at 260nm and 280nm, using an Epoch™ Microplate Spectrophotometer (BioTek).

cDNA was synthesized from 1µg of RNA using the RevertAid First Strand cDNA synthesis kit (K1622, Thermo Fischer,), following the manufacturer's instructions. The synthesized cDNA was diluted in a 1:10 ratio in nuclease-free water before being used for RT-qPCR, which was carried out in a Quant Studio 1 (Applied Biosystems) PCR cycler. RT-qPCR was performed using PowerUp™ SYBR™ Green Master Mix (Applied Biosystems), and mRNA amplification was measured using the delta-delta Ct method (Livak & Schmittgen, 2001), with specific primers for our genes of interest.

Table 10: List of Primers for qPCR

Gene	Forward Primer (5’ – 3’)	Reverse Primer (5’- 3’)
Pgc1α	AAGTGTGGAACTCTCTGGAACTG	GGGTTATCTTGGTTGGCTTTATG
MyoD1	CGCTCCAACTGCTCTGATGGCA	TGCTGCTGCAGTCGATCTCTCA
Myogenin	AAGCGCAGGCTCAAGAAAGT	TTTCGTCTGGGAAGGCAACA
Pax7	TGGAAGTGTCCACCCCTCTTGGC	ATCCAGACGGTTCCCTTTGTCGCC
Il1b	GCAACTGTTCCTGAACTCAACT	ATCTTTTGGGGTCCGTCAACT
Ifn β	CCCTATGGAGATGACGGAGA	CCCAGTGCTGGAGAAATTGT
Il6	GCCCACCAAGAACGATAGTCA	CAAGAAGGCAACTGGATGGAA
Gapdh	AGGTCGGTGTGAACGGATTTG	TGTAGACCATGTAGTTGAGGTCA

The cycling conditions for a standard PCR are shown below.

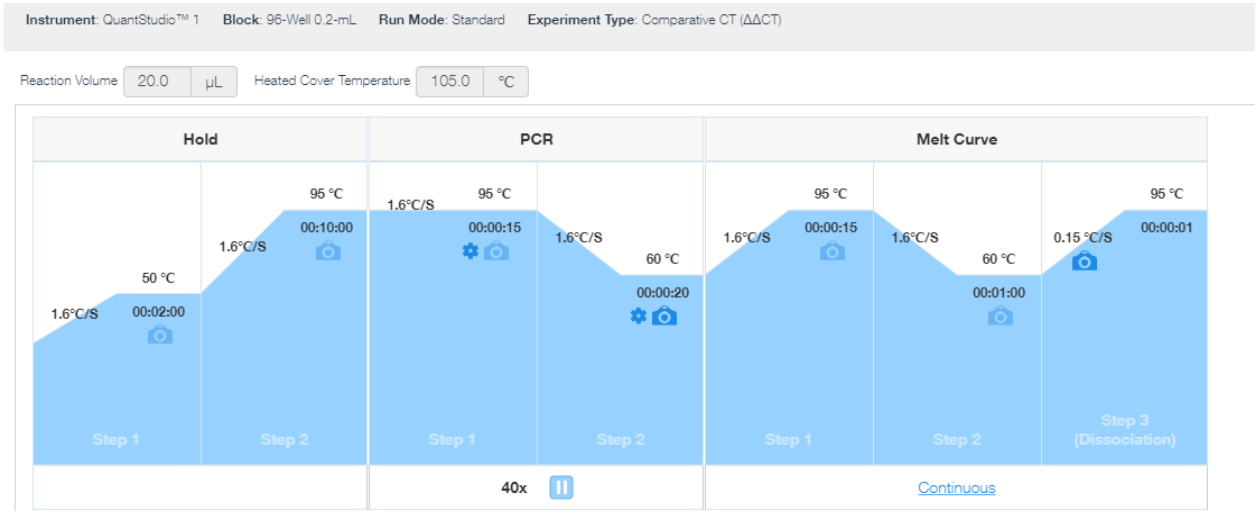

2.10 Protein Isolation and Western Blot Analysis

Proteins were isolated either from cells or from tissues, using RIPA Buffer (150mM NaCl, 1% TritonX-100, 0.5% Sodium deoxycholate, 0.1% SDS, 50mM Tris-HCL (pH 8) in MilliQ water) supplemented with protease inhibitors (Roche). In case of tissues, they were first homogenized using either a 1ml glass homogenizer for larger tissue such as the TA muscle, or a small plastic homogenizer for smaller tissues such as the EDL muscle or the Soleus muscle. Cells were directly suspended in RIPA buffer. After 30 minutes of lysis in RIPA buffer, on ice, with constant vortexing in between, the solution was

centrifuged at 12,000g for 15 minutes. The supernatant was collected, and protein concentration was estimated by Bradford's Assay using a Bovine Serum Albumin (BSA) standard curve, and measuring absorbance at 600 nm using a spectrophotometer (Eppendorf).

First, the proteins were separated using an SDS-PAGE, with a 4.5 % stacking gel, and 10 or 12% resolving gel.

Table 11: Gel composition for SDS PAGE

Resolving Gel – Recipe for 2 gels			**Stacking Gel** - Recipe for 2 gels	
	10%	**12%**		**4.5%**
dH_2O	6.87ml	6.06ml	**dH_2O**	3.5ml
37% Bis Acrylamide	4.05ml	4.86ml	**37% Bis Acrylamide**	1ml
1.5M Tris (pH8.8)	3.75ml	3.75ml	**1.5M Tris (pH6.8)**	1.5ml
10% SDS	150µl	150µl	**10% SDS**	60µl
10% APS	150µl	150µl	**10% APS**	60µl
TEMED	15µl	15µl	**TEMED**	6µl

For the SDS PAGE, 20-30µg of protein samples were prepared together with a 5X Laemmli Buffer (0.3M Tris-HCl pH 6.5, 10% SDS, 30% Glycerol solution, 5% ß-Mercaptoethanol and 0.05% Bromophenol Blue). Most samples were denatured for 10 minutes at 95°C, (except those against which OXPHOS antibodies were to be used), before being loaded onto the SDS-PAGE, with PageRulerTM Prestained as a protein ladder (Thermo Scientific, 26619). Samples were run in 1X running buffer (25mM Tris, 192mM glycine, 0.1% SDS, pH 8.3) at a constant voltage of 100V, for about 2 hours, or till the loading front reached the end of the gel, and then transferred to a polyvinylidene difluoride (PVDF) membrane previously activated in methanol, for 1.5 – 2 hours, at a constant voltage of 100V, at 4°C, in transfer buffer (25mM Tris, 190mM Glycine, 20% Methanol), in a wet transfer apparatus (Bio-Rad). To confirm proper transfer of proteins, the membranes were stained with Ponceau S staining solution (0.1% Ponceau S (Carl Roth), 5% Acetic Acid) and imaged. Ponceau S staining was also used as a loading control, when the housekeeping gene *Gapdh* could not be used.

Following this, the membranes were quickly washed in TBST (1X Tris Buffered Saline, 0.1% Tween20) and blocked (5% Non-fat milk in TBST) for 1 hour at RT, with constant shaking. Membranes were incubated on a rotator overnight at 4°C, with the following primary antibodies: mouse anti- total OXPHOS cocktail (1:1000 dilution, Abcam), rabbit anti-V5 (1:1000 dilution, Cell Signalling Technology), chicken anti-Gapdh (1:2000 dilution, Abcam)

After washing with TBST, the membranes were incubated with the corresponding HRP-conjugated secondary antibodies: goat anti-mouse, goat anti-rabbit or goat anti-chicken (Novex, Life technologies, 1:6000 – 1:10000 dilution, in blocking solution), for an hour at RT, and washed again in TBST. To visualize the proteins, membranes were incubated in the enhanced chemiluminescence substrate Western Lighting Plus-ECL (Perkin Elmer, NEL104001EA) for a minute, and the respective protein bands were detected using the ImageQuant LAS 500 Chemiluminescence CCD Camera (GE Healthcare Life Sciences). Quantification of the relative intensity of blots was performed using ImageJ.

2.11 Isolation and culture of Muscle Satellite Cells

2.11.1 Isolation

To study proliferation and differentiation of MuSCs in vitro, 8-10 week old mice were sacrificed by cervical dislocation and the posterior hindlimb muscles (TA, GN (Gastrocnemius) and QD (Quadriceps) were collected in 1X Dulbecco's Phosphate-Buffered Saline (DPBS). Muscles were cleaned in three successive DPBS washes; tendons, fascia, hair and fat were removed and the muscles were minced into 2-4mm sized pieces. Minced muscles were digested in a gentle digestion buffer (10 mg/mL Collagenase II, 4 mg/mL Dispase and 2.5 mM $CaCl_2$ in PBS, sterile filtered), at 37°C, on a shaker for 1 hour. Muscle satellite cells were isolated using gentleMACS dissociator (Milteny Biotec), a satellite cell isolation kit (Milteny Biotec, 130-104-268) and LS

magnetic separation columns (Milteny Biotec, 130-042-401), according to the manufacturer's protocol. Briefly, after collagenase digestion, muscles were further dissociated in a MACs C-tube using a gentleMACS dissociator (program m_muscle_001). Digestion was stopped with Ham's F10 media, containing 10% FBS. After a brief centrifugation step for 3 minutes, 300g, the supernatant was filtered through a 70µm filter, which had been previously equilibrated with Ham's F-10 media, containing 10% FBS. The filtered solution was then centrifuged at 1000g for 7 minutes and the supernatant was discarded. This was followed by reconstitution of the pellet in Red Blood Cell Lysis Buffer (Milteny Biotec, 130-094-183) and another centrifugation step at 1000g for 5 minutes. The supernatant was discarded and the cell pellet was resuspended in 500µl of PEB Buffer (0.5% BSA, 2mM EDTA in PBS, pH 7.2). 25ul of satellite cell isolation kit was added to each cell pellet, incubated on ice for 30 minutes, followed by filtration through a 40µm filter, equilibrated with PEB buffer. This cell suspension was then applied to a LS Magnetic column (equilibrated with PEB buffer. After centrifugation at 1000g for 5 minutes, cells were either frozen for further use, or were cultured. All isolation steps, after sacrificing the animals, were carried out under cell culture hoods with LAF. Forceps and scissors were autoclaved, all media and reagents were filter sterilized before use.

2.11.2 Culture of MuSCs

Once the MuSCs were isolated, they were cultured in 6 well cell culture dishes (TPP), in special MuSC growth medium (40% DMEM (containing 4.5g/L Glucose + Glutamax), 40% Ham's F10 solution, 20% FBS, 2.5ng/µl bFGF, 1x chick embryo extract and 1x penicillin/streptomycin). MuSCs were maintained at 37°C, with 5% CO2. After allowing the MuSCs to grow to 60-70% confluency, expression of K320E-Twinkle was induced with 10µM 4-hydrooxytamoxifen (4-OH Tmx, Sigma,). Differentiation was initiated by replacing the high serum growth media, with low serum MuSC differentiation medium (DMEM containing 4.5g/L Glucose + Glutamax, 2% Horse Serum (HS), and 1x penicillin/streptomycin. Media was replaced every second day. MuSCs were differentiated for a maximum of 14 days. Brightfield images of various stages of differentiation were taken. MuSCs were collected at various stages, during proliferation

and following differentiation, to isolate DNA, RNA or protein for further downstream analysis

2.12 Isolation of single EDL myofibers to analyse the satellite cell niche

To observe the MuSCs in their niche, EDL myofibers were isolated following a protocol adapted from Pasut et al., 2013 and Lim et al., 2018. EDL myofibers were isolated from 12 week old mice. The mice were first sacrificed by cervical dislocation, following which the EDL was carefully collected, after first removing the TA, to allow easy isolation of the EDL muscle. The EDL muscles were placed in a 0.5% w/v Collagenase B (Roche) solution, and incubated at 37°C in a water bath, for 40-60 minutes, with very gentle shaking every 10 minutes. Digestion was stopped by transferring the muscle to a HS-coated p60 tissue culture dish containing wash media (DMEM supplemented with 1% Penicillin/streptomycin and 1mM sodium pyruvate). The muscles were first fixed in 4% PFA, washed with DPBS, and triturated with a wide-bore HS coated, flame-polished glass Pasteur pipette, under a stereo dissecting microscope using transmitted bright field illumination. Trituration of muscle was done by gently pipetting up and down against the edge of the dish, in order to loosen the individual fibres. Once the desired number of fibres had been released, a small bore HS coated, flame-polished glass pipette was used to collect individual intact muscle fibres. These fibres were stored in DPBS, in HS coated microcentrifuge tubes, at 4°C until further use. All apparatus were coated with HS to prevent myofibre attachment.

2.13 EDL Myofibre Immunofluorescence

Immunofluorescence of EDL myofibres was done to visualize the MuSCs. To do so, around 10-12 single fibres were collected per animal, and transferred to a freshly labelled HS coated microcentrifuge tube, using a small-bore HS coated, glass Pasteur pipette. The fibres were suspended in 1x PBS, permeabilized in 0.1% TritonX-100, 0.1M Glycine

in PBS for 10 minutes at RT. After blocking (5% HS, 2% BSA, 0.1% TritonX-100 in PBS), for 1 hour at RT, samples were incubated in primary antibodies mouse anti-Pax7 (1:50, DSHB) and rabbit anti-Tom20 (1:1000, Proteintech) ON at 4°C.

After washing thrice in PBS, 5 minutes per wash, fibres were incubated in secondary antibodies for an hour. Following this, they were washed again, then the fibres were transferred carefully to charged slides (SuperfrostPlus™ Gold Adhesion Microscope Slides, Epredia). Excess PBS was aspired from the slide and the myofibres were mounted in Fluoromount G + DAPI. Slides were allowed to dry overnight at RT, before being imaged. Whole fibre images were captured using the navigation setting on the confocal microscope, Stellaris 5 (Leica).

2.14 Generation and culture of C2C12 cells

C2C12 cells were purchased from American Type Culture Collection (ATTC). Cells were maintained in C2C12 growth media, composed of DMEM 4.5g/L Glucose + GlutaMax, supplemented with 20% FBS, 1X Penicillin/Streptomycin and 1x Plasmocin. Cells were passaged on reaching a maximum of 70% confluency. To initiate differentiation, at almost 100% confluency, C2C12 cells were shifted from high serum media to a low serum differentiation medium (DMEM 4.5g/L Glucose + GlutaMax, supplemented with 2% HS, 1µM Insulin, 1x Penicillin/Streptomycin, and 1x Plasmocin), and the media was replaced every 48 hours. Cells were maintained at 37°C, in a humidified incubator with 5% CO_2, during both growth and differentiation. Cells were either collected during proliferation or after differentiation for 8, 16 and 28 days, to isolate DNA, RNA or protein.

2.15 Generation of C2C12 cells expressing WT and K320E Twinkle Apex

C2C12 cell lines expressing the WT or the mutated version of Twinkle (K320E Twinkle), were generated by stable pBABE-Puro retroviral transduction. Briefly, 2.5 million HEK293 cells were seeded on a P100 tissue culture dish. On reaching 70-80% confluency, these cells were transfected with pCL-ECO (10µg) and pBABE-Puro (10µg, WT Twinkle or K320E Twinkle) plasmids, in reduced serum media (OptiMEM), using Polyethylenimine (PEI) for transfection. Media was changed after 24 hours, and 48 hours after transfection media containing viruses was harvested and filtered through a sterile 0.45µm filter, then supplemented with Polybrene at a final concentration of 10 µg/ml. Media containing virus was added to C2C12 cells seeded in T-25 tissue culture flasks. Positive clones were selected 48 hours post transduction, by addition of Puromycin (2.5µg/ml final concentration) to the C2C12 growth media. Following selection, cell lines expressing the pBABE-Puro vectors, continued to be maintained in Puromycin.

2.16 Immunofluorescence in C2C12 cells

In order to assess the mitochondrial morphology upon differentiation, C2C12 cells, were grown on 6 well tissue culture dishes, each well containing 3 sterile coverslips. On reaching 80-90% confluency, cells were differentiated in low serum C2C12 differentiation medium (See section 4.15), for 8 days. They were then fixed in 4% PFA in DPBS for 15 minutes, washed thrice and stored in PBS at 4°C till further use. For immunofluorescence, one coverslip was taken per replicate, and placed on labelled parafilm, in a humidified chamber. Cells were first permeabilized in PBS (+0.02% TritonX-100) for 20 minutes at room temperature, and blocked (5% fat-free milk powder, 10% FBS, 1% BSA and 0.1% Triton-X100 in PBS) for one hour. Incubation with primary antibodies: rabbit anti-Tom20 (1:1000, Proteintech) and mouse anti-dsDNA (1:1000, Abcam) was performed overnight at 4°C. Cells were washed thrice in PBS, incubated with secondary antibodies: goat anti-rabbit Alexa 555 (1:1000, Invitrogen) and goat anti-mouse Alexa 488 (1:1000, Invitrogen), for 1 hour, and again washed thrice in PBS. Finally, the coverslips were mounted on glass microscope slides, with Fluoromount + DAPI, and allowed to air dry, before imaging. Imaging was performed using the SP8 (Leica) Confocal Microscope.

2.17 APEX2 Proximity Biotinylation and Mass Spectrometry

C2C12 cells were transduced with either Twinkle-APEX2-V5, K320E-APEX2-V5, and mitochondrial matrix targeted APEX2-V5 (mitoAPEX2), and were used for proximity biotinylation. The transgenic cells were labelled with biotin-phenol, by incubating with 2.5mM biotin-phenol for 7 hours. For cross-linking, cells were incubated shortly in 1mM H202, for 1 minute at RT. The reaction was quenched by washing four times with wash buffer (1 mM sodium azide, 1 mM sodium ascorbate, and 5 mM Trolox in PBS). The cells were then recovered and solubilized in RIPA buffer, for protein isolation. The biotinylation reaction was verified by SDS-PAGE using Streptavidin-HRP (1:2000, Merck), following which the samples were analysed by mass spectrometry (MS).

APEX2-induced crosslinked proteins were purified using streptavidin-magnetic beads. For MS analysis, 500 µg of total protein extracts containing biotinylated proteins were used. First, the samples were washed thrice with RIPA buffer, followed by three washed with ABC buffer. Then, they were denatured with 50 µl of urea buffer (6M urea, 2M thiourea), followed by disulphide-bridge reduction using dithiothreitol (DTT), at a final concentration of 5mM, for 1 hour at RT. Samples were then incubated in 2-Iodoacetamide, at a final concentration of 40mM, and incubated for 30 minutes in the dark, to alkylate oxidized cysteines. To this, Lys-C was added in a ratio of 1:100 (i.e. 0.1 µg enzyme for 10µg protein) and incubated for 2-3 hours. Finally, samples were diluted with ABC buffer, to reach 2M urea concentration. Proteins were digested overnight with trypsin 1:100. Samples were acidified with 1% formic acid and desalted using a modified version of the Stop and Go extraction tip (StageTip) protocol. Proximity biotinylation and MS analysis was performed in collaboration with Prof. Dr. David Pla-Martín and Dr. Sebastian Kallabis.

2.18 Measurement of respiration using Oroboros in intact cells

Respirometry measurements were performed on proliferating C2C12 cells, as well as on differentiated C2C12 cells using Oroboros O2k.Respirometer. For proliferating C2C12

cells, around 1 million cells were seeded on a p100 tissue culture dish, at least 2 days prior to measurements. For differentiated cells, cells were differentiated at 89-90% confluency, in p60 dishes, for 7 days prior to measurements. For the measurement, the Oroboros chambers were first calibrated in the media in which C2C12 cells were grown or differentiated respectively. After cells were detached from the plates by trypsinzation, cell number and viability was assayed using Trypan Blue, with an automatic cell counter EVE (NanoEntek). Cells were resuspended at a final concentration of 500,000 cells per ml, ensuring a total amount of 1million cells per Oroboros chamber.

Following the addition of cells to the respective Oroboros chamber, basal (routine) respiration was measured for at least 15 minutes. Oligomycin independent respiration, or leak respiration was achieved by the addition of Oligomycin at a final concentration of 2µg/ml, since oligomycin inhibits ATP synthase (State 4). Uncoupling of oxidative phosphorylation was achieved by stepwise titration with CCCP (5mM final concentration). This gave readings for maximal respiration. Finally, residual oxygen consumption (ROX) was measured after addition of rotenone (1µg/ml final concentration). The final oxygen consumption rates were depicted as O2 flux per volume.

2.19 Image Analysis

All image analysis was performed on ImageJ (FIJI, NIH, Bethesda). Cross-sectional area of the muscle was analysed by using the free hand tool on ImageJ, and drawing along the perimeter of the muscle fibre. Analysis was performed on at least 5 regions of a muscle section, with each region having an area of ~120000µm^2 (260µm x 460µm). Fibre number per µm2 was calculated manually, using the cell counter plug-in in ImageJ on 3-4 regions of a section. The percentage of centrally nucleated fibres was calculated by manually counting the centrally nucleated fibres in the entire muscle, and dividing this value by the approximated total number of fibres present in the muscle section.

Analysis of red/green fluorescent ratio of mitoTIMER fluorescence was performed by imaging 5-8 random regions of the muscle through the LAS X software (Leica). All images for each channel were taken with the exact same settings. ROIs (regions of interest) were

selected, with each ROI corresponding to a single muscle fibre. The image was then split into individual channels, and the mean grey intensity was measured in each ROI for the red and green channel, from which the ratio of red/green fluorescent intensity was obtained. To analyse the number of mitophagosomes in the muscle sections expressing mitoTIMER fluorescence in the skeletal muscle, the number of red puncta per fibre was manually counted. Each red puncta, with absence of green fluorescence represents a mitophagosome, or mitochondria targeted for removal by autophagy (Laker et al., 2014a).

Analysis of mitochondrial morphology in differentiated C2C12 was carried out using the Mitochondrial Analysis Tool for FIJI using the mitoMorph plugin (Yim et al., 2020). The myogenic fusion index in the differentiated C2C12 myoblasts was calculated by determining the number of nuclei inside myotubes (that contain 2 or more nuclei), divided by the total number of nuclei present in the field of vision.

Fibre type composition and the area occupied by F4/80stained macrophages, was calculated by selecting the ROI, splitting the image into individual channels, adjusting the threshold, the measuring the area percentage occupied.

2.20 Statistical Analysis

Statistical analysis and generation of corresponding graphs was carried out using GraphPad Prism 8.0 (GraphPad Software Inc., San Diego, CA, USA). Comparisons between two groups were performed using unpaired Student's t-test. For more than 2 groups, with a single independent variable, comparison was done using one way analysis of variance (ANOVA), followed by a Tukey's post-hoc test. For comparisons between multiple groups, with two independent variables, a two-way ANOVA was performed for multiple comparisons with Sidak's post-hoc test. All data are expressed as mean ± standard error of mean. *P*-values less than 0.05 were considered to be statistically significant.

3 Results

3.1 K320E-Twinkle expression in skeletal muscle causes differential mitochondrial quality control in different muscle fibre types

Ageing is linked to a decline in mitochondrial quality control mechanisms, with increased accumulation of mtDNA mutations and mitochondrial dysfunction (Larsson, 2010; Srivastava, 2017). Likewise, dysfunctional mitochondria may play a role in skeletal muscle ageing and a consequent decline in muscle function (Chatzinikita et al., 2023; Peterson et al., 2012). To determine the effects of mtDNA mutations in K320E-Twinkle^{Skm} mice, and to visualize mitochondrial quality control in skeletal muscles *in vivo*, we used the mitoTIMER reporter system. The mitoTIMER reporter encodes a mitochondrial fluorescent protein which shifts irreversibly from green to red upon oxidation(Laker et al., 2014b). The age-dependent shift in fluorescence emission from the mitoTIMER protein thus allows estimation of mitochondrial age. Green fluorescence depicts newly synthesized mitoTIMER protein and hence, “young” mitochondria, whereas red fluorescence marks “old" mitochondria. Lower red to green ratios signify a higher mitochondrial turnover ((Cerqueira et al., 2020; Ferree et al., 2013) with reduced oxidation, thus resulting in higher numbers of new, well-functioning mitochondria. Conversely, higher ratios signify a reduced mitochondrial turnover, resulting in higher numbers of older or “oxidized” mitochondria (Cerqueira et al., 2020; Ferree et al., 2013).

To evaluate mitochondrial quality control *in vivo* in skeletal muscle in an age-dependent manner, we isolated the TA and Soleus muscles from 6, 12, and 24 months old mitoTIMER^{Skm} and mitoTIMER/K320E-Twinkle^{Skm} mice. Since the M. tibialis anterior (TA) contains mostly glycolytic fibres and the M. soleus contains mostly oxidative fibres, we chose these to obtain a comprehensive insight into mitochondrial quality control in different fibre types.

At 6 months and at 12 months, we did not observe any differences in the average red/green ratios between the control and the K320E-Twinkle^{Skm} muscle fibres (*Figure* 24A, 24B, 24D). A frequency distribution of the fluorescence ratios (*Figure* 24C, 24E) showed that although there were no significant differences in the average ratios, there was a higher frequency of control fibres with lower mitoTIMER red/green ratios, and a higher frequency of K320E-Twinkle^{Skm} fibres with high fluorescence ratios at 6 months.

Then we analysed the Soleus muscle (*Figure* 25A), and did not observe any differences in the mitoTIMER red/green fluorescence ratio at 6 and 12 months of age (*Figure* 25B, 25D). Unlike in the TA, we did not observe any differences in the frequency distribution of fluorescence ratios of the muscle fibres, at both time points (*Figure* 25C, 25E).

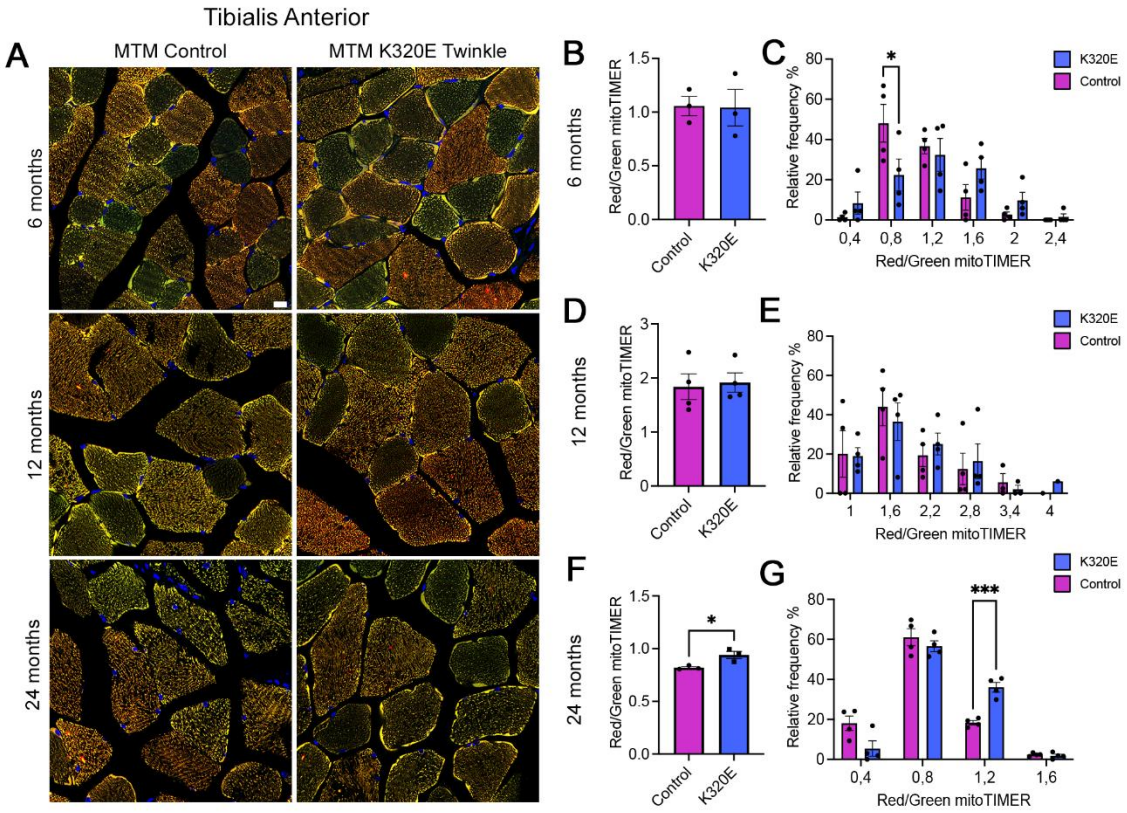

Figure 24: K320E-Twinkle expression in TA increases fibres with oxidized mitochondria (A) mitoTIMER fluorescence in TA muscle at 6, 12 and 24 months. (B, D, F) Average mitoTIMER red/green fluorescence ratio in muscle fibres of control and K320E mice at 6, 12 and 24 months. (C, E, G) Relative frequency distribution of the individual fibres with their red/green mitoTIMER ratio at 6, 12 and 24 months. Data expressed at mean +- SEM.

No of animals (n): 3-4 animals per group, 80-100 fibres per analysis. P values - * <0.05. Scale bar 10µm.

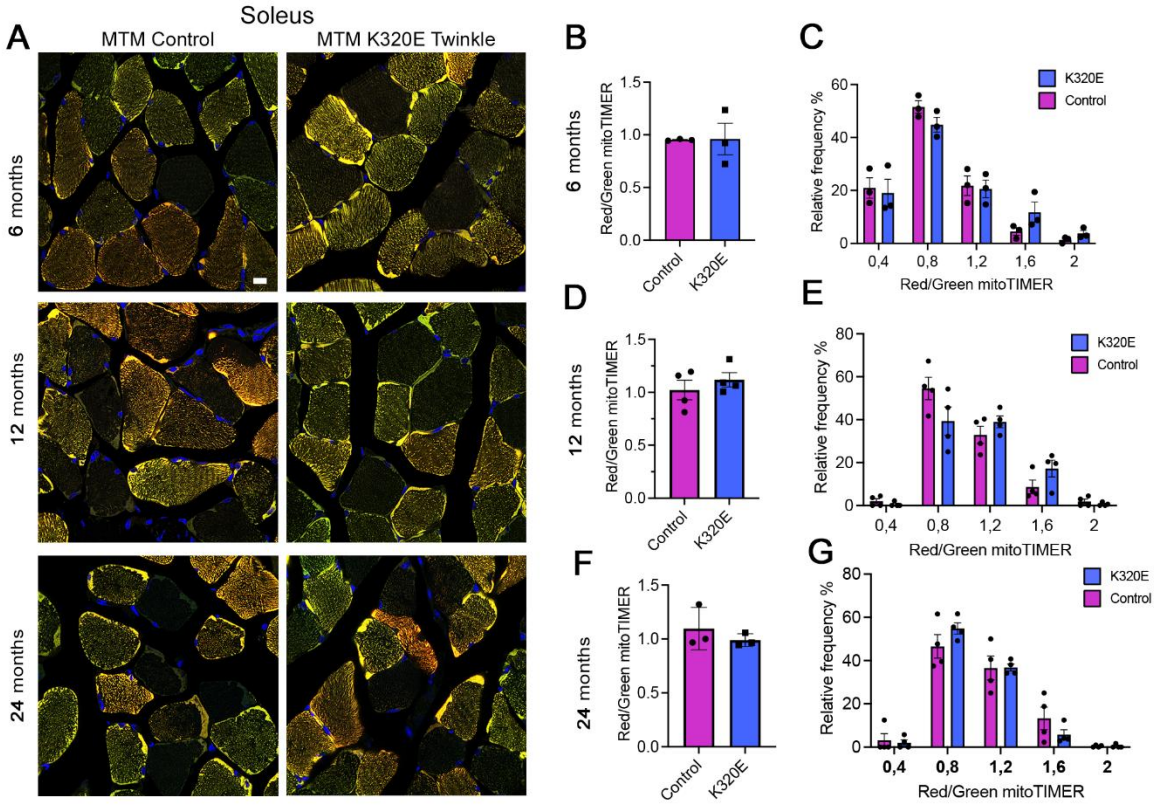

Figure 25: K320E-Twinkle expression in Soleus does not increase fibres with oxidized mitochondria. (A) mitoTIMER fluorescence in Soleus muscle at 6, 12 and 24 months. (B, D, F) Average mitoTIMER red/green fluorescence ratio in muscle fibres of control and K320E mice at 6, 12 and 24 months. (C, E, G) Relative frequency distribution of the individual fibres with their red/green mitoTIMER ratio at 6, 12 and 24 months. Data expressed as mean ± SEM. No of animals (n) / 3-4 animals per group, 80-100 fibres per analysis. Scale bar 10µm

Recently, we showed that K320E-Twinkle expression in skeletal muscle leads to mtDNA alterations and COX-deficient fibres, which are lower at 12 months compared to aged mice (Kimoloi et al., 2022). We hypothesized that mitochondrial quality control mechanisms control the accumulation of mtDNA damage. However, since ageing is linked to a decline in mitochondrial quality control and a reduced induction of autophagy (O'Leary et al., 2013; Srivastava, 2017), this might cause an increase in the accumulation of mtDNA alterations. Consequently, we tested if the expression of K320E-Twinkle reduces macroautophagy in the skeletal muscles. We monitored the autophagic flux by

measuring the conversion of the autophagy adaptor LC3-II to LC3-I. Since steady-state levels of autophagy adaptors could reflect both an increase or decrease in autophagy, we measured autophagic flux by blocking autophagy by injecting the mice with chloroquine, an inhibitor of autophagolysosome formation (*Figure* 26A). An accumulation of the lipidated form of LC3 would reflect an increase in autophagic flux, while a reduction would indicate a decrease in autophagic flux (Liebl et al., 2022). We did not observe any differences in the autophagic flux in the TA muscle expressing K320E-Twinkle (*Figure* 26B). However, in the soleus, we observed that the autophagic flux was significantly higher in the K320E-Twinkle muscles compared to the relevant controls.

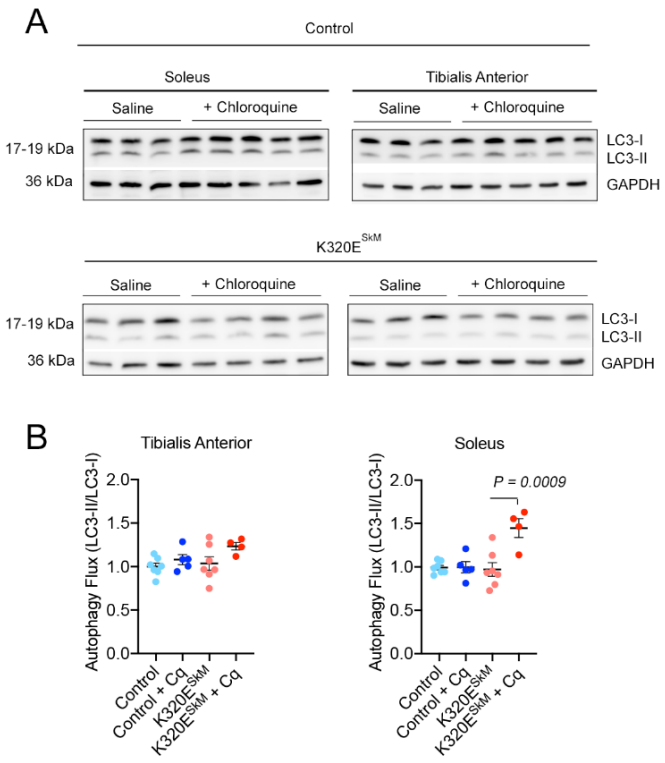

Figure 26: K320E expression causes increased autophagic flux in soleus but not in TA. (A). Western blot showing levels of LC3-I and LC3-II in control and mutant TA and Soleus, when mice are injected (i.p) with either saline or chloroquine for 4 hours prior to collection. GAPDH is the housekeeping gene. (B) Quantification of LC3-II/LC3-I from western blots, as a measure of autophagic flux. (Modified from Sen et al., 2022)

Then, we analysed the fluorescence ratios in 24-month-old animals. In accordance with the flux data, we observed a significant increase in the red/green fluorescence ratio in the TA (*Figure* 24F, 24G), but not in the case of the Soleus (*Figure* 25F, 25G).

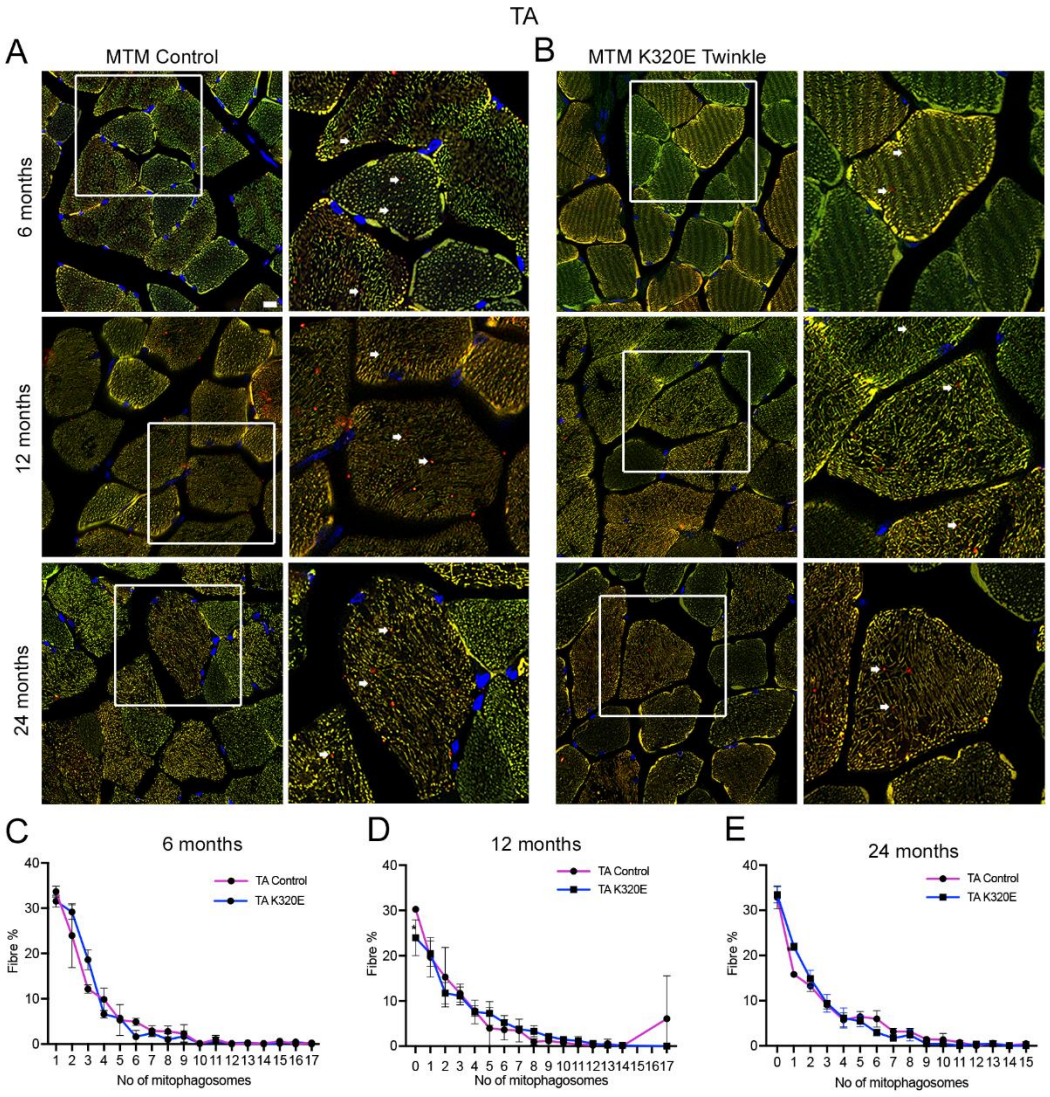

Figure 27: K320-Twinkle expression in TA does not induce classical mitophagy (A). mitoTIMER fluorescence in TA muscles at 6,12 and 24 months, inset showing single fibre cross section, with white arrowheads indicating red puncta (mitophagosomes). (B, C, D) Quantification of the percentage of fibres with the specified number of mitophagosomes in TA at 6,12 and 24 months. Data expressed as mean ± SEM. No of animals (n) / 3-4 animals per group, 80-100 fibres per analysis. P values - * <0.05, ** < 0.001. Scale bar 10μm.

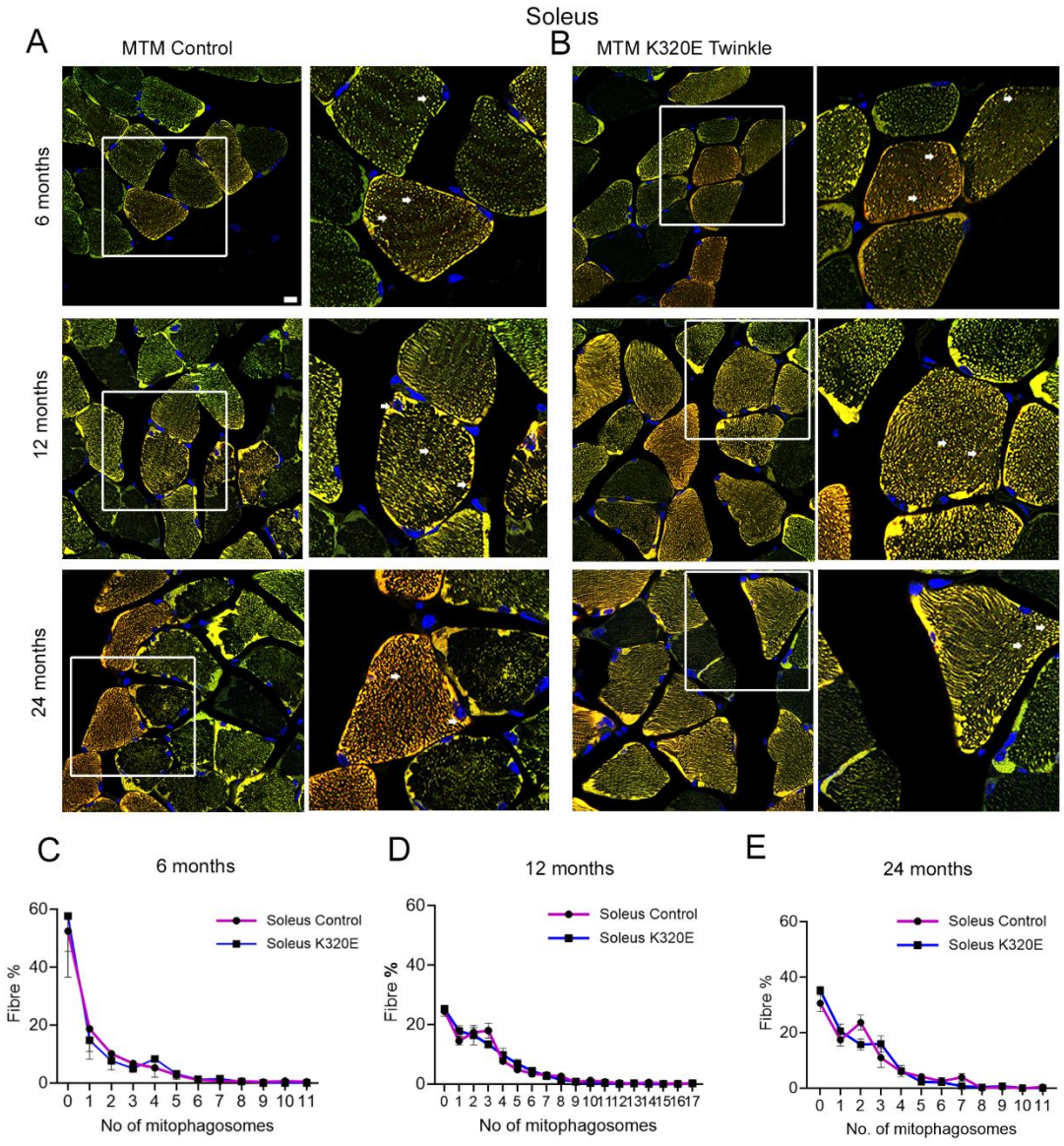

Figure 28: K320-Twinkle expression in Soleus does not induce classical mitophagy (A). mitoTIMER fluorescence in Soleus muscles at 6,12 and 24 months, inset showing single fibre cross section, with white arrowheads indicating red puncta (mitophagosomes). (B, C, D) Quantification of the percentage of fibres with the specified number of mitophagosomes in Soleus at 6,12 and 24 months. Data expressed as mean ± SEM. No of animals (n) / 3-4 animals per group, 80-100 fibres per analysis. Scale bar 10μm.

Next, we tested if the expression of K320E-Twinkle induced mitophagy. Previous reports have shown that the pure red puncta observed in the muscle fibres, with only red mitoTIMER fluorescence, are indicative of mitophagosomes, and consequently mitophagy (Laker et al., 2014). We therefore quantified the number of mitophagosomes

in the muscle fibres of control animals compared to the K320E-Twinkle^{Skm} animals. We did not observe any differences in the number of mitophagosomes between the fibres of the control and K320E-Twinkle animals, in both the TA and the soleus (*Figure 27A-E, 28A-E)*.

These results suggest that since there were no changes in the autophagic flux in the TA upon K320E-Twinkle expression, this indicates a low mitochondrial turnover, thus accumulating a higher number of “oxidized” mitochondria. Conversely, increased autophagic flux in the Soleus and increased mitochondrial turnover might allow better clearance of oxidized mitochondria, therefore preventing the accumulation of oxidized mitochondria in the muscle fibres. Taken together, we conclude that upon K320E-Twinkle expression in skeletal muscles, *in vivo* mitochondrial quality control mechanisms in the Soleus are more efficient than in the TA. Nevertheless, the fact that mitophagy is not activated in the muscle fibres expressing K320E-Twinkle, despite an increased autophagic flux in the Soleus, suggests the activation of complementary pathways besides canonical mitophagy to deal with mtDNA defects.

3.2 K320E-Twinkle expression in MuSCs simulates a fibre-type shift as observed in aged sarcopenic muscles

3.2.1 Acute muscle damage to K320E-Twinkle^{MuSC} mice impairs regeneration

Previous studies with K320E induction in mouse skeletal muscles showed the presence of mtDNA alterations only in very old mice (Kimoloi et al., 2022), with no effect on muscle mass and performance. Since we saw centrally nucleated fibres in mutant muscles, we therefore hypothesized that the detrimental effects on skeletal muscles containing mutated mtDNA molecules were alleviated by the regenerative function of MuSCs. We thus generated a new mouse model, where K320E-Twinkle is expressed specifically in the MuSCs (K320E-Twinkle^{MuSC}), under the control of a tamoxifen-inducible promoter. To induce muscle regeneration and MuSC activation, we used cardiotoxin (CTX), a drug

derived from *Nasa mossambica mossambica*, which is known to induce a reproducible acute injury, followed by synchronous regeneration (Ramadasan-Nair et al., 2014; Wang et al., 2022). Mice at 12 weeks of age, were injected with Tamoxifen for 5 days, rested for 2 days, then were subjected to CTX injury in the TA, followed by regeneration for 7 days (*Figure* 29A).

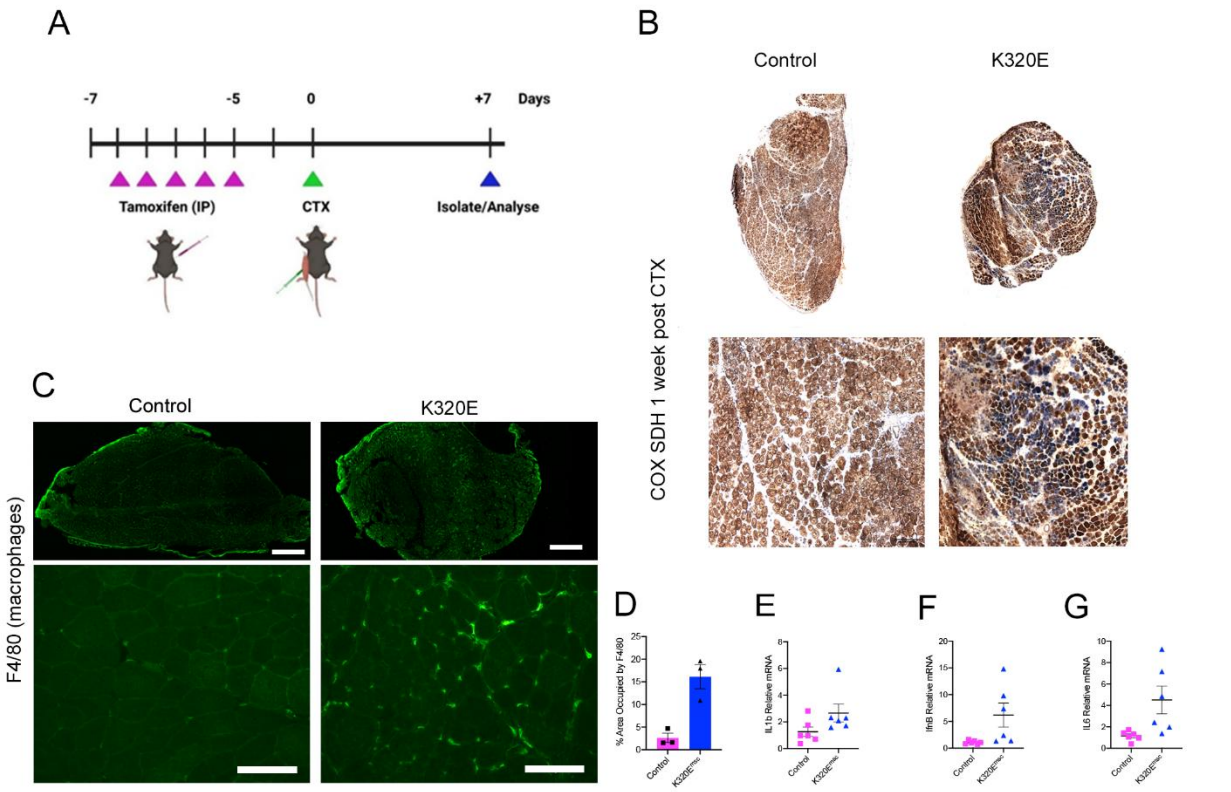

Figure 29: Acute expression of K320E-Twinkle in MuSCs causes mitochondrial dysfunction and enhanced inflammation after regeneration. (A) Schematic for K320E induction with tamoxifen injection (i.p) for 5 days, followed by CTX injection in the TA and subsequent collection of the muscle. (B) Representative images showing COX SDH histochemical analysis for mitochondrial dysfunction in regenerated TA, 1 week post CTX. (C) Representative confocal images of immunofluorescence for F4/80 (macrophage infiltration) in sections from control and K320E-Twinkle mice, 1 week post CTX, showing increased macrophage infiltration. (D) Quantification of area occupied by F4/80-stained macrophages. (E-G) qPCR analysis showing expression of proinflammatory markers interleukin 1b (*Il1b*), interferon β (*Ifnβ*) and interleukin 6 (*Il6*) in RNA isolated from TA of control and K320E muscles, 1 week post CTX (C-G modified from (Kimoloi et al., 2022). Data expressed as mean ± SEM. No of animals (n): 3 animals per group for F4/80 staining, 6 animals per group for qPCR analysis. P values - * <0.05, ** < 0.01. Scale bar 10µm.

First, we tested the effect of K320E-Twinkle expression in MuSCs on mitochondrial function in the regenerated muscle. For this, we performed a double-sequential COX/ SDH histochemical analysis, which assesses the functional integrity of the respiratory chain complexes of the OXPHOS pathway (Ross, 2011). Given that the COX reactive reagent reacts with Complex IV (CIV) activity (three mtDNA encoded subunits) and the SDH reactive reagent reacts with Complex II activity (only nucDNA encoded subunits), the presence of blue fibres (COX-) connotes impaired CIV function, thus indicating that these cells have mtDNA mutations followed by mitochondrial dysfunction. Accordingly, we analysed the TA muscle, 1-week post-CTX injection and observed the presence of a large number of blue cells in the regenerated muscle of K320E-Twinkle animals (*Figure* 29B). Hence, we confirmed that expression of K320E-Twinkle in MuSCs leads to mitochondrial dysfunction and impairs regeneration of intact fibres.

Then, we tested whether the mitochondrial dysfunction in the K320E-Twinkle expressing fibres affected an inflammatory response. We thus performed F4/80 staining and a qRT-PCR to check for the mRNA levels of inflammatory markers 1-week post-CTX damage. We observed an increased infiltration of F4/80-stained macrophages in the regenerated K320E-Twinkle^{MuSC} muscles compared to controls (*Figure* 29C, D). We also observed an upregulation of the proinflammatory markers, interferon β (*Ifnβ*) and interleukin 6 (*Il6* (*Figure* 29E-G). These data indicate enhanced inflammation upon regeneration in the case of K320E-Twinkle^{MuSC} muscle fibres.

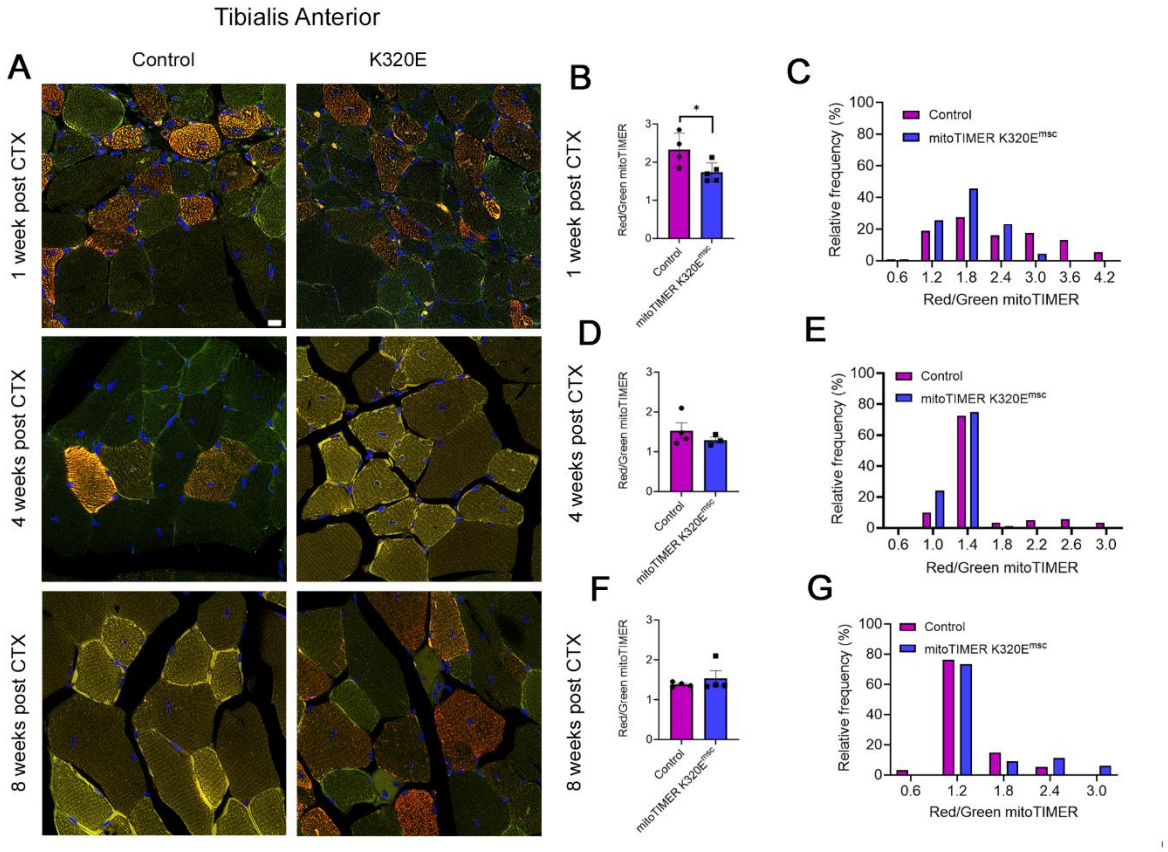

Figure 30: K320E expression in MuSCs induced in an acute manner, increases mitochondrial turnover, but is normalized later. A) Representative confocal images of mitoTIMER fluorescence in control and K320E TA isolated 1 week, 4 weeks and 8 weeks post CTX injury. (B, C, D) Quantification of average red/green mitoTIMER fluorescence ratio between control and K320E fibres at the abovementioned time points. (E, F, G) Relative frequency distribution of fibres showing the depicted red/green fluorescence ratios at the abovementioned time points. Data expressed as mean ± SEM. No of animals (n): 3-4 animals per group for mitoTIMER fluorescence analysis, 25-50 fibres per analysis. P values - * <0.05, ** < 0.01. Scale bar 10µm.

Finally, to observe quality control in MuSCs *in vivo*, upon induction of K320E-Twinkle and activation through acute CTX damage, we used the K320E-Twinkle^{MuSC} mice expressing the mitoTIMER fluorescent reporter (*Figure* 30A) and analysed red/green fluorescence intensity. Following tamoxifen induction, we collected animals 1 week, 4 weeks and 8 weeks post CTX damage. At 1-week post CTX damage, we observed a decrease in the average red/green mitoTIMER fluorescence ratio in case of the fibres expressing K320E-Twinkle compared to controls (*Figure* 30B). The frequency distribution also showed that

there was a higher percentage of mutant fibres with lower ratio compared to regenerated controls (*Figure* 30E), further confirming increased turnover in K320E-Twinkle^{MuSC} fibres. However, when the muscles were analysed 4 weeks and 8 weeks post CTX injection, the differences in red/green ratio were no longer observed (*Figure* 30C, D, F and G)).

Our data indicates that muscle damage causes mitochondrial dysfunction and increased inflammation in fibres regenerated from satellite cells expressing K320E-Twinkle^{MuSC}. This might be caused by the accumulation of mtDNA alterations during MuSC proliferation, growth and differentiation to muscle fibres (Kimoloi et al., 2022; Sen et al., 2022). Additionally, these fibres show reduced oxidation and increased turnover 1 week post CTX, indicating a compensatory mechanism. However, this was obviously lost upon subsequent muscle regeneration.

3.2.2 K320E-Twinkle expression in MuSCs, during development, impairs muscle fibre differentiation

Since the accumulation of mtDNA mutations during ageing occurs in a gradual manner, we aimed to induce mutations in muscle from MuSCs in a more physiological approach. Thus, we injected tamoxifen in nursing dams for 5 days, when the pups were 1-2 weeks old (*Figure* 31A). In this manner, tamoxifen would be passed to the pups through the mother´s milk. We reasoned that mtDNA mutations may be induced by the expression of K320E-Twinkle in MuSCs of pups, when they are highly active and proliferating to differentiate into adult muscle fibres rich in mitochondria.

3.2.2.1 K320E-Twinkle^{MuSC} muscles do not exhibit mitochondrial dysfunction during development

First, we aimed to validate our strategy for K320E-Twinkle induction. K320E-Twinkle mice were originally generated by cloning the gene containing the K320E point mutation into a ROSA-26 STOP construct, with a downstream GFP cassette (Baris et al, 2015). Accordingly, GFP expression can be used to monitor if the transgene has been activated.

Therefore, we isolated RNA from the quadriceps (QD) muscle of these animals at 3 months and 12 months post induction, and quantified the mRNA levels of GFP.

At 3 months, we observed that the GFP mRNA levels in K320E-Twinkle^{MuSC} fibres was 50 times higher than in controls (*Figure* 31B). This result confirmed the successful induction of the K320E mutation in the satellite cells. At 12 months, GFP expression was still significantly high in the K320E-Twinkle fibres, but lower than at the earlier time point (*Figure* 31B).

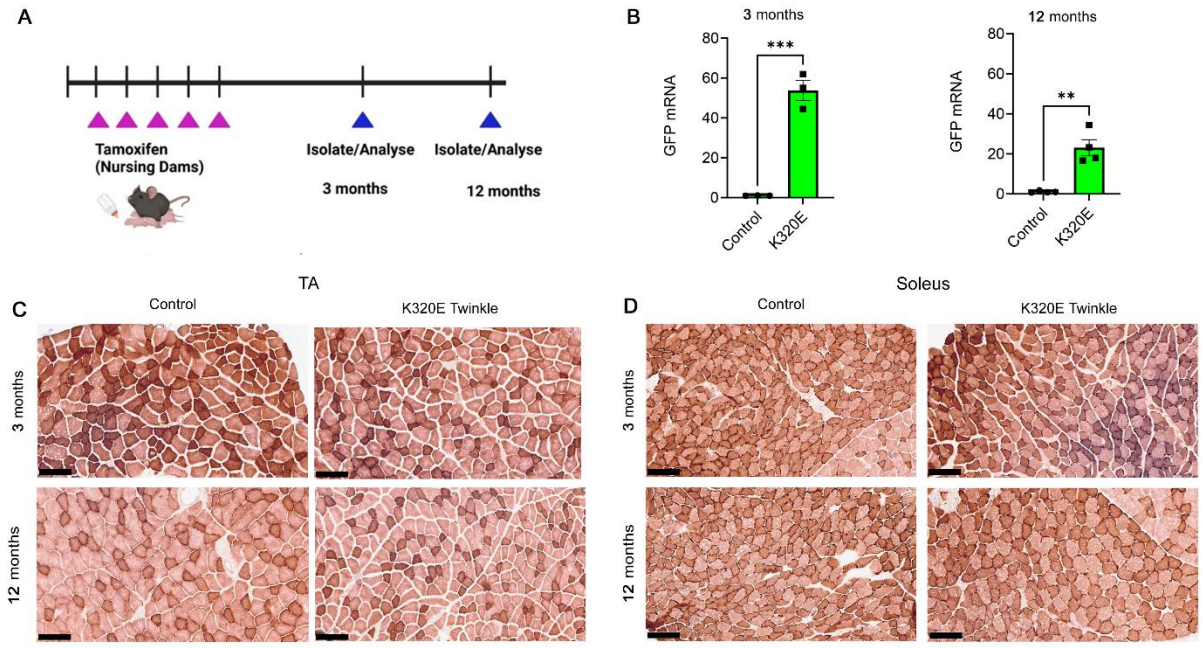

Figure 31: Expression of K320E-Twinkle in MuSCs, during development, does not cause mitochondrial dysfunction. (A) Schematic to induce K320E expression in K320E-Twinkle MUSC pups, where tamoxifen in injected for 5 days to the nursing dams. (B) qPCR analysis showing GFP expression in quadriceps muscle isolated from K320E-Twinkle animals at 12 weeks compared to control animals. Representative images showing COX SDH histochemical analysis for mitochondrial dysfunction in TA (C) and in Soleus (D) at 3 months and 12 months post induction in pups. Data expressed as mean ± SEM. No of animals (n): 3 3-4 animals per group for qPCR analysis and for COX SDH. P values - * <0.05, ** < 0.01, ***< 0.001. Scale bar 100µm.

Next, we aimed to determine if K320E-Twinkle expression, with this approach, also induced mitochondrial dysfunction, as observed when K320E-Twinkle was induced after

acute muscle regeneration (Figure 31B; Kimoloi et al., 2022; Sen et al 2022). Therefore, we performed a COX/SDH histochemical staining and analysed the TA and Soleus muscles, collected at 3 months and at 12 months post-induction. In the TA, we did not observe any blue COX-deficient fibres at 3 months, nor at 12 months (*Figure* 31C). Similarly, the Soleus muscle also did not exhibit any COX-deficient fibres at both 3 months and 12 months (*Figure* 31D).

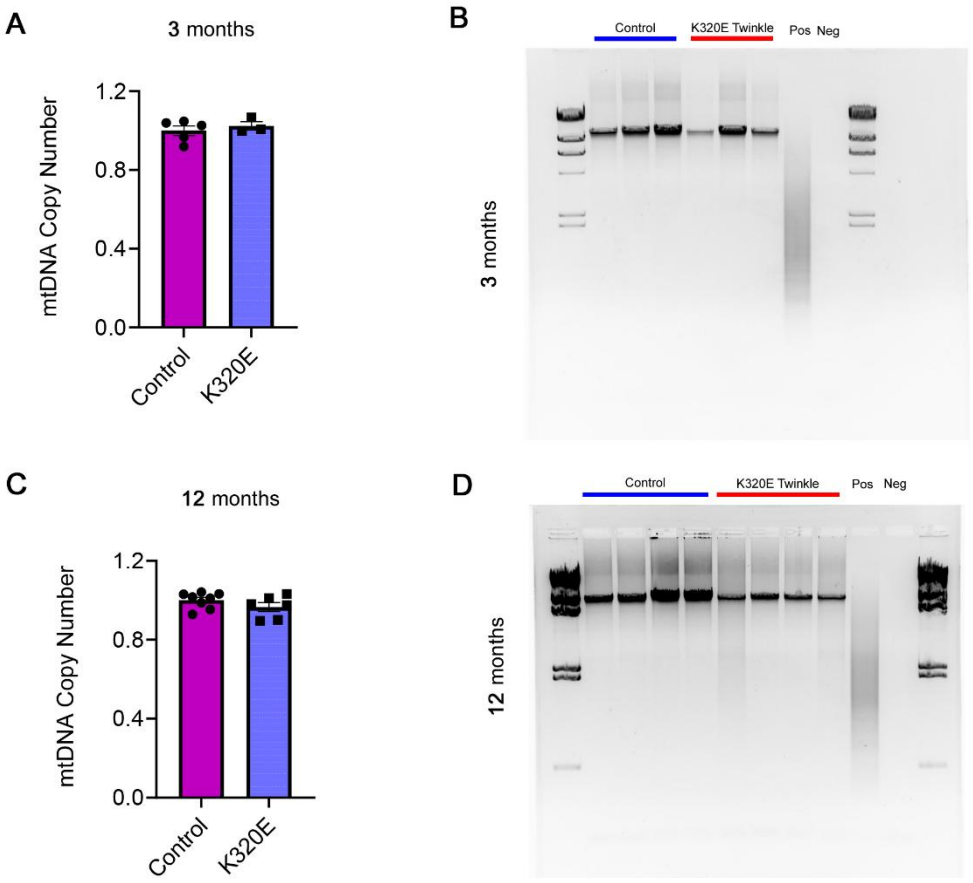

Figure 32: Physiologically induced expression of K320E-Twinkle in MuSCs does not cause accumulation of mtDNA alterations or mtDNA depletion in MuSCs. mtDNA copy number quantification by qPCR in control and K320E MuSCs at 3 months (A) and at 12 months (B). Long range PCR to detect the presence of mtDNA alterations in MuSCs at 3 months (C) and at 12 months (D). Data expressed as mean ± SEM. No of animals (n): 3-4 animals per group at 3 months, and 6-8 animals per group at 12months.

Finally, we determined the effect of K320E-Twinkle expression on mtDNA mutagenesis in MuSCs. First, we isolated MuSCs from the mice at 3 months and at 12 months post

induction via mother's milk. Analysis of the mtDNA copy number by qPCR showed no differences between the control and the K320E-Twinkle^{MuSC} MuSCs at both 3 months and at 12 months (*Figure* 32A-B). Next, we performed a long-range PCR to analyse mtDNA alterations, however, we did not find any large rearrangements of the mtDNA, at both 3 months and at 12 months (*Figure* 32C-D).

Therefore, expression of K320E-Twinkle in MuSCs did not lead to accumulation of mtDNA alterations or cause mtDNA depletion in these MuSCs, nor did it generate COX-deficient fibres in the muscles coming from these cells during normal development. All together, these data indicate that K320E-Twinkle expression in MuSCs, when induced during development, is not sufficient to cause mitochondrial dysfunction.

3.2.2.2 K320E-Twinkle expression in MuSCs, during development, does not influence MuSC numbers in the niche

The stem cell niche is a heavily regulated environment and alterations to it can affect MuSCs and its regenerative capacity. Thus, we aimed to visualize and count satellite cell numbers in their niche. For this, we utilized muscle fibres from the M. extensor digitorum longus (EDL), a well-established protocol to study MuSCs in their niche. To quantify if the expression of K320-Twinkle alters the MuSC numbers and distribution in the muscle fibres, we isolated the EDL myofibres from 12-week-old mice, and performed immunofluorescence staining for Pax7 (in red) and used aTOMM20 antibody for mitochondria (in green) (*Figure* 33A). We also imaged the fibres with transillumination to be able to visualize the satellite cells residing on the muscle fibres (*Figure* 33B).

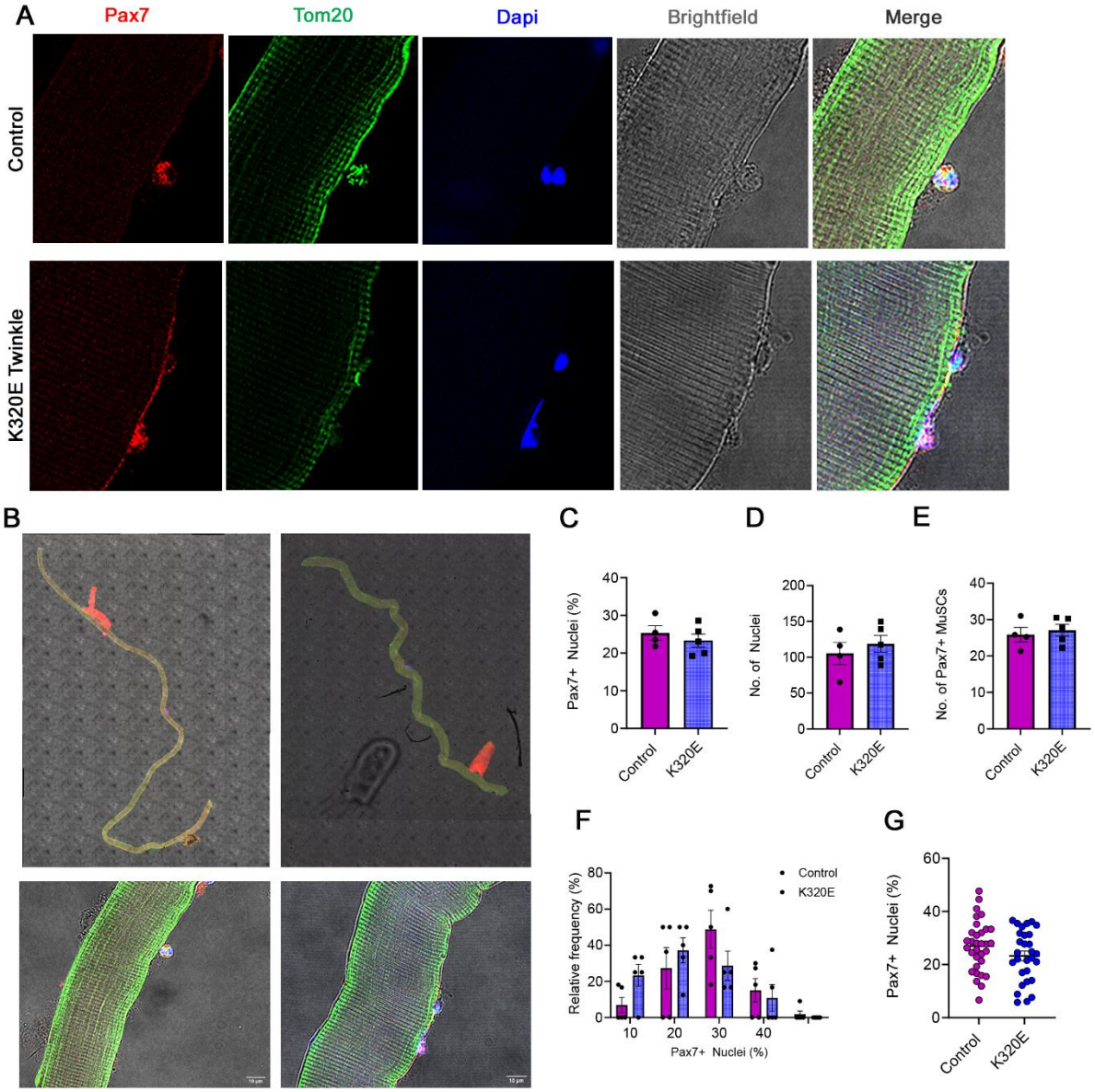

Figure 33: Expression of K320E-Twinkle in MuSCs, during development, does not affect MuSC numbers in the MuSC niche. (A) Representative images of individual channels and merged images of EDL myofibres from control and K320E animals collected at 12 weeks. MuSCs (Pax7) shown in red, mitochondria (Tom 20) shown in green, nucleus (DAPI) shown in blue, along with a brightfield image of the fibre. (B) Representative image of the complete myofibre and MuSCs. Quantification of the number of Pax7 + Dapi stained nuclei (C), total number of DAPI+ Nuclei, and total number of Pax7+ MuSCs per fibre (E). Relative frequency distribution of the percentage of Control and K320E fibres with the depicted number of Pax7+ Dapi nuclei. Data expressed as mean ± SEM. No of animals (n): 3-6 animals per group, 6-11 fibres per animal.

Quantification of the number of Pax7+/DAPI-stained nuclei, indicating MuSCs, revealed no differences between the control and the K320E-Twinkle^{MuSC} fibres (*Figure* 33C-G). Quantification of the number of nuclei, and the number of satellite cells alone also did not reveal any differences either (*Figure* 33D-E). Therefore, the expression of K320E-Twinkle during development, does not affect MuSC numbers within their niche.

3.2.2.3 K320E-Twinkle$^{MuSC(physiological)}$ exhibit change in fibre type composition

To observe the muscle architecture of the fibres generated from K320E-Twinkle expressing MuSCs, induced via the mother's milk, we performed Haematoxylin and Eosin staining on frozen tissue sections in TA (*Figure* 34A) and Soleus (*Figure* 34J) at 3 and 12 months.

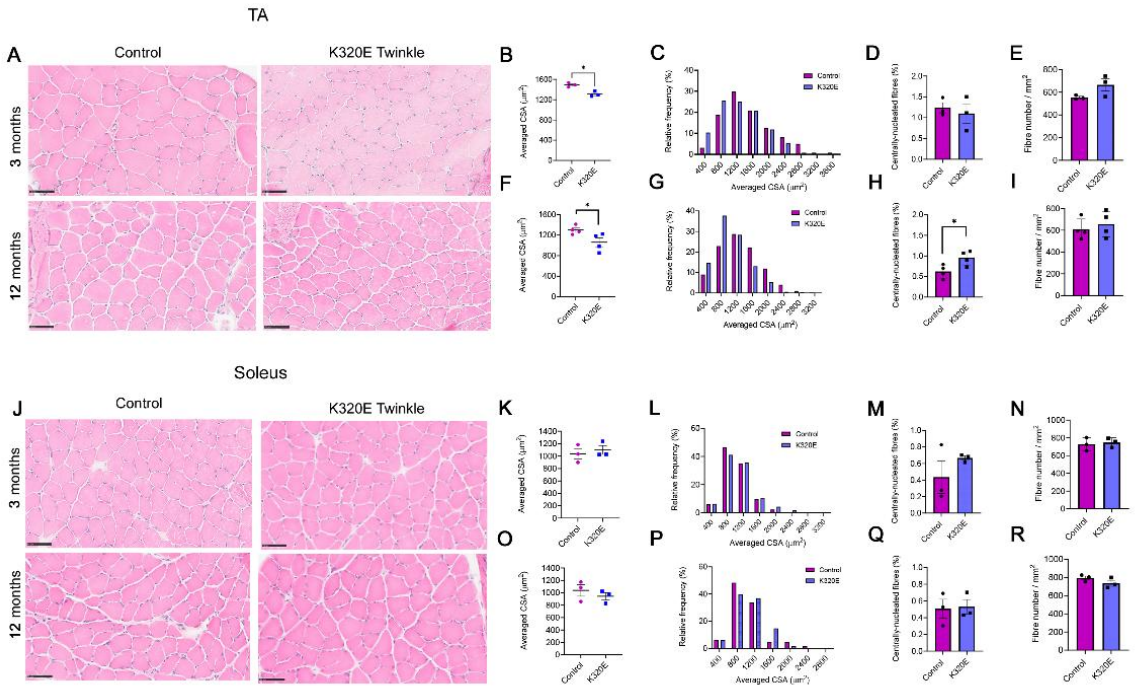

Figure 34: K320E-Twinkle expression in MuSCs influences differentiation in TA but not in Soleus, during development. Representative images showing H&E staining at 3 months and at 12 months in TA (A) and in Soleus (J). Quantification of averaged CSA in control and K320E fibres in TA at 3 months (B) and at 12 months (F). Quantification of averaged CSA in Soleus at 3 months (K) and at 12 months (0). Relative frequency distribution of the percentage of control and K320E-Twinkle fibres with the depicted CSA at 3 and 12 months in TA (C,G) and in Soleus (L,P). Quantification of the percentage of centrally-nucleated fibres at 3 and 12 months in TA (D, H) and in Soleus (M, Q). Quantification of

the fibre number/mm2 at 3 and 12 months in TA (E, I) and in Soleus (N, R). Data expressed as mean ± SEM. No of animals (n): 3-4 animals per group. P values - * <0.05. Scale bar 50μm.

Cross-sectional Area (CSA) measured from the H&E sections in the TA muscle showed a reduction (~13%) in the average CSA at 3 months, with an average CSA of ~1500μm^2 in control fibres compared to ~1300μm^2 in the K320E-Twinkle^{MuSC} fibres (*Figure* 34B). A similar reduction (~20%) was also observed at 12 months, with an average CSA of ~1300μm^2 in the control fibres compared to ~1050μm^2 in the mutant fibres (*Figure* 34F). The frequency distribution of the fibres also indicated a greater percentage of the K320E-Twinkle^{MuSC} fibres with a smaller CSA compared to controls at both ages (*Figure* 34C, G). However, in case of the Soleus, we did not observe any differences in the CSA between control fibres and K320E fibres (*Figure* 34K, O), nor did we observe any differences in the distribution of the fibres at both 3 and 12 months (*Figure* 34L, P).

Next, we checked if K320E-Twinkle expression affected the regeneration of muscle fibres. Hence, we counted the percentage of centrally-nucleated fibres, which signifies regenerating fibres (Gussoni et al., 1997). In the TA muscle, at 3 months, we did not observe any differences in the percentage of centrally-nucleated fibres, with both control and K320E-Twinkle^{MuSC} fibres having an average of ~1.2% regenerated fibres (*Figure* 34D). However, at 12 months, there was a significant increase in percentage of regenerated fibres in the K320E-Twinkle^{MuSC} TA muscle (*Figure* 34H), with ~0.6% in the control muscle and ~0.9% in the K320E muscle. In case of the Soleus muscle, we observed ~0.5% regenerated fibres and no differences between the percentage of centrally-nucleated fibres in control and K320 muscles, at both 3 and 12 months (*Figure* 34M, Q). In addition, we did not observe any difference in the number of fibres per mm^2 between control and K320E-Twinkle expressing muscles, in both TA and Soleus (*Figure* 34E, I, N, R), indicating no fibre loss. This suggests ongoing regeneration upon ageing in the TA of K320E-Twinkle^{MuSC} animals, which is not observed in the Soleus.

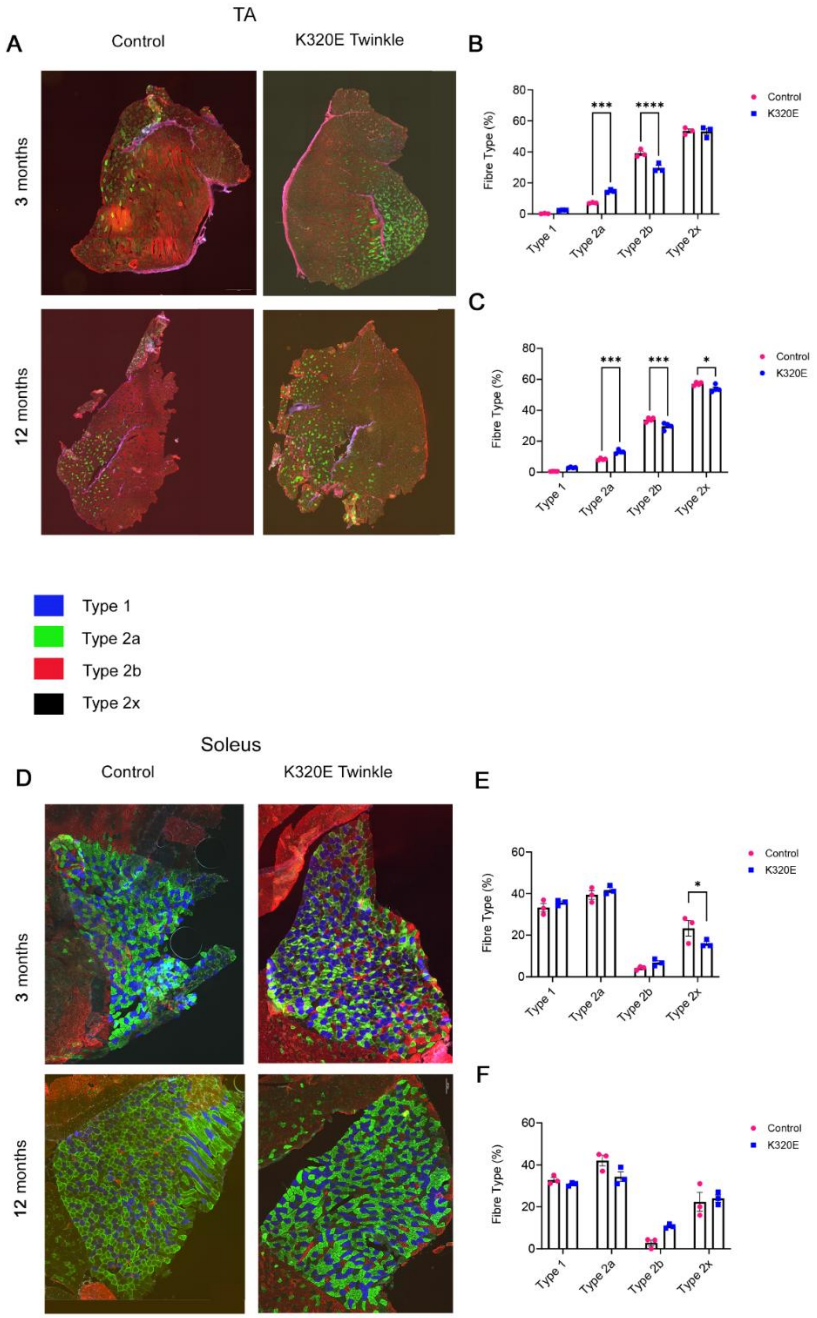

Figure 35: K320E-Twinkle expression in MuSCs, during development, causes a fibre type shift in TA but not in Soleus. Representative images of fibre types in TA (A) and in Soleus (D) at 3 and 12 months in control and K320E-Twinkle mice. Type 1 fibres shown in blue, Type 2a fibres shown in green and Type 2b fibres shown in red. Quantification of fibre type composition in TA at 3 months (B), 12 months (C), and in Soleus at 3 months (E) and 12 months (F). Data expressed as mean ± SEM. No of animals (n): 3-4 animals per group. P values - * <0.05, **<0.01, ***<0.001, ****<0.0001.

Finally, since most muscles are heterogeneous and are composed of different fibre types with different metabolism, we analysed their fibre type composition. We performed an immunofluorescence for fibre type 1 (MyHC-I), fibre type 2a (MyHC-IIA) and fibre type 2b (MyHC-IIB) in muscles at increasing ages, and quantified their respective proportions.

In TA at 3 months, we observed an increase in type 2a oxidative fibres from ~7.1% to ~14.7%, and a decrease in type 2b glycolytic fibres from ~39.1% to ~29.6%. Type 1 oxidative fibres also showed a trend to increase from ~0.2% to ~2.4% (not significant). At 12 months, this change in fibre type was further established (*Figure* 35A-C), with type 2a oxidative fibres increasing from ~8.3% in controls to ~13.2% in K320E-Twinkle fibres. Type 2b fibres decreased from 33.9% to ~29.7%. Type 2x fibres also decreased from ~57.1% to ~54%. Also, Type 1 fibres showed a trend for increase from ~0.5% to 2.9% (not significant). In Soleus, in contrast, we quantified a decrease in Type 2x glycolytic fibres, from ~23.3% to ~16% at 3 months (*Figure* 35D-E). At 12 months we did not see any significant differences in the fibre type percentages between the control and K320E-Twinkle^{MuSC} muscle (*Figure* 35D, 35F).

Therefore, these data suggest that K320E-Twinkle expression in MuSCs in TA causes a change in fibre type composition, which is further established with increasing age. In contrast, K320E-Twinkle expression in MuSCs does not influence the fibre type composition in Soleus. In conclusion, K320E-Twinkle expression in MuSCs leads to ongoing regeneration in the TA with a shift to oxidative fibre types with a smaller diameter, whereas the muscle architecture is not affected in the soleus. Taken together, physiological expression of K320E-Twinkle in MuSCs affects differentiation of new muscle fibres in the TA, but not in the Soleus.

3.2.2.4 K320E-Twinkle expression in MuSCs (in vitro) lowers mitochondrial biogenesis after differentiation

To better understand the contribution of mtDNA integrity to MuSCs homeostasis, we shifted to an *in vitro* approach. MuSCs were isolated from 8-week-old mice and,

expression of K320E-Twinkle was induced using 4-hydroxy tamoxifen. The MuSCs were either collected in their proliferative phase or induced for differentiation to myotubes and collected after 14 days (*Figure* 36A).

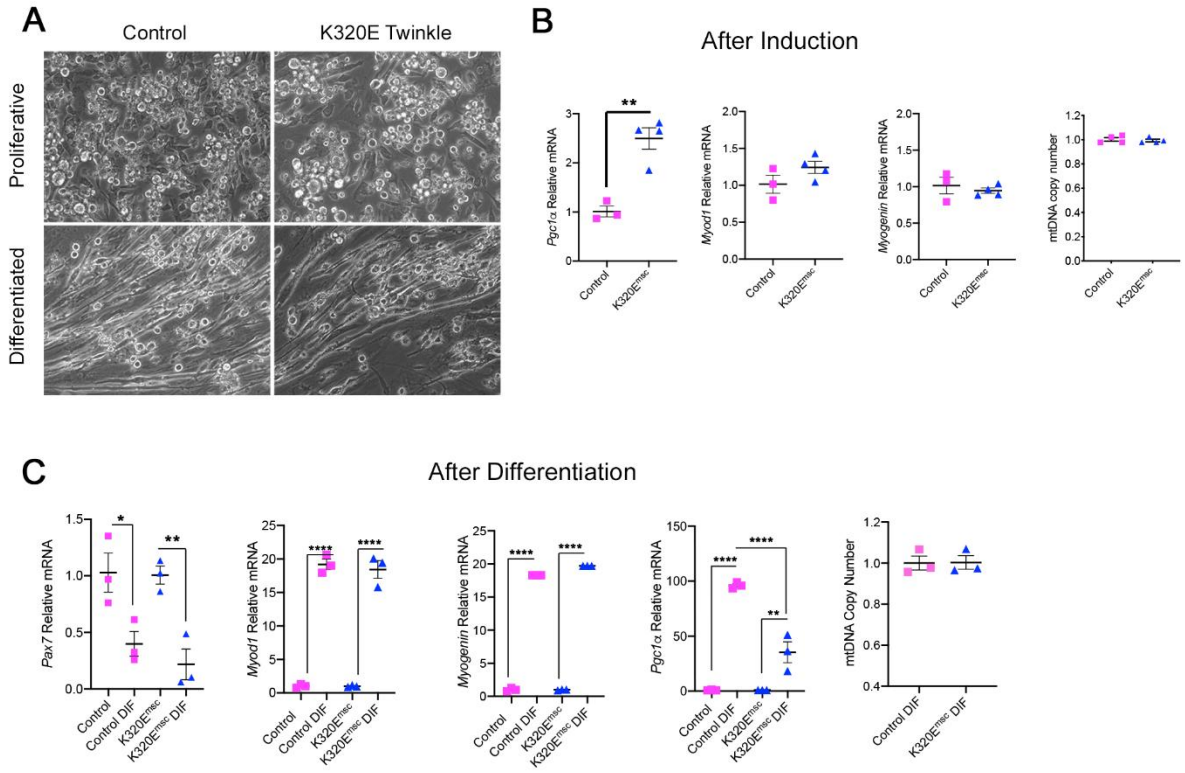

Figure 36: K320E expression in MuSCs in vitro. Representative brightfield images of proliferating and differentiated, control and K320E MuSCs. (B) qPCR analysis showing relative mRNA of PGC1α (for mitochondrial biogenesis), MyoD1 and Myogenin (MuSC differentiation markers) and mtDNA copy number analysis in MuSCs which were immediately collected after K320E induction. (C) qPCR analysis showing relative mRNA of MyoD and Myogenin, Pax7 (MuSC stemness marker), Pgc1 alpha and mtDNA copy number analysis in Control and K320E MuSCs differentiated for 14 days. Data expressed as mean ± SEM. No of animals (n): 3 animals per group. P values - * <0.05, **<0.01, ***<0.001, ****<0.0001. (modified from Kimoloi et al., 2022)

Following induction of K320E-Twinkle expression, we observed an increase in the levels of PGC1α, the master regulator of mitochondrial biogenesis (*Figure* 36B), in the mutant MuSCs. MyoD1 and Myogenin levels, which represent late proliferation and early differentiation steps of myogenesis, were similar between control and mutant MuSCs, confirming that MuSCs were activated but had not yet undergone differentiation.

After 14 days of differentiation, we observed a decrease of the stemness marker Pax7, in both control and K320E-Twinkle^{MuSC} cells. Consistently, we observed a prominent increase in the mRNA levels of MyoD and Myogenin in myotubes of both origins. However, we observed a lower increase in PGC1α levels upon differentiation in the K320E-Twinkle cells (*Figure* 36C). In addition, we did not observe changes in mtDNA copy number, neither in proliferative nor in differentiated cells (*Figure* 36B, C).

Taken together, this data suggests that immediately after activation; MuSCs undergo a compensatory mechanism to deal with K320E-Twinkle expression by increasing mitochondrial biogenesis. However, after differentiation, mitochondrial biogenesis is lower in the K320E-Twinkle cells.

3.2.2.5 K320E-Twinkle$^{MuSC\ (physiological)}$ do not exhibit changes in body weight and exercise performance

Since CSA in TA of the K320E-Twinkle^{MuSC} mice is reduced, we sought to test its impact on body or muscle weight. Animals were weighed every 2 weeks till they reached 12 weeks. Then they were weighed every 4 weeks till 54 weeks of age. No differences in body weights were observed between control and K320E animals, neither in females nor in males (*Figure* 37A-B).

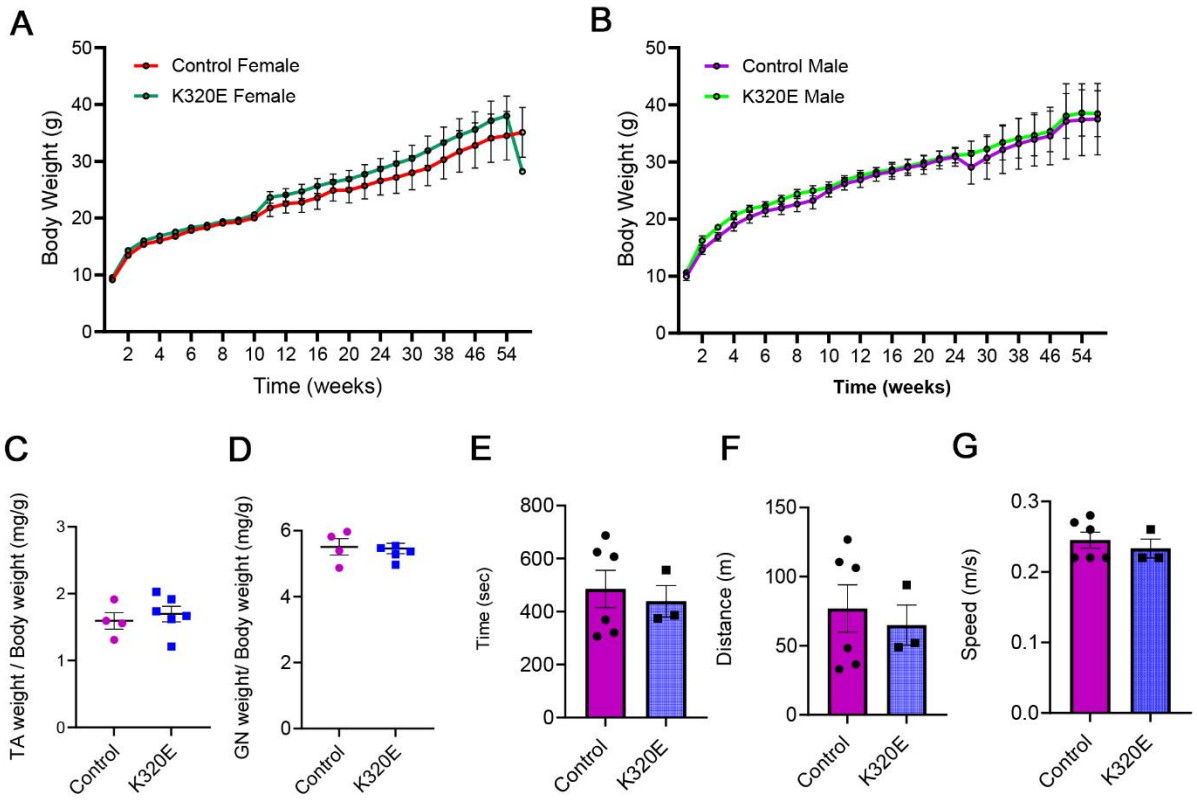

Figure 37: Physiological K320E-Twinkle expression in MuSCs does not cause loss in muscle mass, body weight or exercise performance. (A, B) Comparison of body weights over time, between Control and K320E animals, in females and males, up to 54 weeks. (C, D) Muscle weight per total body weight in TA and GN at 3 months. Maximum speed attained (E), total time (F) and total distance (G) run by control and K320E animals on a treadmill. Data expressed as mean ± SEM. No of animals (n): 3-6 animals per group.

Next, we measured the wet weight of TA and Gastrocnemius (GN) muscle, and depicted them in reference to the total body weight. Remarkably, although the TA showed a reduction in CSA at 3 months, there were no differences in the wet weight (*Figure* 37C). In line with this, there were no differences in the wet weight of the gastrocnemius as well (*Figure* 37D).

Since a fibre type shift was observed in the TA, and differentiation was affected by K320E-Twinkle expression, we tested exercise performance and endurance capacity of these animals. For this, 3-month-old animals were subjected to a forced treadmill test. As can

be seen in *Figure* 37E-G, neither the running performance (maximal speed attained) nor the endurance (distance run) was impaired in K320E-Twinkle^{MuSC} mice.

Therefore, although muscle fibre differentiation is affected by the expression of K320E-Twinkle, this does not impair muscle performance, nor does it lead to loss of muscle mass.

3.2.2.6 K320E Twinkle expression in C2C12 cells impairs mitochondrial function

C2C12 cells are immortalized mouse myoblast cells, which can be used as an *in vitro* model for studying satellite cells. Hence, we generated C2C12 stably expressing WT Twinkle and K320E Twinkle. In growing medium, C2C12 cells proliferate as single cells. When these cells are incubated in low serum conditions, they start forming myotubes (*Figure* 38A) and upregulate differentiation markers such as Myogenin (*Figure* 38B).

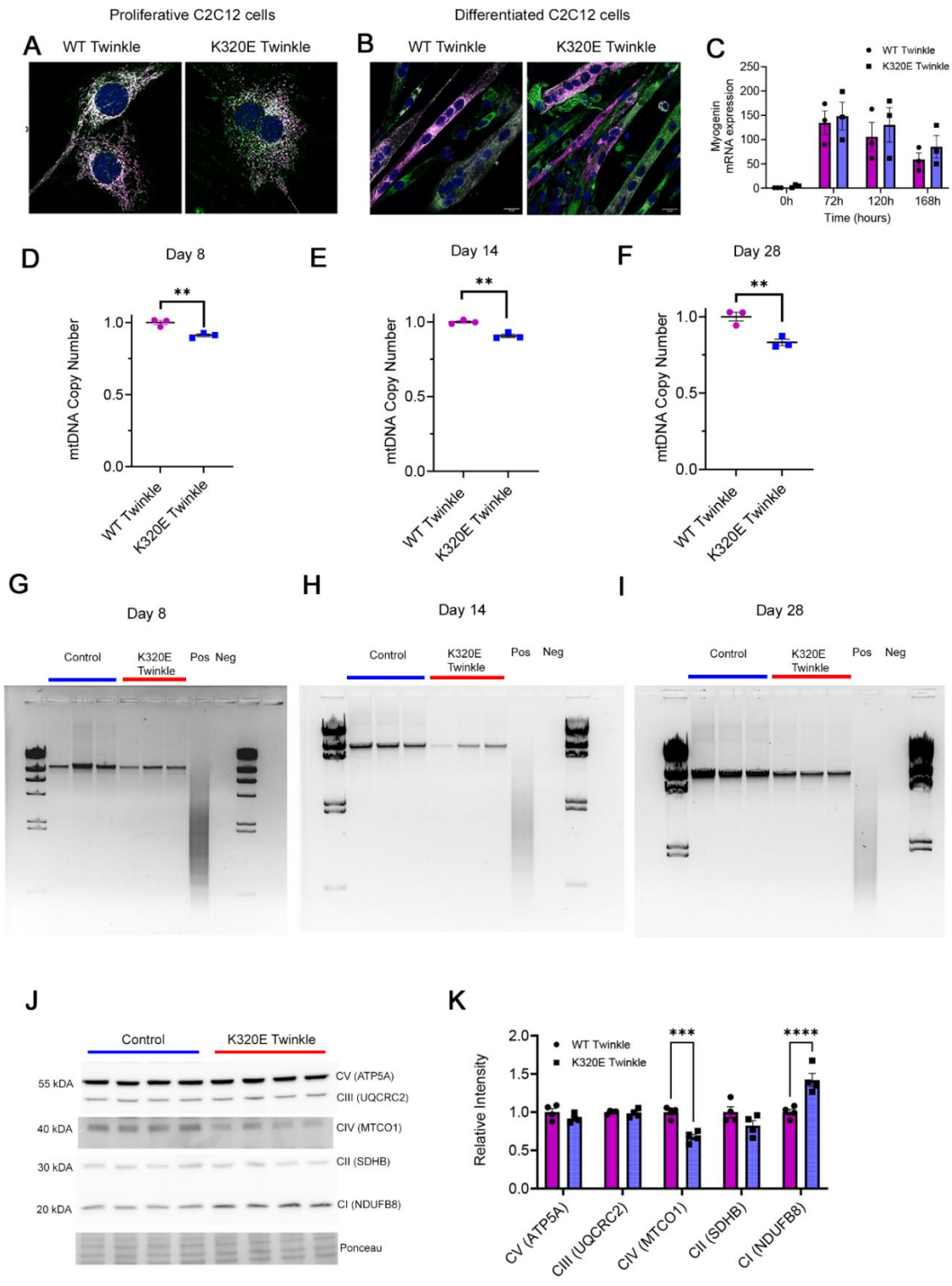

Figure 38: C2C12 cells expressing K320E Twinkle cause mtDNA depletion and alter respiratory chain composition upon differentiation. (A) Representative confocal images of

C2C12 cells expressing WT and K320E Twinkle during proliferation and upon differentiation. (B qPCR analysis showing mRNA levels of differentiation marker Myogenin in differentiated C2C12 cells. (C) mtDNA copy number analysis through qPCR and long-range PCR (E) for detecting mtDNA alterations in C2C12 cells differentiated for 8, 14 and 28 days. (D, F) Western blot analysis and quantification of relative intensity of respiratory chain subunits in C2C12 cells differentiated for 14 days. Data expressed as mean ± SEM. No of replicates (n): 3 replicates per genotype. P values - **<0.01, ***<0.001, ****<0.0001. Scale bar 10μm

Analysis of mtDNA copy number confirmed mtDNA depletion in differentiated C2C12 cells expressing K320E-Twinkle, with a progressive reduction in copy number upon differentiation with time (*Figure* 38C). After 8 days of differentiation, mtDNA copy number was reduced by ~8.9%, after 14 days by ~9.3% and after 28 days, the copy number was reduced by ~16.8% in the differentiated cells expressing K320E- Twinkle. However, these cells do not show any mtDNA structural alterations using long range PCR, even after 28 days of differentiation (*Figure* 38E).

An immunoblot for respiratory chain complexes showed a reduction (~32.6%) in the CIV subunit MTCO1, and an increase (~41.9%) in CI subunit NDUFB8 (*Figure* 38D).

To elucidate the changes occurring in the mitochondria upon cell differentiation, we performed proximity proteomics using ascorbate peroxidase (APEX2) (Han et al., 2017). We transduced C2C12 cells with a plasmid encoding WT-Twinkle-APEX2, K320E-Twinkle APEX2 and mitochondrial matrix APEX2. APEX2 is an enzyme, which in the presence of a short pulse of peroxidase, catalyses the biotinylation of neighbouring proteins. The biotinylated proteins can be purified and identified by mass spectrometry, enabling the identification of the neighbouring proteins (Han et al., 2017).

Mass spectroscopy showed enrichment of mitochondrial proteins in the mitoAPEX2 compared to the empty vector, confirming that the biotinylation reaction was specific for the mitochondrial compartment (*Figure* 39B). Next, we analysed the enriched proteins of the proximity proteome for wild-type Twinkle and K320E-Twinkle expressing cells. Hierarchical clustering of z-score normalized protein targets showed enrichment of proteins annotated in MitoCarta3.0 along with the sub-cellular localization (*Figure* 39C). The heat map generated shows upregulated mitochondrial proteins in red and

downregulated mitochondrial proteins in green (*Figure* 39C). This analysis revealed an evident lack of mitochondrial proteins upon differentiation in cells expressing K320E-Twinkle. Precisely, 20 outer membrane proteins, 127 inner membrane proteins and 101 matrix proteins were lowered in the K320E-Twinkle cells (*Figure* 39D).

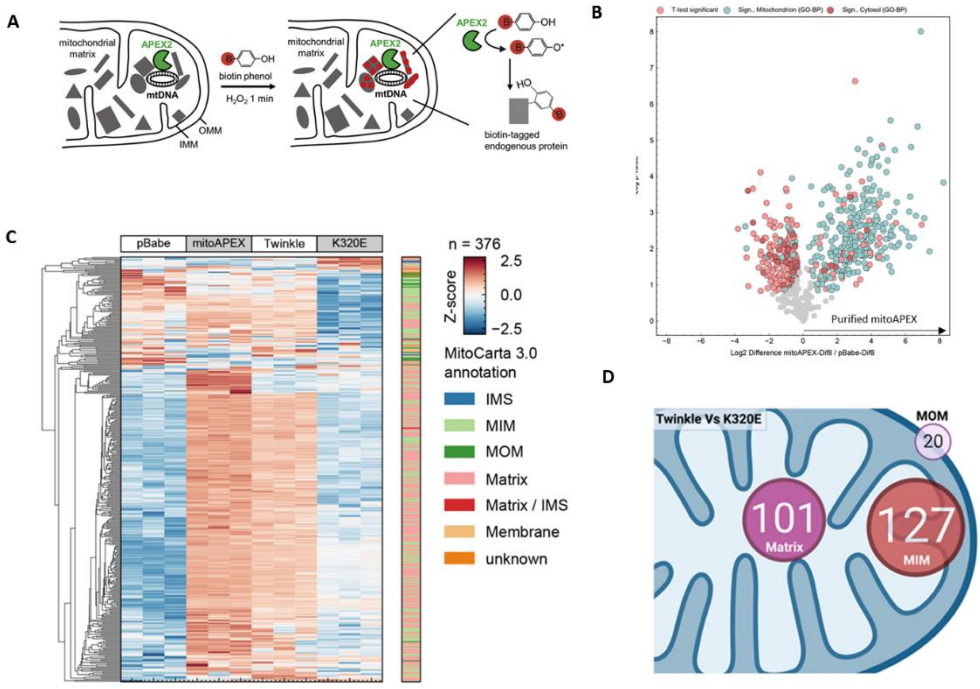

Figure 39: Proximity proteomics of differentiated C2C12-K320E-Twinkle Apex cells reveal evident lack of mitochondrial proteins. (A) Schematic of proximity proteomics upon APEX2 biotinylation (Han et al., 2017). (B) Volcano plot showing proteins enriched after crosslinking and purification of Twinkle and K320E-APEX2-V5. Differentially enriched proteins compared with cells transfected with empty vector pBabe (significant: q value < −0.05 and absolute log2 fold change >1) are highlighted in blue. (C) Hierarchical clustering of z-score normalized protein targets, showing enrichment of proteins annotated in MitoCarta3.0 along with sub-cellular localization of said proteins. (D) Graphical representation of the localization of the differentially enriched proteins.

Next, we aimed to assess changes in the mitochondrial morphology in C2C12 cells upon differentiation (*Figure* 40A). Mitochondrial morphology was characterized as filamentous, intermediate, fragmented (puncta), or swollen organelles. However, despite the lack of mitochondrial proteins, we did not observe any differences in the mitochondrial

morphology between the differentiated WT and the K320E-Twinkle expressing cells (*Figure* 40B).

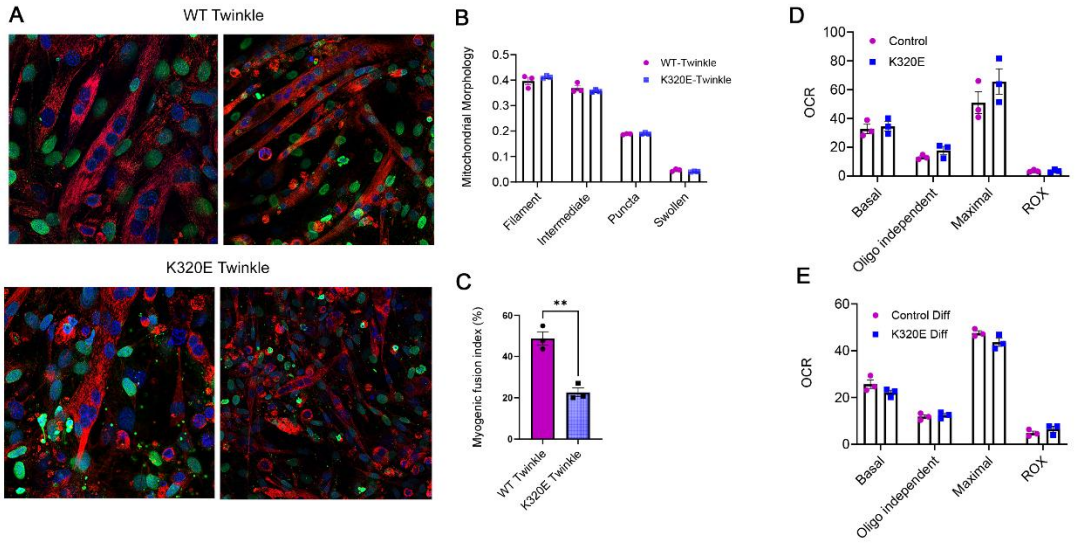

Figure 40: Mitochondrial morphology and cellular respiration is not affected, but myogenic fusion index is reduced in differentiated K320E C2C12 cells. (A) Representative confocal images of WT Twinkle and K320E Twinkle expressing 8 days differentiated C2C12 cells, with nucleus (Dapi) in blue, dsDNA in green and mitochondria (Tom 20) in red. (B) Quantification of mitochondrial morphology and (C) myogenic fusion index after 8 days of differentiation. Respirometry measurements in proliferating (D) C2C12 cells and 8 day differentiated (E) C2C12 cells. ROX – Residual Oxygen Consumption. P values - **<0.01. Scale bar 10µm

We then tested the potency of the C2C12 cells expressing K320E-Twinkle to differentiate into myotubes. We analysed the myogenic fusion index, a well-accepted parameter to determine the amount of myoblast fusion and quantify myogenic potency. Myogenic fusion index is defined as the number of nuclei in myotubes containing 2 or more nuclei, divided by the total number of nuclei in a given frame. As can be seen in figure 40C, we observed a remarkable reduction in the myogenic fusion index in K320E-Twinkle differentiated C2C12 cells.

We finally checked if the cellular respiration was affected by K320E-Twinkle expression using high-resolution Oroboros respirometry. However, we did not observe any

differences in respiration parameters, neither in proliferative cells (***Figure*** 40D) nor after differentiation (***Figure*** 40E).

Thus, the expression of K320E-Twinkle in C2C12 cells causes progressive mtDNA depletion upon differentiation, alters the composition of the respiratory chain complexes, and changes the composition of the mitochondrial proteome. Importantly, the reduced myogenic fusion capacity of K320E-Twinkle cells further evidences compromised differentiation due to impaired mitochondrial function upon K320E-Twinkle expression.

4 Discussion

The decline of mitochondrial function upon ageing has been well-established, with mitochondrial dysfunction playing a key role in various age-related disorders (Wallace, 2005). Mitochondrial dysfunction manifests as altered mitochondrial morphology, decreased number of mitochondria, decreased mtDNA copy number, altered levels of mitochondrial proteins and impaired respiratory chain complexes (Chen et al., 2023; Srinivasan et al., 2017). In long-lived organisms such as humans, ageing is associated with accumulation of mtDNA alterations such as deletions and duplications, in the muscles of such organisms (Larsson, 2010; López-Otín et al., 2013). Mutations in the mitochondrial Twinkle helicase gene (*PEO1*) have been implicated in Progressive external opthalmoplegia (PEO), recessively inherited infantile-onset spinocerebellar ataxia, rare forms of mtDNA depletion syndrome along with other diseases related to mtDNA instability(Copeland, 2012; Spelbrink et al., 2001). Since mitochondrial deficiency has been implicated in ageing and age-related diseases, there is a high likelihood that the maintenance of mtDNA integrity, which is essential for proper tissue function, is compromised during ageing.

Ageing is also associated with the loss of skeletal muscle mass, called sarcopenia, and a decline in the regenerative capacity of MuSCs (Morley, 2016; Xie et al., 2023). The importance of mitochondrial function is heavily implicated in MuSCs, where an increase in mtDNA copy number and mitochondrial mass is required for the differentiation of the MuSCs into large muscle fibres (Phanie Duguez et al., 2002; Remels et al., 2010). MuSCs lose both their mitogenic and myogenic capabilities, and also decrease in number upon ageing (Barbieri et al., 2011; Sahin & Depinho, 2010). It is well known that the regenerative capacity of skeletal muscles is reliant on MuSCs. MuSC quiescence, which is necessary to maintain the stem cell pool, relies in turn on basal autophagy. A decline in basal autophagy upon ageing results in the accumulation of misfolded proteins and other deleterious cellular waste, which forces the entry of MuSC into senescence (García-Prat et al., 2016). This decline is directly connected to the decline in regenerative capacity of the MuSC, thereby indicating that this decline in autophagy may lead to sarcopenia.

Sarcopenia contributes to frailty, significantly deteriorates the quality of life (Tsekoura et al., 2017), and has been proven to increase the risk of mortality in the elderly (Xu et al., 2022). Considering that the age of the global population is ever increasing, it is essential to understand the maintenance of mtDNA integrity and the consequences of disturbed mtDNA integrity in MuSCs, in the context of sarcopenia.

To study the consequences of disturbed mitochondrial function due to mtDNA instability, we generated a mouse line with an accelerated accumulation of mtDNA mutations by expressing a dominant-negative mutant of the mitochondrial helicase Twinkle. Overexpression of K320E-Twinkle simulates age-related accumulation of mitochondrial DNA defects (Baris et al., 2015). Along with respiratory chain defects, it results in the accumulation of mtDNA alterations/deletions in post-mitotic tissues such as the heart and muscle (Baris et al., 2015; Kimoloi et al., 2022; Oexner et al., 2020), and causes mtDNA depletion in proliferative tissues such as the epidermis (Weiland et al., 2018). K320E-Twinkle expression also leads to respiratory chain defects in chondrocytes (Bubb et al., 2021) and during B-cell differentiation (Urbanczyk et al., 2022). This approach is thus well established, and can be used to study disturbances of mtDNA integrity and its consequences in the pathophysiology of sarcopenia.

Skeletal muscle homeostasis is maintained by a fine balance between anabolic and catabolic processes (Rocchi et al., 2016). The nutrient and stress-sensing capacity of skeletal muscles governs the lifespan and the overall age of an organism (Demontis et al., 2013). Previous studies in our laboratory have shown that K320E-Twinkle^{Skm} mice (K320E-Twinkle specifically expressed in skeletal muscle) exhibit accumulation of mtDNA mutations and COX deficient fibres with mitochondrial dysfunction upon ageing, albeit with no impairment in muscle mass or performance (Kimoloi et al., 2022). The expression of K320E-Twinkle in the skeletal muscle was not sufficient to cause a sarcopenic phenotype, even in very old animals (Kimoloi et al., 2022). Since K320E-Twinkle^{Skm} mice did not show any impaired physical performance, nor a loss in muscle mass, there is a high likelihood that the detrimental effects of skeletal muscles containing mtDNA mutations were replaced by the regenerative function of MuSCs (Bischoff & Heintz, 1994; Chargé & Rudnicki, 2004). In order to explore the role of MuSCs in alleviating the

detrimental effects of skeletal muscle containing mtDNA mutations, we expressed the K320E-Twinkle specifically in the muscle satellite cells, K320E-Twinkle^{MuSC}, under the control of a tamoxifen inducible promoter. Earlier studies in the laboratory showed that when K320E-Twinkle was induced in adult mice in Pax7^{+} MuSCs, when these cells were in a quiescent state, it led to the accumulation of mtDNA depletion, however only in very old mice (Kimoloi et al., 2022).

Upon acute injury, our results showed that expression of K320E-Twinkle in MuSCs led to mitochondrial dysfunction in the regenerated muscle. During the regeneration process, activation of MuSCs is accompanied by inflammation (Carosio et al., 2011a). Proper muscle regeneration is dependent on the timely shift from a pro-inflammatory to an anti-inflammatory tissue environment (Marzetti et al., 2024). Proliferation of MuSCs is facilitated by the pro-inflammatory cytokines that are produced by M1 macrophages, whereas the myoblast fusion and myofibre growth are facilitated by the anti-inflammatory cytokine IL-10, produced by M2 macrophages (Marzetti et al., 2024; Tidball, 2017). We observed that the mitochondrial dysfunction caused by the expression of K320E-Twinkle leads to increased macrophage infiltration and upregulation of the pro-inflammatory cytokines interferon B (*Ifnβ*) and interleukin 6 (*Il6*) in the mutant muscles, compared to controls. The enhanced inflammation suggests a delayed regeneration due to the presence of mitochondrial dysfunction. Moreover, the balance between M1 and M2 macrophages is crucial for proper muscle regeneration, with even slight changes in the M1/M2 macrophage ratio being sufficient to adversely affect myogenesis (Marzetti et al., 2024). During ageing, a similar dysregulation of the cytokine environment is observed, accompanied by poor regeneration, and increased fibrosis. The enhanced inflammation observed in our mutant animals could similarly cause this imbalance in the macrophages, thereby affecting myogenesis. In this manner, the mitochondrial dysfunction in the MuSCs could cause impaired muscle regeneration. Ageing in MuSC is associated with accumulation of damaged mtDNA and mitochondrial dysfunction (Hong et al., 2022). This suggests a role for mitochondria in the activation of innate immunity, which regulates the cytokine environment during muscle regeneration.

Following muscle damage, or muscle injury, muscle regeneration occurs through myogenesis. Differentiation is a process which demands high energy, therefore a metabolic switch from a high glycolytic state, to one predominantly relying on OXPHOS, is required (Leary et al., 1998; Wagatsuma & Sakuma, 2013). Myogenesis is characterized by a highly regulated, rapid turnover of poorly functioning mitochondria, which are cleared out and instead replaced by the synthesis of "high function" mitochondria that are better suited to meet the regeneration needs (Chatzinikita et al., 2023). This is supported by studies which demonstrate that myogenesis first involves an initial increase in mitophagy for mitochondrial clearance which are suited for the glycolytic needs of myoblasts. Following mitophagy, a dramatic reorganization of the mitochondrial network (Remels et al., 2010), through mitochondrial biogenesis, is responsible for generating new mature mitochondria to handle the oxidative needs of differentiating myotubes (Sin et al., 2016). Hence, muscle regeneration is followed by increased mitochondrial turnover. In line with this, we observed a significant reduction in the mitoTIMER red/green ratio in the muscles of mutant mice 1 week post injury. This indicates that there was reduced oxidation and increased mitochondrial turnover in mutant muscle fibres (Cerqueira et al., 2020; Ferree et al., 2013). The fact that the mitochondrial turnover increases compared to controls could point to the presence of a compensatory mechanism that is taking care of the mtDNA defects in the mutant fibres. Consistently, we observed an increase in PGC1α mRNA in K320E-Twinkle cells, during MuSC activation *in vitro*, suggesting an upregulation of mitochondrial biogenesis. However, the reduced mitoTIMER red/green ratio is normalized after 4 weeks, indicating that the initial burst of compensation is short lived and not long term. This is further supported by the fact that the regenerated muscle continues to show reduced mass, as shown previously in the lab (Kimoloi et al., 2022).

While the data obtained from K320E-Twinkle expression in MuSCs after their activation is essential to show the importance of maintaining mtDNA integrity during acute MuSC regeneration, studying the maintenance of mtDNA integrity in a physiological manner is even more relevant in the context of ageing. In this case, we did not observe any accumulation of mtDNA alterations, nor the presence of COX-deficient fibres.

Interestingly, while the expression of K320E-Twinkle, in this physiological manner did not cause mitochondrial dysfunction or affect the MuSC niche, it did cause a reduction in the cross-sectional area of the muscle fibres. K320E-Twinkle differentially affected different muscles, and the reduced CSA was only observed in the TA at 3 and 12 months, but not in the Soleus.

Skeletal muscles are made up of three different fibre types, 1, 2a and 2b, along with other hybrid fibre types (Schiaffino, 2010). The fibre type composition was altered in the muscles when K320E-Twinkle was expressed in the MuSCs in a physiological manner, during development. In the TA muscle, we observed an increase in the percentage of smaller oxidative fibres and a reduction in the percentage of larger glycolytic fibres. This shift in fibre type is therefore in line with the observed reduction in TA CSA, since the type 1 fibres are smaller. At the same time, the total number of fibres per unit area was not affected, showing that overall number of fibres remained unchanged, but the fibres have shifted from larger to smaller. This could explain why, despite the reduced CSA, no loss of muscle mass was observed in the muscles of the K320E-Twinkle^{MuSC} animals. An increase in the percentage of centrally nucleated fibres in the TA of mutant mice at 12 months implies that there is enhanced regeneration, possibly to alleviate the effect of K320E-Twinkle expression. However, since this percentage of centrally nucleated fibres is less than 2%, which is expected in normal muscle (Schmalbruch & Lewis, 2000), it is not sufficient to truly quell any effect.

In line with this, when Twinkle expression was disturbed in differentiating C2C12 cells, it led to the reduction of a large number of mitochondrial proteins and progressive mtDNA depletion. Importantly, the myogenic fusion potential of the differentiating cells was impaired, suggesting that differentiation was affected. A possible reason for this could be disturbances in mitophagy and/or mitochondrial biogenesis, which is required for the remodelling of the mitochondrial network. Inadequate mitochondrial clearance, along with the inability to generate new mitochondria to meet the oxidative demands of the cells could explain the reduction of some mitochondrial proteins. Additionally, the imbalance in the respiratory chain complex subunits could contribute to the impaired differentiation. Therefore, one could speculate that tampering with the replication machinery, while not

sufficient to cause mitochondrial dysfunction, is still adequate to influence myogenesis and could be a major reason behind the altered fibre type composition that we observe.

Accordingly, *in vitro* studies with MuSCs show that upon differentiation, both control and mutant cells express similar levels of markers of differentiation (or rather the myogenic regulatory factors). Nevertheless, despite differentiation *in vitro* appearing normal, the fact that PGC1α is not increased to the same level as in differentiated control cells reveals a disturbance in proper differentiation, albeit without any physical manifestation. PGC1α is controlled by mTORC levels, therefore increased mTOR activity increases PGC1α activity, which in turn causes a fibre type shift (Cunningham et al., 2007; Rocchi et al., 2016). Therefore, the increase in PGC1α levels could play a role in the metabolic shift in fibre type composition. In our case, the increased PGC1α expression upon immediate induction could support this hypothesis. It is also entirely possible that the shift in fibre type is not dependent on PGC1α overexpression and is a consequence of the general shift in phenotype that is observed during ageing. The fact that PGC1α is not increased to the same level as in control cells upon differentiation might possibly indicate a feedback mechanism to prevent excessive metabolic shift. Moreover, studies have also shown that decreased mitochondrial biogenesis tends to blunt myogenesis (Marzetti et al., 2024). This is in line with the reduced mitochondrial biogenesis, i.e. lower PGC1α expression that we observe in our differentiated K320E-Twinkle MuSCs compared to controls. Additionally, PGC1α buffers oxidative stress that occurs during differentiation, by promoting the expression of antioxidant enzymes (Baldelli et al., 2014). Consequently, downregulation of PGC1α is accompanied by increased oxidative damage as well as a decrease in mitochondrial mass and function (Baldelli et al., 2014). A shift in fibre type from glycolytic to oxidative is seen in spinal and bulbar muscular atrophy (SBMA), with skeletal muscle atrophy being one of the main clinical manifestations of this disease (Rocchi et al., 2016). Here, the fibre type shift is brought about by overexpression of PGC1α (Li et al., 2002; Rocchi et al., 2016). Additionally, this shift has been observed in Amyotrophic lateral sclerosis (ALS) as well. However, in case of ALS, the shift is PGC1α independent, because in this case the shift is accompanied by a reduction of PGC1α

levels (Palamiuc et al., 2015). These findings further show that expression of K320E-Twinkle in MuSCs interferes with differentiation of myofibres.

During ageing, muscle atrophy is seen more in weight bearing muscles, with markedly high atrophy in muscles which are primarily composed of fast-twitch glycolytic fibres (Holloszy et al., 1991). Changes in the composition of fibre type occur due to various physiological adaptations with various molecular and cellular modifications in the skeletal muscle tissue being responsible for altered protein expression patterns (Gelfi et al., 2011). While slow to fast transition occurs during muscle disuse, microgravity, and extended bed rest, in contrast, endurance exercise, chronic low frequency stimulation, hyper excitability and ageing are the factors that trigger fast to slow muscle transition or transformation (Canepari et al., 2010).

There have been various studies with senescent animals, including proteomic profiling of aged rodent skeletal muscles, which reveal a drastic increase in the abundance and phosphorylation levels of slow myosin light chain MLC2 levels, clearly confirming the pathophysiological shift to a slower muscle phenotype (Gannon et al., 2009). In humans too, this trend of fast to slow transitions have been observed, and this is most likely due to or associated with a preferential susceptibility of fast-twitching muscle fibres to muscle atrophy (Dowling et al., 2023). The shift in muscle type to oxidative is characterized by a drastic decrease in glycolytic enzymes and a concomitant increase in mitochondrial markers of oxidative metabolism (Donoghue et al., 2010).

Various crucial regulatory and contractile elements such as myosin heavy chains, myosin light chains, actin and tropomyosin were shown to exhibit a switch to slower isoforms during ageing (Donoghue et al., 2010; Gelfi et al., 2011; O'Connell et al., 2007; Ohlendieck, 2011; Piec et al., 2005). Glycolytic enzymes are lower in senescent muscles (Capitanio et al., 2009; Gelfi et al., 2011), whereas mitochondrial enzymes are elevated during ageing (O'Connell et al., 2007). Most interestingly, a disturbance in the supramolecular organization of mitochondrial complexes that are involved in OXPHOS was shown to occur in aged muscle (Lombardi et al., 2009).

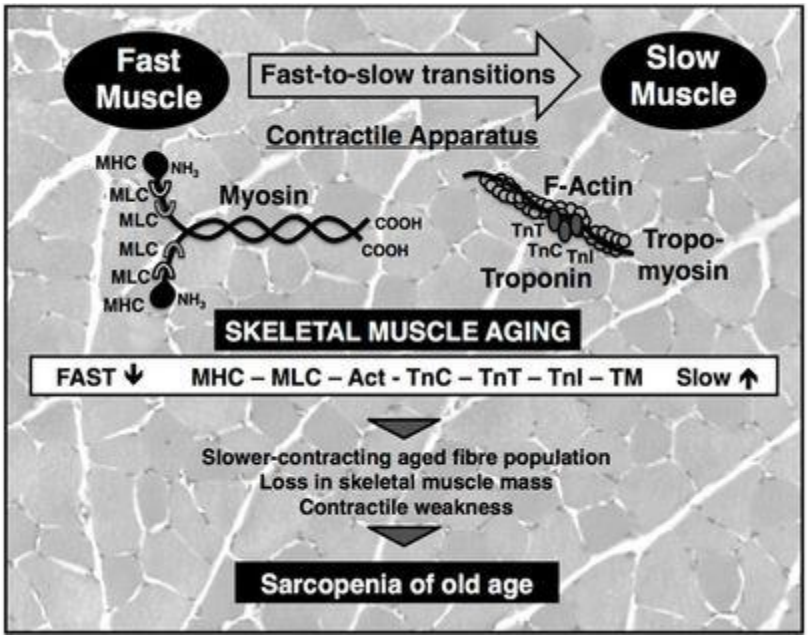

Figure 41: Proteomic profile of fast to slow transitions during ageing. (Ohlendieck, 2011)

These studies show that the higher susceptibility of fast twitch type II fibres leads to fast-to-slow transition in senescent muscle. This age-related shift in fibre type and accompanying changes in MyHC isoforms can only generate low maximum force levels in senescent or aged skeletal muscles compared to young and adult muscles (M. Li & Larsson, 2010). Consequently, the alterations in overall composition of motor units play a vital or central role in the gradual loss of skeletal muscle strength during ageing (Verdijk et al., 2010).

Unlike the TA, the CSA of the soleus was not affected, nor was the fibre type composition altered. Perhaps in case of the soleus muscle, since it already comprises of mostly oxidative fibres, it has better quality control mechanisms that are taking care of the effects of K320E-Twinkle expression.

In line with this, expression of K320E-Twinkle in skeletal muscles, also expressing mitoTIMER, exhibit differential mitochondrial turnover, along with differences in the autophagic capacity between the TA and the soleus. The unchanged autophagic flux in the mutant TA muscle fibres could be responsible for the inefficient mitochondrial turnover. On the other hand, in the oxidative soleus muscle, we observe an increase in

the autophagic flux, which results in increased mitochondrial turnover. Autophagy plays a protective role in sarcopenia and is one of the main reasons for myofibre atrophy (Bonaldo & Sandri, 2013; Jiao & Demontis, 2017). Reduction in autophagic capacity contributes to sarcopenia, supported by various studies which show that autophagy becomes progressively dysfunctional with ageing in rodent and human muscle (Jiao & Demontis, 2017; O'Leary et al., 2013). This differential autophagic mechanism in the TA compared to the soleus is possibly because the predominantly glycolytic TA is more prone to age related failure (Nilwik et al., 2013;Fernando et al., 2020). In contrast, oxidative muscles have better mitochondrial homeostasis and exhibit more functional autophagy during ageing, thereby maintaining mitochondrial function (Crupi et al., 2018; Fernando et al., 2020).

Likewise, ageing is associated with impaired mitophagy. However, we do not observe the activation of classical mitophagy pathways. This is in agreement with previous data, showing that protein levels of the mitophagy adaptor, Optineurin, were not altered (Sen et al., 2022). Nonetheless, the mtDNA defects, caused by K320E-Twinkle expression in skeletal muscle, were unmistakenly being cleared, at least in case of the soleus. This suggests that alternative or complementary pathways, besides canonical mitophagy, have been activated in these muscles with mtDNA defects. One possible explanation for this is that the elimination of mutated mtDNA molecules was carried out by selective removal through a specialized endosomal-mediated mitophagy pathway, recently described by us (Sen et al., 2022). This non-canonical mitophagy pathway is independent of autophagosome formation and upon mtDNA damage, mitochondrial nucleoids are eliminated via recruitment to endosomes, while at the same time avoiding an exacerbated immune response (Sen et al., 2022, 2023). Collectively, expression of K320E-Twinkle differentially affects mitochondrial quality control, depending on the predominant muscle metabolism, and unquestionably confirms the susceptibility of glycolytic muscles to mtDNA defects.

It is noteworthy that this shift in fibre type from glycolytic to oxidative has been observed during ageing and is linked to sarcopenia (Dowling et al., 2023). Therefore, during ageing,

since muscle atrophy is preferentially seen in glycolytic fibres, these fibres are more susceptible to sarcopenia.

Albeit the changes observed in muscle fibre composition, we did not perceive any differences in endurance strength of the mutant animals. A possible explanation for this is that the difference in fibre composition is probably not altered to adequate levels required to show a physical manifestation of the change.

Altogether, we can conclude that expression of K320E-Twinkle in MuSCs, induced in a physiological manner affects the mtDNA replication process. Of course, it is necessary to point out that this study has its limitations, especially since we were unable to show how exactly the expression of K320E-Twinkle is affecting the replication process in the satellite cells. A further deep sequencing analysis would be able to shed light into this query. Since K320E-Twinkle expression did not result in mtDNA alterations or mtDNA depletion, we speculate that point mutations may occur, since similar mutations were observed when K320E-Twinkle was expressed in dopaminergic neurons (Paß et al., 2024).

The shift in fibre type from glycolytic to oxidative, and the fibre atrophy that we observe, are well-established characteristics of sarcopenia. The differential mitochondrial quality control between muscles, corroborates the increased susceptibility of glycolytic fibres to sarcopenia. While K320E-Twinkle expression in the MuSCs did not cause any measurable mitochondrial dysfunction, it was sufficient to alter the myoblast differentiation process. Moreover, the remarkable decrease in mitochondrial proteins in the C2C12 cells expressing K320E-Twinkle, with consequent reduction in myogenic capabilities further substantiates that the mitochondrial reorganization required for proper myogenesis was distinctly altered. This showcases that the expression of K320E-Twinkle, which interferes with mtDNA replication, subsequently influences mtDNA integrity. Thus, one could postulate that mtDNA integrity has a key role in the ageing muscle phenotype, and disturbances to the mtDNA replication machinery (through Twinkle-K320E expression) could be a reason for the altered metabolic fibre profile observed in aged sarcopenic muscles.

5 Bibliography

1. Ahlqvist, K. J., Hämäläinen, R. H., Yatsuga, S., Uutela, M., Terzioglu, M., Götz, A., Forsström, S., Salven, P., Angers-Loustau, A., Kopra, O. H., Tyynismaa, H., Larsson, N. G., Wartiovaara, K., Prolla, T., Trifunovic, A., & Suomalainen, A. (2012). Somatic progenitor cell vulnerability to mitochondrial DNA mutagenesis underlies progeroid phenotypes in polg mutator mice. *Cell Metabolism*, *15*(1), 100–109. https://doi.org/10.1016/j.cmet.2011.11.012
2. Alam, T. I., Kanki, T., Muta, T., Ukaji, K., Abe, Y., Nakayama, H., Takio, K., Hamasaki, N., & Kang, D. (2003). Human mitochondrial DNA is packaged with TFAM. In *Nucleic Acids Research* (Vol. 31, Issue 6, pp. 1640–1645). https://doi.org/10.1093/nar/gkg251
3. Alberts, B., Johnson, A., Lewis, J., Raff, M., Roberts, K., & Walter, P. (2002). *Molecular Biology of the Cell* (4th edition). Garland Science.
4. Anderson, S., Bankier, A. T., Barrell, B. G., De Bruijn, M. H. L., Coulson, A. R., Drouin, J., Eperon, I. C., Nierlich, D. P., Roe, B. A., Sanger, F., Schreier, P. H., Smith, A. J. H., Staden, R., & Young, I. G. (1981). Sequence and organization of the human mitochondrial genome. In *Greenberg. R. As'r. 1* (Vol. 290, Issue 6).
5. Area-Gomez, E., & Schon, E. A. (2014). Mitochondrial genetics and disease. *Journal of Child Neurology*, *29*(9), 1208–1215. https://doi.org/10.1177/0883073814539561
6. Baldelli, S., Aquilano, K., & Ciriolo, M. R. (2014). PGC-1α buffers ROS-mediated removal of mitochondria during myogenesis. *Cell Death and Disease*, *5*(11). https://doi.org/10.1038/cddis.2014.458
7. Barbieri, E., Battistelli, M., Casadei, L., Vallorani, L., Piccoli, G., Guescini, M., Gioacchini, A. M., Polidori, E., Zeppa, S., Ceccaroli, P., Stocchi, L., Stocchi, V., & Falcieri, E. (2011). Morphofunctional and biochemical approaches for studying mitochondrial changes during myoblasts differentiation. *Journal of Aging Research*, *2011*. https://doi.org/10.4061/2011/845379
8. Baris, O. R., Ederer, S., Neuhaus, J. F. G., von Kleist-Retzow, J. C., Wunderlich, C. M., Pal, M., Wunderlich, F. T., Peeva, V., Zsurka, G., Kunz, W. S., Hickethier, T., Bunck, A. C., Stöckigt, F., Schrickel, J. W., & Wiesner, R. J. (2015). Mosaic Deficiency in Mitochondrial Oxidative Metabolism Promotes Cardiac Arrhythmia during Aging. *Cell Metabolism*, *21*(5), 667–677. https://doi.org/10.1016/j.cmet.2015.04.005
9. Baumgartner, R. N. (2000). Body composition in healthy aging. *Annals of the New York Academy of Sciences*, *904*, 437–448. https://doi.org/10.1111/j.1749-6632.2000.tb06498.x
10. Bellanti, F., Buglio, A. Lo, & Vendemiale, G. (2021). Mitochondrial impairment in sarcopenia. In *Biology* (Vol. 10, Issue 1, pp. 1–16). MDPI AG. https://doi.org/10.3390/biology10010031
11. Berk, A. J., & Clayton, D. A. (1974). Mechanism of Mitochondrial DNA Replication in Mouse L-cells : Asynchronous Replication of Strands, Segregation of Circular

Daughter Molecules, Aspects of Topology and Turnover of an Initiation Sequence. *J. Mol. Biol*, *86*, 824.

12. Bhattacharya, D., & Scimè, A. (2020). Mitochondrial Function in Muscle Stem Cell Fates. In *Frontiers in Cell and Developmental Biology* (Vol. 8). Frontiers Media S.A. https://doi.org/10.3389/fcell.2020.00480
13. Bibb, M. J., Van Etten, R. A., Wright, C. T., Walberg, M. W., & Clayton, D. A. (1981). Sequence and Gene Organization of Mouse Mitochondrial DNA. In *Cell* (Vol. 26).
14. Bischoff, R., & Heintz, C. (1994). Enhancement of skeletal muscle regeneration. *Developmental Dynamics*, *201*(1), 41–54. https://doi.org/10.1002/aja.1002010105
15. Bjornson, C. R. R., Cheung, T. H., Liu, L., Tripathi, P. V., Steeper, K. M., & Rando, T. A. (2012). Notch signaling is necessary to maintain quiescence in adult muscle stem cells. *Stem Cells*, *30*(2), 232–242. https://doi.org/10.1002/stem.773
16. Boczonadi, V., Ricci, G., & Horvath, R. (2018). Mitochondrial DNA transcription and translation: Clinical syndromes. In *Essays in Biochemistry* (Vol. 62, Issue 3, pp. 321–340). Portland Press Ltd. https://doi.org/10.1042/EBC20170103
17. Bogenhagen, D. F., Rousseau, D., & Burke, S. (2008). The layered structure of human mitochondrial DNA nucleoids. *Journal of Biological Chemistry*, *283*(6), 3665–3675. https://doi.org/10.1074/jbc.M708444200
18. Bonaldo, P., & Sandri, M. (2013). Cellular and molecular mechanisms of muscle atrophy. In *DMM Disease Models and Mechanisms* (Vol. 6, Issue 1, pp. 25–39). https://doi.org/10.1242/dmm.010389
19. Boppart, M. D., De Lisio, M., & Witkowski, S. (2015). Exercise and Stem Cells. *Progress in Molecular Biology and Translational Science*, *135*, 423–456.
20. Bratic, A., & Larsson, N. G. (2013). The role of mitochondria in aging. In *Journal of Clinical Investigation* (Vol. 123, Issue 3, pp. 951–957). https://doi.org/10.1172/JCI64125
21. Bubb, K., Holzer, T., Nolte, J. L., Krüger, M., Wilson, R., Schlötzer-Schrehardt, U., Brinckmann, J., Altmüller, J., Aszodi, A., Fleischhauer, L., Clausen-Schaumann, H., Probst, K., & Brachvogel, B. (2021). Mitochondrial respiratory chain function promotes extracellular matrix integrity in cartilage. *Journal of Biological Chemistry*, *279*(4). https://doi.org/10.1016/j.jbc.2021.101224
22. Cadot, B., Gache, V., & Gomes, E. R. (2015). Moving and positioning the nucleus in skeletal muscle-one step at a time. In *Nucleus* (Vol. 6, Issue 5, pp. 373–381). Taylor and Francis Inc. https://doi.org/10.1080/19491034.2015.1090073
23. Cairns, J. (1975). Mutation selection and the natural history of cancer. *Nature*, *255*.
24. Calvani, R., Joseph, A. M., Adhihetty, P. J., Miccheli, A., Bossola, M., Leeuwenburgh, C., Bernabei, R., & Marzetti, E. (2013). Mitochondrial pathways in sarcopenia of aging and disuse muscle atrophy. In *Biological Chemistry* (Vol. 394, Issue 3, pp. 393–414). https://doi.org/10.1515/hsz-2012-0247
25. Capitanio, D., Vasso, M., Fania, C., Moriggi, M., Viganò, A., Procacci, P., Magnaghi, V., & Gelfi, C. (2009). Comparative proteomic profile of rat sciatic nerve and

gastrocnemius muscle tissues in ageing by 2-D DIGE. *Proteomics*, *9*(7), 2004–2020. https://doi.org/10.1002/pmic.200701162

26. Carosio, S., Berardinelli, M. G., Aucello, M., & Musarò, A. (2011a). Impact of ageing on muscle cell regeneration. In *Ageing Research Reviews* (Vol. 10, Issue 1, pp. 35–42). https://doi.org/10.1016/j.arr.2009.08.001
27. Carosio, S., Berardinelli, M. G., Aucello, M., & Musarò, A. (2011b). Impact of ageing on muscle cell regeneration. In *Ageing Research Reviews* (Vol. 10, Issue 1, pp. 35–42). https://doi.org/10.1016/j.arr.2009.08.001
28. Cerqueira, F. M., Kozer, N., Petcherski, A., Baranovski, B. M., Wolf, D., Assali, E. A., Roth, Y., Gazit, R., Barr, H., Lewis, E. C., Las, G., & Shirihai, O. S. (2020). MitoTimer-based high-content screen identifies two chemically-related benzothiophene derivatives that enhance basal mitophagy. *Biochemical Journal*, *477*(2), 461–475. https://doi.org/10.1042/BCJ20190616
29. Chan, D. C. (2006). Mitochondrial fusion and fission in mammals. In *Annual Review of Cell and Developmental Biology* (Vol. 22, pp. 79–99). https://doi.org/10.1146/annurev.cellbio.22.010305.104638
30. Chan, D. C. (2012). Fusion and fission: Interlinked processes critical for mitochondrial health. *Annual Review of Genetics*, *46*, 265–287. https://doi.org/10.1146/annurev-genet-110410-132529
31. Chargé, S. B. P., & Rudnicki, M. A. (2004). *Cellular and Molecular Regulation of Muscle Regeneration*. https://doi.org/10.1152/physrev.00019.2003.-Under
32. Chatzinikita, E., Maridaki, M., Palikaras, K., Koutsilieris, M., & Philippou, A. (2023). The Role of Mitophagy in Skeletal Muscle Damage and Regeneration. In *Cells* (Vol. 12, Issue 5). MDPI. https://doi.org/10.3390/cells12050716
33. Chen, W., Datzkiw, D., & Rudnicki, M. A. (2020). Satellite cells in ageing: Use it or lose it. In *Open Biology* (Vol. 10, Issue 5). Royal Society Publishing. https://doi.org/10.1098/rsob.200048
34. Chen, W., Zhao, H., & Li, Y. (2023). Mitochondrial dynamics in health and disease: mechanisms and potential targets. *Signal Transduction and Targeted Therapy*, *8*(1). https://doi.org/10.1038/s41392-023-01547-9
35. Clark, W. E. L. G. (1946). An experimental study of the regeneration of mammalian striped muscle. *Journal of Anatomy*, *80*, 24–36.
36. Cohen, H. Y., Miller, C., Bitterman, K. J., Wall, N. R., Hekking, B., Kessler, B., Howitz, K. T., Gorospe, M., De Cabo, R., & Sinclair, D. A. (2004). Calorie restriction promotes mammalian cell survival by inducing the SIRT1 deacetylase. *Science*, *305*(5682), 390–392. https://doi.org/10.1126/science.1099196
37. Colman, R. J., Anderson, R. M., Johnson, S. C., Kastman, E. K., Kosmatka, K. J., Beasley, T. M., Allison, D. B., Cruzen, C., Simmons, H. A., Kemnitz, J. W., & Weindruch, R. (2009). Caloric restriction delays disease onset and mortality in rhesus monkeys. *Science*, *325*(5937), 201–204. https://doi.org/10.1126/science.1173635
38. Cooper, G. (2000). *The Cell: A Molecular Approach.* (2nd edition.). Sinauer Associates.

39. Copeland, W. C. (2012). Defects in mitochondrial DNA replication and human disease. In *Critical Reviews in Biochemistry and Molecular Biology* (Vol. 47, Issue 1, pp. 64–74). https://doi.org/10.3109/10409238.2011.632763
40. Crupi, A. N., Nunnelee, J. S., Taylor, D. J., Thomas, A., Vit, J.-P., Riera, C. E., Gottlieb, R. A., & Goodridge, H. S. (2018). Oxidative muscles have better mitochondrial homeostasis than glycolytic muscles throughout life and maintain mitochondrial function during aging. *Aging (Albany NY)*, *10*(11), 3327–3352.
41. Cruz-Jentoft, A. J., Baeyens, J. P., Bauer, J. M., Boirie, Y., Cederholm, T., Landi, F., Martin, F. C., Michel, J. P., Rolland, Y., Schneider, S. M., Topinková, E., Vandewoude, M., & Zamboni, M. (2010). Sarcopenia: European consensus on definition and diagnosis. *Age and Ageing*, *39*(4), 412–423. https://doi.org/10.1093/ageing/afq034
42. Cunningham, J. T., Rodgers, J. T., Arlow, D. H., Vazquez, F., Mootha, V. K., & Puigserver, P. (2007). mTOR controls mitochondrial oxidative function through a YY1-PGC-1α transcriptional complex. *Nature*, *450*(7170), 736–740. https://doi.org/10.1038/nature06322
43. DeBalsi, K. L., Hoff, K. E., & Copeland, W. C. (2017). Role of the mitochondrial DNA replication machinery in mitochondrial DNA mutagenesis, aging and age-related diseases. In *Ageing Research Reviews* (Vol. 33, pp. 89–104). Elsevier Ireland Ltd. https://doi.org/10.1016/j.arr.2016.04.006
44. Demontis, F., Piccirillo, R., Goldberg, A. L., & Perrimon, N. (2013). The influence of skeletal muscle on systemic aging and lifespan. In *Aging Cell* (Vol. 12, Issue 6, pp. 943–949). https://doi.org/10.1111/acel.12126
45. Dimauro, S., & Schon, E. A. (2003). *mechanisms of disease Mitochondrial Respiratory-Chain Diseases*. www.nejm.org
46. Donoghue, P., Staunton, L., Mullen, E., Manning, G., & Ohlendieck, K. (2010). DIGE analysis of rat skeletal muscle proteins using nonionic detergent phase extraction of young adult versus aged gastrocnemius tissue. *Journal of Proteomics*, *73*(8), 1441–1453. https://doi.org/10.1016/j.jprot.2010.01.014
47. Dowling, P., Gargan, S., Swandulla, D., & Ohlendieck, K. (2023). Fiber-Type Shifting in Sarcopenia of Old Age: Proteomic Profiling of the Contractile Apparatus of Skeletal Muscles. In *International Journal of Molecular Sciences* (Vol. 24, Issue 3). MDPI. https://doi.org/10.3390/ijms24032415
48. Druzhyna, N. M., Wilson, G. L., & LeDoux, S. P. (2008). Mitochondrial DNA repair in aging and disease. *Mechanisms of Ageing and Development*, *129*(7–8), 383–390. https://doi.org/10.1016/j.mad.2008.03.002
49. D'Souza, A. R., & Minczuk, M. (2018). Mitochondrial transcription and translation: Overview. In *Essays in Biochemistry* (Vol. 62, Issue 3, pp. 309–320). Portland Press Ltd. https://doi.org/10.1042/EBC20170102
50. Dumont, N. A., Wang, Y. X., & Rudnicki, M. A. (2015). Intrinsic and extrinsic mechanisms regulating satellite cell function. *Development (Cambridge)*, *142*(9), 1572–1581. https://doi.org/10.1242/dev.114223

51. Dyall, S. D., Brown, M. T., & Johnson, P. J. (2000). 14. E. Suss-Toby. In *28. R. Ménard, Cell Microbiol* (Vol. 290, Issue 9). https://www.science.org
52. Evano, B., & Tajbakhsh, S. (2018). Skeletal muscle stem cells in comfort and stress. In *npj Regenerative Medicine* (Vol. 3, Issue 1). Nature Publishing Group. https://doi.org/10.1038/s41536-018-0062-3
53. Falkenberg, M. (2018). Mitochondrial DNA replication in mammalian cells: Overview of the pathway. In *Essays in Biochemistry* (Vol. 62, Issue 3, pp. 287–296). Portland Press Ltd. https://doi.org/10.1042/EBC20170100
54. Falkenberg, M., & Gustafsson, C. M. (2020). Mammalian mitochondrial DNA replication and mechanisms of deletion formation. In *Critical Reviews in Biochemistry and Molecular Biology* (Vol. 55, Issue 6, pp. 509–524). Taylor and Francis Ltd. https://doi.org/10.1080/10409238.2020.1818684
55. Falkenberg, M., Larsson, N. G., & Gustafsson, C. M. (2007). DNA replication and transcription in mammalian mitochondria. In *Annual Review of Biochemistry* (Vol. 76, pp. 679–699). https://doi.org/10.1146/annurev.biochem.76.060305.152028
56. Farge, G. É. R., & Falkenberg, M. (2019). Organization of DNA in mammalian mitochondria. In *International Journal of Molecular Sciences* (Vol. 20, Issue 11). MDPI AG. https://doi.org/10.3390/ijms20112770
57. Fernando, R., Castro, J. P., Flore, T., Deubel, S., Grune, T., & Ott, C. (2020). Age-Related Maintenance of the Autophagy-Lysosomal System Is Dependent on Skeletal Muscle Type. *Oxidative Medicine and Cellular Longevity*, *2020*. https://doi.org/10.1155/2020/4908162
58. Ferree, A. W., Trudeau, K., Zik, E., Benador, I. Y., Twig, G., Gottlieb, R. A., & Shirihai, O. S. (2013). MitoTimer probe reveals the impact of autophagy, fusion, and motility on subcellular distribution of young and old mitochondrial protein and on relative mitochondrial protein age. *Autophagy*, *9*(11), 1887–1896. https://doi.org/10.4161/auto.26503
59. Ferri, E., Marzetti, E., Calvani, R., Picca, A., Cesari, M., & Arosio, B. (2020). Role of age-related mitochondrial dysfunction in sarcopenia. In *International Journal of Molecular Sciences* (Vol. 21, Issue 15, pp. 1–12). MDPI AG. https://doi.org/10.3390/ijms21155236
60. Fielding, R. A., Vellas, B., Evans, W. J., Bhasin, S., Morley, J. E., Newman, A. B., Abellan van Kan, G., Andrieu, S., Bauer, J., Breuille, D., Cederholm, T., Chandler, J., De Meynard, C., Donini, L., Harris, T., Kannt, A., Keime Guibert, F., Onder, G., Papanicolaou, D., … Zamboni, M. (2011). Sarcopenia: An Undiagnosed Condition in Older Adults. Current Consensus Definition: Prevalence, Etiology, and Consequences. International Working Group on Sarcopenia. *Journal of the American Medical Directors Association*, *12*(4), 249–256. https://doi.org/10.1016/j.jamda.2011.01.003
61. Franzini-Armstrong, C., & Boncompagni, S. (2011). The evolution of the mitochondria-to-calcium release units relationship in vertebrate skeletal muscles. In

Journal of Biomedicine and Biotechnology (Vol. 2011). https://doi.org/10.1155/2011/830573

62. Frontera, W. R., & Ochala, J. (2015). Skeletal Muscle: A Brief Review of Structure and Function. In *Behavior Genetics* (Vol. 45, Issue 2, pp. 183–195). Springer New York LLC. https://doi.org/10.1007/s00223-014-9915-y
63. Fu, X., Zhuang, C. le, & Hu, P. (2022). Regulation of muscle stem cell fate. In *Cell Regeneration* (Vol. 11, Issue 1). Springer. https://doi.org/10.1186/s13619-022-00142-7
64. Fukada, S., Uezumi, A., Ikemoto, M., Masuda, S., Segawa, M., Tanimura, N., Yamamoto, H., Miyagoe-Suzuki, Y., & Takeda, S. (2007). Molecular Signature of Quiescent Satellite Cells in Adult Skeletal Muscle. *Stem Cells*, *25*(10), 2448–2459. https://doi.org/10.1634/stemcells.2007-0019
65. Gannon, J., Doran, P., Kirwan, A., & Ohlendieck, K. (2009). Drastic increase of myosin light chain MLC-2 in senescent skeletal muscle indicates fast-to-slow fibre transition in sarcopenia of old age. *European Journal of Cell Biology*, *88*(11), 685–700. https://doi.org/10.1016/j.ejcb.2009.06.004
66. García-Prat, L., Martínez-Vicente, M., Perdiguero, E., Ortet, L., Rodríguez-Ubreva, J., Rebollo, E., Ruiz-Bonilla, V., Gutarra, S., Ballestar, E., Serrano, A. L., Sandri, M., & Muñoz-Cánoves, P. (2016). Autophagy maintains stemness by preventing senescence. *Nature*, *529*(7584), 37–42. https://doi.org/10.1038/nature16187
67. García-Prat, L., Perdiguero, E., Alonso-Martín, S., Dell'Orso, S., Ravichandran, S., Brooks, S. R., Juan, A. H., Campanario, S., Jiang, K., Hong, X., Ortet, L., Ruiz-Bonilla, V., Flández, M., Moiseeva, V., Rebollo, E., Jardí, M., Sun, H. W., Musarò, A., Sandri, M., … Muñoz-Cánoves, P. (2020). FoxO maintains a genuine muscle stem-cell quiescent state until geriatric age. *Nature Cell Biology*, *22*(11), 1307–1318. https://doi.org/10.1038/s41556-020-00593-7
68. Garrido, N., Griparic, L., Jokitalo, E., Wartiovaara, J., Van der Bliek, A. M., & Spelbrink, J. N. (2003). Composition and dynamics of human mitochondrial nucleoids. *Molecular Biology of the Cell*, *14*(4), 1583–1596. https://doi.org/10.1091/mbc.E02-07-0399
69. Gelfi, C., Vasso, M., & Cerretelli, P. (2011). Diversity of human skeletal muscle in health and disease: Contribution of proteomics. In *Journal of Proteomics* (Vol. 74, Issue 6, pp. 774–795). https://doi.org/10.1016/j.jprot.2011.02.028
70. Gnocchi, V. F., White, R. B., Ono, Y., Ellis, J. A., & Zammit, P. S. (2009). Further characterisation of the molecular signature of quiescent and activated mouse muscle satellite cells. *PLoS ONE*, *4*(4). https://doi.org/10.1371/journal.pone.0005205
71. Goffart, S., & Wiesner, R. J. (2003). Regulation and co-ordination of nuclear gene expression during mitochondrial biogenesis. *Experimental Physiology*, *88*(1), 33–40. https://doi.org/10.1113/eph8802500
72. Gomes, L. C., Benedetto, G. Di, & Scorrano, L. (2011). During autophagy mitochondria elongate, are spared from degradation and sustain cell viability. *Nature Cell Biology*, *13*(5), 589–598. https://doi.org/10.1038/ncb2220

73. Gussoni, E., Blau, H. M., & Kunkel, L. M. (1997). The fate of individual myoblasts after transplantation into muscles of DMD patients. *Nature Medicine*, 990–997. https://doi.org/10.1038/nm0997-970
74. Gustafsson, C. M., Falkenberg, M., & Larsson, N. G. (2016). Maintenance and Expression of Mammalian Mitochondrial DNA. *Annual Review of Biochemistry*, *85*, 133–160. https://doi.org/10.1146/annurev-biochem-060815-014402
75. Habbane, M., Montoya, J., Rhouda, T., Sbaoui, Y., Radallah, D., & Emperador, S. (2021). Human mitochondrial DNA: Particularities and diseases. In *Biomedicines* (Vol. 9, Issue 10). MDPI. https://doi.org/10.3390/biomedicines9101364
76. Hall-Craggs, E. C. B., & Singh Seyan, H. (1975). Histochemical Changes in Innervated and Denervated Skeletal Muscle Fibers Following Treatment With Bupivacaine (Marcain). In *EXPERIMENTAL NEUROLOGY* (Vol. 46).
77. Han, S., Udeshi, N. D., Deerinck, T. J., Svinkina, T., Ellisman, M. H., Carr, S. A., & Ting, A. Y. (2017). Proximity Biotinylation as a Method for Mapping Proteins Associated with mtDNA in Living Cells. *Cell Chemical Biology*, *24*(3), 404–414. https://doi.org/10.1016/j.chembiol.2017.02.002
78. Harman, D. (1956). AGING: A THEORY BASED ON FREE RADICAL AND RADIATION CHEMISTRY. *Aging: Free Radical Theory*. https://academic.oup.com/geronj/article/11/3/298/616585
79. Harman, D. (1972). The Biologic Clock: The Mitochondria? *Journal of the American Geriatrics Society*, *20*(4), 145–147. https://doi.org/10.1111/j.1532-5415.1972.tb00787.x
80. Herbst, A., Lee, C. C., Vandiver, A. R., Aiken, J. M., McKenzie, D., Hoang, A., Allison, D., Liu, N., & Wanagat, J. (2021). Mitochondrial DNA deletion mutations increase exponentially with age in human skeletal muscle. *Aging Clinical and Experimental Research*, *33*(7), 1811–1820. https://doi.org/10.1007/s40520-020-01698-7
81. Hillen, H. S., Temiakov, D., & Cramer, P. (2018). Structural basis of mitochondrial transcription. In *Nature Structural and Molecular Biology* (Vol. 25, Issue 9, pp. 754–765). Nature Publishing Group. https://doi.org/10.1038/s41594-018-0122-9
82. Holloszy, J. O., Chen, M., Cartee, G. D., & Young, J. C. (1991). Skeletal muscle atrophy in old rats: differential changes in the three fiber types. *Mechanisms of Ageing and Development*, *60*(2), 199–213.
83. Holt, I. J., Lorimer, H. E., & Jacobs, H. T. (2000). Coupled Leading-and Lagging-Strand Synthesis of Mammalian Mitochondrial DNA eubacteria. Replication of the H strand on this model is proposed to initiate at a single site (O H), and to proceed unidirectionally until two-thirds of the way around the These replication intermediates were compared with. In *Cell* (Vol. 100).
84. Holzenberger, M., Dupont, J., Ducos, B., Leneuve, P., Géloën, A., Evens, P. C., Cervera, P., & Le Bouc, Y. (2003). IGF-1 receptor regulates lifespan and resistance to oxidative stress in mice. *Nature*, *421*(6919), 182–187.
85. Hong, X., Isern, J., Campanario, S., Perdiguero, E., Ramírez-Pardo, I., Segalés, J., Hernansanz-Agustín, P., Curtabbi, A., Deryagin, O., Pollán, A., González-Reyes, J.

A., Villalba, J. M., Sandri, M., Serrano, A. L., Enríquez, J. A., & Muñoz-Cánoves, P. (2022). Mitochondrial dynamics maintain muscle stem cell regenerative competence throughout adult life by regulating metabolism and mitophagy. *Cell Stem Cell*, *29*(9), 1298-1314.e10. https://doi.org/10.1016/j.stem.2022.07.009

86. Hood, D. A., Memme, J. M., Oliveira, A. N., & Triolo, M. (2019). Maintenance of Skeletal Muscle Mitochondria in Health, Exercise, and Aging. *The Annual Review of Physiology Is Online At*, *81*, 19–41. https://doi.org/10.1146/annurev-physiol-020518
87. Jiao, J., & Demontis, F. (2017). Skeletal muscle autophagy and its role in sarcopenia and organismal aging. In *Current Opinion in Pharmacology* (Vol. 34, pp. 1–6). Elsevier Ltd. https://doi.org/10.1016/j.coph.2017.03.009
88. Kapahi, P., Zid, B. M., Harper, T., Koslover, D., Sapin, V., & Benzer, S. (2004). Regulation of lifespan in Drosophila by modulation of genes in the TOR signaling pathway. *Current Biology*, *14*(10), 885–890. https://doi.org/10.1016/j.cub.2004.03.059
89. Kauppila, T. E. S., Kauppila, J. H. K., & Larsson, N. G. (2017). Mammalian Mitochondria and Aging: An Update. In *Cell Metabolism* (Vol. 25, Issue 1, pp. 57–71). Cell Press. https://doi.org/10.1016/j.cmet.2016.09.017
90. Kimoloi, S., Sen, A., Guenther, S., Braun, T., Brügmann, T., Sasse, P., Wiesner, R. J., Pla-Martín, D., & Baris, O. R. (2022). Combined fibre atrophy and decreased muscle regeneration capacity driven by mitochondrial DNA alterations underlie the development of sarcopenia. *Journal of Cachexia, Sarcopenia and Muscle*, *13*(4), 2132–2145. https://doi.org/10.1002/jcsm.13026
91. Korhonen, J. A., Pham, X. H., Pellegrini, M., & Falkenberg, M. (2004). Reconstitution of a minimal mtDNA replisome in vitro. *EMBO Journal*, *23*(12), 2423–2429. https://doi.org/10.1038/sj.emboj.7600257
92. Korthuis, R. J. (2011). *Skeletal Muscle Circulation*. Morgan & Claypool Life Sciences.
93. Krasich, R., & Copeland, W. C. (2017). DNA polymerases in the mitochondria: A critical review of the evidence. *Frontier Bioscience*, *22*, 692–709.
94. Kuang, S., Kuroda, K., Le Grand, F., & Rudnicki, M. A. (2007). Asymmetric Self-Renewal and Commitment of Satellite Stem Cells in Muscle. *Cell*, *129*(5), 999–1010. https://doi.org/10.1016/j.cell.2007.03.044
95. Kwon, Y. N., & Yoon, S. S. (2017). Sarcopenia: Neurological Point of View. *Journal of Bone Metabolism*, *24*(2), 83. https://doi.org/10.11005/jbm.2017.24.2.83
96. Laker, R. C., Xu, P., Ryall, K. A., Sujkowski, A., Kenwood, B. M., Chain, K. H., Zhang, M., Royal, M. A., Hoehn, K. L., Driscoll, M., Adler, P. N., Wessells, R. J., Saucerman, J. J., & Yan, Z. (2014a). A novel mitotimer reporter gene for mitochondrial content, structure, stress, and damage in vivo. *Journal of Biological Chemistry*, *289*(17), 12005–12015. https://doi.org/10.1074/jbc.M113.530527
97. Laker, R. C., Xu, P., Ryall, K. A., Sujkowski, A., Kenwood, B. M., Chain, K. H., Zhang, M., Royal, M. A., Hoehn, K. L., Driscoll, M., Adler, P. N., Wessells, R. J., Saucerman, J. J., & Yan, Z. (2014b). A novel mitotimer reporter gene for mitochondrial content,

structure, stress, and damage in vivo. *Journal of Biological Chemistry*, *289*(17), 12005–12015. https://doi.org/10.1074/jbc.M113.530527

98. Larsson, L., Sjodin, B., & Karlsson, J. (1978). Histochemical and biochemical changes in human skeletal muscle with age in sedentary males, age 22-65 years. *Acta Physiologica Scandinavica*, *103*(1), 31–39.
99. Larsson, N. G. (2010). Somatic mitochondrial DNA mutations in mammalian aging. *Annual Review of Biochemistry*, *79*, 683–706. https://doi.org/10.1146/annurev-biochem-060408-093701
100. Latil, M., Rocheteau, P., Châtre, L., Sanulli, S., Mémet, S., Ricchetti, M., Tajbakhsh, S., & Chrétien, F. (2012). Skeletal muscle stem cells adopt a dormant cell state post mortem and retain regenerative capacity. *Nature Communications*, *3*. https://doi.org/10.1038/ncomms1890
101. Leary, S. C., Battersby, B. J., Hansford, R. G., & Moyes, C. D. (1998). Interactions between bioenergetics and mitochondrial biogenesis. *Biochimica et Biophysica Acta* , 522–530.
102. Lee, C.-K., Allison, D. B., Brand, J., Weindruch, R., & Prolla, T. A. (2002). Transcriptional profiles associated with aging and middle age-onset caloric restriction in mouse hearts. *Proc Natl Acad Sci U S A*, *99*(23), 14988–14993. www.pnas.orgcgidoi10.1073pnas.232308999
103. Lemasters, J. J. (2005). Perspective Selective Mitochondrial Autophagy, or Mitophagy, as a Targeted Defense Against Oxidative Stress, Mitochondrial Dysfunction, and Aging. In *REJUVENATION RESEARCH* (Vol. 8, Issue 1). www.liebertpub.com
104. Lexell, J., Henriksson-Larsén, K., Winblad, B., & Sjöström, M. (1983). Distribution of different fiber types in human skeletal muscles: Effects of aging studied in whole muscle cross sections. *Muscle & Nerve*, *6*(8), 588–595. https://doi.org/10.1002/mus.880060809
105. Li, J., Kinoshita, T., Pandey, S., Ng, C. K. Y., Gygi, S. P., Shimazaki, K. I., & Assmann, S. M. (2002). Modulation of an RNA-binding protein by abscisic-acid-activated protein kinase. *Nature*, *418*(6899), 793–797. https://doi.org/10.1038/nature00936
106. Li, M., & Larsson, L. (2010). Force-generating capacity of human myosin isoforms extracted from single muscle fibre segments. *Journal of Physiology*, *588*(24), 5105–5114. https://doi.org/10.1113/jphysiol.2010.199067
107. Liebl, M. P., Meister, S. C., Frey, L., Hendrich, K., Klemmer, A., Wohlfart, B., Untucht, C., Nuber, J., Pohl, C., & Lakics, V. (2022). Robust LC3B lipidation analysis by precisely adjusting autophagic flux. *Scientific Reports*, *12*(1). https://doi.org/10.1038/s41598-021-03875-8
108. Liesa, M., & Shirihai, O. S. (2013). Mitochondrial dynamics in the regulation of nutrient utilization and energy expenditure. In *Cell Metabolism* (Vol. 17, Issue 4, pp. 491–506). https://doi.org/10.1016/j.cmet.2013.03.002
109. Lim, C. L., Ling, K.-H., & Cheah, P.-S. (2018). Isolation, cultivation and immunostaining of single myofibers: An improved approach to study the behavior of

satellite cells. *Journal of Biological Methods*, *5*(1), e87. https://doi.org/10.14440/jbm.2018.219

110. Lin, J., Handschin, C., & Spiegelman, B. M. (2005). Metabolic control through the PGC-1 family of transcription coactivators. In *Cell Metabolism* (Vol. 1, Issue 6, pp. 361–370). https://doi.org/10.1016/j.cmet.2005.05.004
111. Litonin, D., Sologub, M., Shi, Y., Savkina, M., Anikin, M., Falkenberg, M., Gustafsson, C. M., & Temiakov, D. (2010). Human mitochondrial transcription revisited: Only TFAM and TFB2M are required for transcription of the mitochondrial genes in vitro. *Journal of Biological Chemistry*, *285*(24), 18129–18133. https://doi.org/10.1074/jbc.C110.128918
112. Liu, D., Sartor, M. A., Nader, G. A., Pistilli, E. E., Tanton, L., Lilly, C., Gutmann, L., Iglayreger, H. B., Visich, P. S., Hoffman, E. P., & Gordon, P. M. (2013). Microarray analysis reveals novel features of the muscle aging process in men and women. *Journals of Gerontology - Series A Biological Sciences and Medical Sciences*, *68*(9), 1035–1044. https://doi.org/10.1093/gerona/glt015
113. Liu, L., Li, Y., Chen, G., & Chen, Q. (2023). Crosstalk between mitochondrial biogenesis and mitophagy to maintain mitochondrial homeostasis. In *Journal of Biomedical Science* (Vol. 30, Issue 1). BioMed Central Ltd. https://doi.org/10.1186/s12929-023-00975-7
114. Livak, K. J., & Schmittgen, T. D. (2001). Analysis of relative gene expression data using real-time quantitative PCR and the 2-ΔΔCT method. *Methods*, *25*(4), 402–408. https://doi.org/10.1006/meth.2001.1262
115. Lombardi, A., Silvestri, E., Cioffi, F., Senese, R., Lanni, A., Goglia, F., de Lange, P., & Moreno, M. (2009). Defining the transcriptomic and proteomic profiles of rat ageing skeletal muscle by the use of a cDNA array, 2D- and Blue native-PAGE approach. *Journal of Proteomics*, *72*(4), 708–721. https://doi.org/10.1016/j.jprot.2009.02.007
116. López-Lluch, G., Hunt, N., Jones, B., Zhu, M., Jamieson, H., Hilmer, S., Cascajo, M. V, Allard, J., Ingram, D. K., Navas, P., & De Cabo, R. (2006). Calorie restriction induces mitochondrial biogenesis and bioenergetic efficiency. *Proc Natl Acad Sci U S A.*, *103*(6), 1768–1773. www.pnas.orgcgidoi10.1073pnas.0510452103
117. López-Otín, C., Blasco, M. A., Partridge, L., Serrano, M., & Kroemer, G. (2013). The hallmarks of aging. In *Cell* (Vol. 153, Issue 6, p. 1194). Elsevier B.V. https://doi.org/10.1016/j.cell.2013.05.039
118. Lu, Y., Li, Z., Zhang, S., Zhang, T., Liu, Y., & Zhang, L. (2023). Cellular mitophagy: Mechanism, roles in diseases and small molecule pharmacological regulation. *Theranostics*, *13*(2), 736–766. https://doi.org/10.7150/thno.79876
119. Marcus, R. L., Addison, O., Kidde, J. P., Dibble, L. E., & Lastayo, P. C. (n.d.). *Skeletal muscle fat infiltration: impact of age, inactivity, and exercise*.
120. Marzetti, E., Lozanoska-Ochser, B., Calvani, R., Landi, F., Coelho-Júnior, H. J., & Picca, A. (2024). Restoring Mitochondrial Function and Muscle Satellite Cell Signaling: Remedies against Age-Related Sarcopenia. *Biomolecules*, *14*(4), 415. https://doi.org/10.3390/biom14040415

121. Mauro, A. (1961). SATELLITE CELL OF SKELETAL MUSCLE FIBERS. *The Journal of Biophysical and Biochemical Cytology*, *9*(2), 493–495.
122. McCuller, C., Jessu, R., & Callahan, A. L. (2024). *Physiology, Skeletal Muscle*. StatPearls Publishing.
123. Metter, E. J., Conwit, R., Tobin, J., & Fozard, J. L. (1997). Age-Associated Loss of Power and Strength in the Upper Extremities in Women and Men. *Journal of Gerontology: BIOLOGICAL SCIENCES*, *52A*(5), B267–B276. https://academic.oup.com/biomedgerontology/article/52A/5/B267/617501
124. Mizushima, N. (2007). Autophagy: Process and function. In *Genes and Development* (Vol. 21, Issue 22, pp. 2861–2873). https://doi.org/10.1101/gad.1599207
125. Morley, J. E. (2016). Frailty and sarcopenia in elderly. *Wiener Klinische Wochenschrift*, *128*, 439–445. https://doi.org/10.1007/s00508-016-1087-5
126. Muscaritoli, M., Anker, S. D., Argilés, J., Aversa, Z., Bauer, J. M., Biolo, G., Boirie, Y., Bosaeus, I., Cederholm, T., Costelli, P., Fearon, K. C., Laviano, A., Maggio, M., Fanelli, F. R., Schneider, S. M., Schols, A., & Sieber, C. C. (2010). Consensus definition of sarcopenia, cachexia and pre-cachexia: Joint document elaborated by Special Interest Groups (SIG) " cachexia-anorexia in chronic wasting diseases" and " nutrition in geriatrics." *Clinical Nutrition*, *29*(2), 154–159. https://doi.org/10.1016/j.clnu.2009.12.004
127. Narici, M. V., & Maffulli, N. (2010). Sarcopenia: Characteristics, mechanisms and functional significance. In *British Medical Bulletin* (Vol. 95, Issue 1, pp. 139–159). https://doi.org/10.1093/bmb/ldq008
128. Nilwik, R., Snijders, T., Leenders, M., Groen, B. B. L., van Kranenburg, J., Verdijk, L. B., & Van Loon, L. J. C. (2013). The decline in skeletal muscle mass with aging is mainly attributed to a reduction in type II muscle fiber size. *Experimental Gerontology*, *48*(5), 492–498. https://doi.org/10.1016/j.exger.2013.02.012
129. O'Connell, K., Gannon, J., Doran, P., & Ohlendieck, K. (2007). Proteomic profiling reveals a severely perturbed protein expression pattern in aged skeletal muscle. *International Journal of Molecular Medicine*, 145–153. https://doi.org/10.3892/ijmm.20.2.145
130. Oexner, R. R., Pla-Martín, D., Paß, T., Wiesen, M. H. J., Zentis, P., Schauss, A., Baris, O. R., Kimoloi, S., & Wiesner, R. J. (2020). Extraocular muscle reveals selective vulnerability of type IIB fibers to respiratory chain defects induced by mitochondrial DNA alterations. *Investigative Ophthalmology and Visual Science*, *61*(12). https://doi.org/10.1167/IOVS.61.12.14
131. Ohlendieck, K. (2011). Proteomic profiling of fast-to-slow muscle transitions during aging. *Frontiers in Physiology*, *2 DEC*. https://doi.org/10.3389/fphys.2011.00105
132. Ohsumi, Y. (2014). Historical landmarks of autophagy research. In *Cell Research* (Vol. 24, Issue 1, pp. 9–23). https://doi.org/10.1038/cr.2013.169
133. O'Leary, M. F., Vainshtein, A., Iqbal, S., Ostojic, O., & Hood, D. A. (2013). Adaptive plasticity of autophagic proteins to denervation in aging skeletal muscle. *American*

Journal of Physiology - Cell Physiology, *304*(5). https://doi.org/10.1152/ajpcell.00240.2012

134. Pacifico, J., Geerlings, M. A. J., Reijnierse, E. M., Phassouliotis, C., Lim, W. K., & Maier, A. B. (2020). Prevalence of sarcopenia as a comorbid disease: A systematic review and meta-analysis. In *Experimental Gerontology* (Vol. 131). Elsevier Inc. https://doi.org/10.1016/j.exger.2019.110801
135. Palamiuc, L., Schlagowski, A., Ngo, S. T., Vernay, A., Dirrig-Grosch, S., Henriques, A., Boutillier, A., Zoll, J., Echaniz-Laguna, A., Loeffler, J., & René, F. (2015). A metabolic switch toward lipid use in glycolytic muscle is an early pathologic event in a mouse model of amyotrophic lateral sclerosis. *EMBO Molecular Medicine*, *7*(5), 526–546. https://doi.org/10.15252/emmm.201404433
136. Palikaras, K., Lionaki, E., & Tavernarakis, N. (2015). Coordination of mitophagy and mitochondrial biogenesis during ageing in C. elegans. *Nature*, *521*(7553), 525–528. https://doi.org/10.1038/nature14300
137. Palikaras, K., Lionaki, E., & Tavernarakis, N. (2018). Mechanisms of mitophagy in cellular homeostasis, physiology and pathology. In *Nature Cell Biology* (Vol. 20, Issue 9, pp. 1013–1022). Nature Publishing Group. https://doi.org/10.1038/s41556-018-0176-2
138. Palmer, J. W., Tandler, B., & Hoppel, C. L. (1977). Biochemical Properties of Subsarcolemmal and Interfibrillar Mitochondria Isolated from Rat Cardiac Muscle*. In *BIOLOGICAL. CHEMISTRY* (Vol. 252, Issue 23).
139. Paß, T., Ricke, K. M., Hofmann, P., Chowdhury, R. S., Nie, Y., Endepols, H., Neumaier, B., Carvalho, A., Rigoux, L., Steculorum, M., Prudent, J., Riemer, T., Aswendt, M., Liss, B., & Wiesner, R. J. (2024). Preserved striatal innervation maintains motor function 1 despite severe loss of nigral dopaminergic neurons 2. *Brain*. https://doi.org/10.1093/brain/awae089/7640942
140. Pasut, A., Jones, A. E., & Rudnicki, M. A. (2013). Isolation and culture of individual myofibers and their satellite cells from adult skeletal muscle. *Journal of Visualized Experiments*, *73*. https://doi.org/10.3791/50074
141. Pernas, L., & Scorrano, L. (2016). Mito-Morphosis: Mitochondrial Fusion, Fission, and Cristae Remodeling as Key Mediators of Cellular Function. In *Annual Review of Physiology* (Vol. 78, pp. 505–531). Annual Reviews Inc. https://doi.org/10.1146/annurev-physiol-021115-105011
142. Peter, B., & Falkenberg, M. (2020). TWINKLE and other human mitochondrial DNA helicases: Structure, function and disease. In *Genes* (Vol. 11, Issue 4). MDPI AG. https://doi.org/10.3390/genes11040408
143. Peterson, C. M., Johannsen, D. L., & Ravussin, E. (2012). Skeletal muscle mitochondria and aging: A review. In *Journal of Aging Research* (Vol. 2012). https://doi.org/10.1155/2012/194821
144. Pfanner, N., Warscheid, B., & Wiedemann, N. (2019). Mitochondrial proteins: from biogenesis to functional networks. In *Nature Reviews Molecular Cell Biology* (Vol. 20,

Issue 5, pp. 267–284). Nature Publishing Group. https://doi.org/10.1038/s41580-018-0092-0

145. Pham, S., & Puckett, Y. (2024). *Physiology, Skeletal Muscle Contraction*. StatPearls Publishing.
146. Phanie Duguez, S., Onard Fé Asson, L., Denis, C., & Freyssenet, D. (2002). *Mitochondrial biogenesis during skeletal muscle regeneration*. https://doi.org/10.1152/ajpendo.00343
147. Piec, I., Listrat, A., Alliot, J., Chambon, C., Taylor, R. G., & Bechet, D. (2005). Differential proteome analysis of aging in rat skeletal muscle. *The FASEB Journal*, *19*(9), 1143–1145. https://doi.org/10.1096/fj.04-3084fje
148. Pittis, A. A., & Gabaldón, T. (2016). Late acquisition of mitochondria by a host with chimaeric prokaryotic ancestry. *Nature*, *531*(7592), 101–104. https://doi.org/10.1038/nature16941
149. Pollock, N., Staunton, C. A., Vasilaki, A., McArdle, A., & Jackson, M. J. (2017). Denervated muscle fibers induce mitochondrial peroxide generation in neighboring innervated fibers: Role in muscle aging. *Free Radical Biology and Medicine*, *112*, 84–92. https://doi.org/10.1016/j.freeradbiomed.2017.07.017
150. Posse, V., & Gustafsson, C. M. (2017). Human mitochondrial transcription factor B2 is required for promoter melting during initiation of transcription. *Journal of Biological Chemistry*, *292*(7), 2637–2645. https://doi.org/10.1074/jbc.M116.751008
151. Priego, T., Martín, A. I., González-Hedström, D., Granado, M., López-Calderón, A., & Cardalini, D. (2021). Role of hormones in sarcopenia. In *Vitamins and Hormones* (Vol. 115, pp. 535–570). Academic Press Inc. https://doi.org/10.1016/bs.vh.2020.12.021
152. Ramachandran, A., Basu, U., Sultana, S., Nandakumar, D., & Patel, S. S. (2017). Human mitochondrial transcription factors TFAM and TFB2M work synergistically in promoter melting during transcription initiation. *Nucleic Acids Research*, *45*(2), 861–874. https://doi.org/10.1093/nar/gkw1157
153. Ramadasan-Nair, R., Gayathri, N., Mishra, S., Sunitha, B., Mythri, R. B., Nalini, A., Subbannayya, Y., Harsha, H. C., Kolthur-Seetharam, U., & Bharath, M. M. S. (2014). Mitochondrial alterations and oxidative stress in an acute transient mouse model of muscle degeneration: Implications for Muscular dystrophy and related muscle pathologies. *Journal of Biological Chemistry*, *289*(1), 485–509. https://doi.org/10.1074/jbc.M113.493270
154. Relaix, F., Bencze, M., Borok, M. J., Der Vartanian, A., Gattazzo, F., Mademtzoglou, D., Perez-Diaz, S., Prola, A., Reyes-Fernandez, P. C., Rotini, A., & Taglietti. (2021). Perspectives on skeletal muscle stem cells. In *Nature Communications* (Vol. 12, Issue 1). Nature Research. https://doi.org/10.1038/s41467-020-20760-6
155. Relaix, F., & Zammit, P. S. (2012). Satellite cells are essential for skeletal muscle regeneration: The cell on the edge returns centre stage. In *Development (Cambridge)* (Vol. 139, Issue 16, pp. 2845–2856). https://doi.org/10.1242/dev.069088

156. Remels, A. H. V., Langen, R. C. J., Schrauwen, P., Schaart, G., Schols, A. M. W. J., & Gosker, H. R. (2010). Regulation of mitochondrial biogenesis during myogenesis. *Molecular and Cellular Endocrinology*, *315*(1–2), 113–120. https://doi.org/10.1016/j.mce.2009.09.029
157. Riuzzi, F., Sorci, G., Arcuri, C., Giambanco, I., Bellezza, I., Minelli, A., & Donato, R. (2018). Cellular and molecular mechanisms of sarcopenia: the S100B perspective. In *Journal of Cachexia, Sarcopenia and Muscle* (Vol. 9, Issue 7, pp. 1255–1268). Wiley Blackwell. https://doi.org/10.1002/jcsm.12363
158. Robberson, D. L., Kasamatsu, H., & Vinogradt, J. (1972). *Replication of Mitochondrial DNA. Circular Replicative Intermediates in Mouse L Cells (electron microscopy/separated strands/duplex synthesis/displacement synthesis)* (Vol. 69, Issue 3).
159. Robinson, S., Granic, A., Cruz-Jentoft, A. J., & Sayer, A. A. (2023). The role of nutrition in the prevention of sarcopenia. In *American Journal of Clinical Nutrition* (Vol. 118, Issue 5, pp. 852–864). Elsevier B.V. https://doi.org/10.1016/j.ajcnut.2023.08.015
160. Rocchi, A., Milioto, C., Parodi, S., Armirotti, A., Borgia, D., Pellegrini, M., Urciuolo, A., Molon, S., Morbidoni, V., Marabita, M., Romanello, V., Gatto, P., Blaauw, B., Bonaldo, P., Sambataro, F., Robins, D. M., Lieberman, A. P., Sorarù, G., Vergani, L., … Pennuto, M. (2016). Glycolytic-to-oxidative fiber-type switch and mTOR signaling activation are early-onset features of SBMA muscle modified by high-fat diet. *Acta Neuropathologica*, *132*(1), 127–144. https://doi.org/10.1007/s00401-016-1550-4
161. Rocheteau, P., Gayraud-Morel, B., Siegl-Cachedenier, I., Blasco, M. A., & Tajbakhsh, S. (2012). A subpopulation of adult skeletal muscle stem cells retains all template DNA strands after cell division. *Cell*, *148*(1–2), 112–125. https://doi.org/10.1016/j.cell.2011.11.049
162. Roman, W., & Gomes, E. R. (2018). Nuclear positioning in skeletal muscle. In *Seminars in Cell and Developmental Biology* (Vol. 82, pp. 51–56). Elsevier Ltd. https://doi.org/10.1016/j.semcdb.2017.11.005
163. Rosenber, I. H. (1989). Epidemiologic and Methodologic Problems in Determining Nutritional Status of Older Persons: Summary comments. *The American Journal of Clinical Nutrition*, *50*(5), 1231–1233.
164. Ross, J. M. (2011). Visualization of mitochondrial respiratory function using cytochrome C oxidase/succinate dehydrogenase (COX/SDH) double-labeling histochemistry. *Journal of Visualized Experiments*, *57*. https://doi.org/10.3791/3266
165. Rudnicki, M. A., Grand, F. Le, McKinnell, I., & Kuang, S. (2008). The molecular regulation of muscle stem cell function. *Cold Spring Harb Symp Quant Biol*, *73*, 323–331.
166. Sahin, E., & Depinho, R. A. (2010). Linking functional decline of telomeres, mitochondria and stem cells during ageing. *Nature*, *464*(7288), 520–528. https://doi.org/10.1038/nature08982

167. Satoh, M., & Kuroiwa, T. (1991). Organization of multiple nucleoids and DNA molecules in mitochondria of a human cell. *Experimental Cell Research*, *196*(1), 137–140. https://doi.org/10.1016/0014-4827(91)90467-9
168. Schiaffino, S. (2010). Fibre types in skeletal muscle: A personal account. In *Acta Physiologica* (Vol. 199, Issue 4, pp. 451–463). Blackwell Publishing Ltd. https://doi.org/10.1111/j.1748-1716.2010.02130.x
169. Schiaffino, S., & Reggiani, C. (2011). Fiber Types In Mammalian Skeletal Muscles. *Physiol Rev*, *91*, 1447–1531. https://doi.org/10.1152/physrev.00031.2010.-Mammalian
170. Schmalbruch, H., & Lewis, D. M. (2000). Dynamics of nuclei of muscle fibers and connective tissue cells in normal and denervated rat muscles. *Muscle and Nerve*, *23*(4), 617–626. https://doi.org/10.1002/(SICI)1097-4598(200004)23:4<617::AID-MUS22>3.0.CO;2-Y
171. Schmidt, M., Schüler, S. C., Hüttner, S. S., von Eyss, B., & von Maltzahn, J. (2019). Adult stem cells at work: regenerating skeletal muscle. In *Cellular and Molecular Life Sciences* (Vol. 76, Issue 13, pp. 2559–2570). Birkhauser Verlag AG. https://doi.org/10.1007/s00018-019-03093-6
172. Scott, W. B., Stevens-Lapsley, J. E., & Binder-Macleod, S. A. (2001). Human Skeletal Muscle Fiber Type Classifications. *Physical Therapy*, *81*(11), 1810–1816. https://academic.oup.com/ptj/article/81/11/1810/2857618
173. Sebastián, D., Sorianello, E., Segalés, J., Irazoki, A., Ruiz-Bonilla, V., Sala, D., Planet, E., Berenguer-Llergo, A., Muñoz, J. P., Sánchez-Feutrie, M., Plana, N., Hernández-Álvarez, M. I., Serrano, A. L., Palacín, M., & Zorzano, A. (2016). Mfn2 deficiency links age-related sarcopenia and impaired autophagy to activation of an adaptive mitophagy pathway. *The EMBO Journal*, *35*(15), 1677–1693. https://doi.org/10.15252/embj.201593084
174. Sen, A., Boix, J., & Pla-Martín, D. (2023). Endosomal-dependent mitophagy coordinates mitochondrial nucleoid and mtDNA elimination. *Autophagy*, *19*(9), 2609–2610. https://doi.org/10.1080/15548627.2023.2170959
175. Sen, A., Kallabis, S., Gaedke, F., Jüngst, C., Boix, J., Nüchel, J., Maliphol, K., Hofmann, J., Schauss, A. C., Krüger, M., Wiesner, R. J., & Pla-Martín, D. (2022). Mitochondrial membrane proteins and VPS35 orchestrate selective removal of mtDNA. *Nature Communications*, *13*(1). https://doi.org/10.1038/s41467-022-34205-9
176. Shadrin, I. Y., Khodabukus, A., & Bursac, N. (2016). Striated muscle function, regeneration, and repair. In *Cellular and Molecular Life Sciences* (Vol. 73, Issue 22, pp. 4175–4202). Birkhauser Verlag AG. https://doi.org/10.1007/s00018-016-2285-z
177. Shigenaga, M. K., Hagen, T. M., & Ames, B. N. (1994). Oxidative damage and mitochondrial decay in aging (bloenergetics/mltodcndra DNA/arwdbipn/acetyl-L-cnitlne/neurodeneration). In *Proc. Nail. Acad. Sci. USA* (Vol. 91). https://www.pnas.org

178. Shinin, V., Gayraud-Morel, B., Gomès, D., & Tajbakhsh, S. (2006). Asymmetric division and cosegregation of template DNA strands in adult muscle satellite cells. *Nature Cell Biology*, *8*(7), 677–682. https://doi.org/10.1038/ncb1425
179. Sin, J., Andres, A. M., Taylo R, D. J. R., Weston, T., Hiraumi, Y., Stotland, A., Kim, B. J., Huang, C., Doran, K. S., & Gottlieb, R. A. (2016). Mitophagy is required for mitochondrial biogenesis and myogenic differentiation of C2C12 myoblasts. *Autophagy*, *12*(2), 369–380. https://doi.org/10.1080/15548627.2015.1115172
180. Sousa, J. S., D'Imprima, E., & Vonck, J. (2018). Mitochondrial Respiratory Chain Complexes. *Subcellular Biochemistry*, *87*, 167–227.
181. Spelbrink, J., Li, F. Y., Tiranti, V., Nikali, K., Yuan, Q. P., Tariq, M., Wanrooji, S., Garrido, N., Comi, N., Morandi, L., Santoro, L., Toscano, A., Fabrizi, G. M., Somer, H., Croxen, R., Beeson, D., Poulton, J., Suomalainen, A., Jacobs, H. T., … Larsson, C. (2001). Human mitochondrial DNA deletions associated with mutations in the gene encoding Twinkle, a phage T7 gene 4-like protein localized in mitochondria. *Nature Genetics*, *28*(3), 223–231. https://doi.org/10.1038/90058
182. Srinivasan, S., Guha, M., Kashina, A., & Avadhani, N. G. (2017). Mitochondrial dysfunction and mitochondrial dynamics-The cancer connection. In *Biochimica et Biophysica Acta - Bioenergetics* (Vol. 1858, Issue 8, pp. 602–614). Elsevier B.V. https://doi.org/10.1016/j.bbabio.2017.01.004
183. Srivastava, S. (2017). The mitochondrial basis of aging and age-related disorders. In *Genes* (Vol. 8, Issue 12). MDPI AG. https://doi.org/10.3390/genes8120398
184. Stocco, D. M., Cascarano, J., & Wilson, M. A. (1977). Quantitation of mitochondrial DNA, RNA, and protein in starved and starved-refed rat liver. *Journal of Cellular Physiology*, *90*(2), 295–306. https://doi.org/10.1002/jcp.1040900215
185. Taaffe, D. R., Henwood, T. R., Nalls, M. A., Walker, D. G., Lang, T. F., & Harris, T. B. (2009). Alterations in muscle attenuation following detraining and retraining in resistance-trained older adults. *Gerontology*, *55*(2), 217–223. https://doi.org/10.1159/000182084
186. Tait, S. W. G., & Green, D. R. (2012). Mitochondria and cell signalling. In *Journal of Cell Science* (Vol. 125, Issue 4, pp. 807–815). https://doi.org/10.1242/jcs.099234
187. Tajsharghi, H., & Oldfors, A. (2013). Myosinopathies: Pathology and mechanisms. In *Acta Neuropathologica* (Vol. 125, Issue 1, pp. 3–18). https://doi.org/10.1007/s00401-012-1024-2
188. Tapper, D. P., & Clayton, D. A. (1981). Mechanism of Replication of Human Mitochondrial DNA Localization of the 5' Ends of Nascent Daughter Strands*. In *The Journal of Biological Chemistry* (Vol. 256, Issue 10).
189. Tauchi, H., & Sato, T. (1968). Age Changes in Size and Number of Mitochondria of Human Hepatic Cells. *Journal of Gerontolgy*, *23*(1), 454–461. https://doi.org/10.1093/geronj/23.4.454.
190. Taylor, R. W., Barron, M. J., Borthwick, G. M., Gospel, A., Chinnery, P. F., Samuels, D. C., Taylor, G. A., Plusa, S. M., Needham, S. J., Greaves, L. C., Kirkwood, T. B. L., & Turnbull, D. M. (2003). Mitochondrial DNA mutations in human colonic crypt stem

cells. *Journal of Clinical Investigation*, *112*(9), 1351–1360. https://doi.org/10.1172/jci200319435

191. Tidball, J. G. (2017). Regulation of muscle growth and regeneration by the immune system. In *Nature Reviews Immunology* (Vol. 17, Issue 3, pp. 165–178). Nature Publishing Group. https://doi.org/10.1038/nri.2016.150
192. Tilokani, L., Nagashima, S., Paupe, V., & Prudent, J. (2018). Mitochondrial dynamics: Overview of molecular mechanisms. In *Essays in Biochemistry* (Vol. 62, Issue 3, pp. 341–360). Portland Press Ltd. https://doi.org/10.1042/EBC20170104
193. Tournadre, A., Vial, G., Capel, F., Soubrier, M., & Boirie, Y. (2019). Sarcopenia. In *Joint Bone Spine* (Vol. 86, Issue 3, pp. 309–314). Elsevier Masson SAS. https://doi.org/10.1016/j.jbspin.2018.08.001
194. Trifunovic, A., Wredenberg, A., Falkenberg, M., Spelbrink, J. N., Rovio. Anja T, Bruder, C. E., Bohlooly-Y, M., Gidlöf, S., Oldfors, A., Wibom, R., Törnell, J., Jacobs, H. T., & Larsson, N.-G. (2004). Premature ageing in mice expressing defective mitochondrial DNA polymerase. *Nature*, *429*(6990), 413–417. https://doi.org/10.1038/nature02544
195. Tsekoura, M., Kastrinis, A., Katsoulaki, M., Billis, E., & Gliatis, J. (2017). Sarcopenia and its impact on quality of life. In *Advances in Experimental Medicine and Biology* (Vol. 987, pp. 213–218). Springer New York LLC. https://doi.org/10.1007/978-3-319-57379-3_19
196. Twig, G., & Shirihai, O. S. (2011). The interplay between mitochondrial dynamics and mitophagy. In *Antioxidants and Redox Signaling* (Vol. 14, Issue 10, pp. 1939–1951). https://doi.org/10.1089/ars.2010.3779
197. Urbanczyk, S., Baris, O. R., Hofmann, J., Taudte, R. V., Guegen, N., Golombek, F., Castiglione, K., Meng, X., Bozec, A., Thomas, J., Weckwerth, L., Mougiakakos, D., Schulz, S. R., Schuh, W., Schlötzer-Schrehardt, U., Steinmetz, T. D., Brodesser, S., Wiesner, R. J., & Mielenz, D. (2022). Mitochondrial respiration in B lymphocytes is essential for humoral immunity by controlling the flux of the TCA cycle. *Cell Reports*, *39*(10). https://doi.org/10.1016/j.celrep.2022.110912
198. Verdijk, L. B., Snijders, T., Beelen, M., Savelberg, H. H. C. M., Meijer, K., Kuipers, H., & Van Loon, L. J. C. (2010). Characteristics of muscle fiber type are predictive of skeletal muscle mass and strength in elderly men. *Journal of the American Geriatrics Society*, *58*(11), 2069–2075. https://doi.org/10.1111/j.1532-5415.2010.03150.x
199. Wagatsuma, A., & Sakuma, K. (2013). Mitochondria as a potential regulator of myogenesis. In *The Scientific World Journal* (Vol. 2013). https://doi.org/10.1155/2013/593267
200. Wahwah, N., Kras, K. A., Roust, L. R., & Katsanos, C. S. (2020). Subpopulation-specific differences in skeletal muscle mitochondria in humans with obesity: insights from studies employing acute nutritional and exercise stimuli. *Am J Physiol Endocrinol Metab*, *318*(4), E538–E553. www.physiology.org/journal/ajpendo
201. Wallace, D. C. (2005). A mitochondrial paradigm of metabolic and degenerative diseases, aging, and cancer: A dawn for evolutionary medicine. In *Annual Review of*

Genetics (Vol. 39, pp. 359–407). https://doi.org/10.1146/annurev.genet.39.110304.095751

202. Walston, J. D. (2012). Sarcopenia in older adults. In *Current Opinion in Rheumatology* (Vol. 24, Issue 6, pp. 623–627). https://doi.org/10.1097/BOR.0b013e328358d59b
203. Wang, Y., Lu, J., & Liu, Y. (2022). Skeletal Muscle Regeneration in Cardiotoxin-Induced Muscle Injury Models. In *International Journal of Molecular Sciences* (Vol. 23, Issue 21). MDPI. https://doi.org/10.3390/ijms232113380
204. Wang, Y. X., Dumont, N. A., & Rudnicki, M. A. (2014). Muscle stem cells at a glance. *Journal of Cell Science*, *127*(21), 4543–4548. https://doi.org/10.1242/jcs.151209
205. Weiland, D., Brachvogel, B., Hornig-Do, H. T., Neuhaus, J. F. G., Holzer, T., Tobin, D. J., Niessen, C. M., Wiesner, R. J., & Baris, O. R. (2018). Imbalance of Mitochondrial Respiratory Chain Complexes in the Epidermis Induces Severe Skin Inflammation. *Journal of Investigative Dermatology*, *138*(1), 132–140. https://doi.org/10.1016/j.jid.2017.08.019
206. Wiesner, R. J., Zsurka, G., & Kunz, W. S. (2006). Mitochondrial DNA damage and the aging process-facts and imaginations. *Free Radical Research*, *40*(12), 1284–1294. https://doi.org/10.1080/10715760600913168
207. Wilkinson, D. J., Piasecki, M., & Atherton, P. J. (2018). The age-related loss of skeletal muscle mass and function: Measurement and physiology of muscle fibre atrophy and muscle fibre loss in humans. In *Ageing Research Reviews* (Vol. 47, pp. 123–132). Elsevier Ireland Ltd. https://doi.org/10.1016/j.arr.2018.07.005
208. Williams, A. H., Liu, N., van Rooij, E., & Olson, E. N. (2009). MicroRNA control of muscle development and disease. In *Current Opinion in Cell Biology* (Vol. 21, Issue 3, pp. 461–469). https://doi.org/10.1016/j.ceb.2009.01.029
209. Xie, G., Jin, H., Mikhail, H., Pavel, V., Yang, G., Ji, B., Lu, B., & Li, Y. (2023). Autophagy in sarcopenia: Possible mechanisms and novel therapies. In *Biomedicine and Pharmacotherapy* (Vol. 165). Elsevier Masson s.r.l. https://doi.org/10.1016/j.biopha.2023.115147
210. Xu, J., Wan, C. S., Ktoris, K., Reijnierse, E. M., & Maier, A. B. (2022). Sarcopenia Is Associated with Mortality in Adults: A Systematic Review and Meta-Analysis. In *Gerontology* (Vol. 68, Issue 4, pp. 361–376). S. Karger AG. https://doi.org/10.1159/000517099
211. Yang, Q., & Chan, P. (2022). Skeletal Muscle Metabolic Alternation Develops Sarcopenia. In *Aging and Disease* (Vol. 13, Issue 3, pp. 801–814). International Society on Aging and Disease. https://doi.org/10.14336/AD.2021.1107
212. Yim, A., Koti, P., Bonnard, A., Marchiano, F., Dürrbaum, M., Garcia-Perez, C., Villaveces, J., Gamal, S., Cardone, G., Perocchi, F., Storchova, Z., & Habermann, B. H. (2020). MitoXplorer, a visual data mining platform to systematically analyze and visualize mitochondrial expression dynamics and mutations. *Nucleic Acids Research*, *48*(2), 605–632. https://doi.org/10.1093/nar/gkz1128

213. Yin, H., Price, F., & Rudnicki, M. A. (2013). Satellite cells and the muscle stem cell niche. *Physiological Reviews*, *93*(1), 23–67. https://doi.org/10.1152/physrev.00043.2011
214. Youle, R. J., & Van Der Bliek, A. M. (2012). Mitochondrial fission, fusion, and stress. In *Science* (Vol. 337, Issue 6098, pp. 1062–1065). American Association for the Advancement of Science. https://doi.org/10.1126/science.1219855
215. Yuan, Q., Zeng, Z. L., Yang, S., Li, A., Zu, X., & Liu, J. (2022). Mitochondrial Stress in Metabolic Inflammation: Modest Benefits and Full Losses. In *Oxidative Medicine and Cellular Longevity* (Vol. 2022). Hindawi Limited. https://doi.org/10.1155/2022/8803404
216. Zhong, F., Liang, S., & Zhong, Z. (2019). Emerging Role of Mitochondrial DNA as a Major Driver of Inflammation and Disease Progression. In *Trends in Immunology* (Vol. 40, Issue 12, pp. 1120–1133). Elsevier Ltd. https://doi.org/10.1016/j.it.2019.10.008

6 Appendix

6.1 List of Figures

6.7 List of Tables

6.3 List of Abbreviations

Abbreviation	Full Form
acetyl CoA	acetyl coenzyme A
ADP	Adenosine diphosphate
ALS	Amyotrophic lateral sclerosis
ANOVA	one way analysis of variance
ATP	Adenosine triphosphate
BSA	Bovine serum albumin
$CaCl_2$	Calcium Chloride
COX	Cytochrome c oxidase
CR	Calorie restriction
CSA	Cross-sectional Area
CTX	cardiotoxin
D Loop	displacement-loop
DAPI	4′,6-diamidino-2-phenylindole
DEPC	Diethly Pyrocarbonate
DNM2	dynamin 2
DPBS	Dulbecco's Phosphate-Buffered Saline
DRP1	dynamin-related protein 1
ECM	extra cellular matrix
EDL	extensor digitorum longus
EDTA	Ethylenediaminetetraacetic acid
ERT	Estrogen Receptor
ETC	Electron transport chain
FAD	Flavin adenine dinucleotide
$FADH_2$	Flavin adenine dinucleotide (hydroquinone form)
FAO	fatty acid oxidation
FIS 1	fission 1 protein
FMN	flavin mononucleotide
FoxO	Forkhead Box O
G-actin	Globular actin
GAPDH	Glyceraldehyde 3-phosphate dehydrogenase
gDNA	genomic DNA
GN	Gastrocnemius
H & E	Haematoxylin and Eosin
HCl	Hydrochloric acid
HIF1α	hypoxia-inducible factor 1-alpha
HS	Horse serum
HSP	Heavy strand promoter
IIS	Insulin/IGF1 signalling
IL 10	interleukin 10
IL1	interleukin 1

IM	inner membrane
IMF	intermyofibrillar
IMS	intermembrane space
kcal/mol	kilocalorie/mole
LAF	Laminar Air flow
LANUV	Landesamt für Natur, Umwelt und Verbraucherschutz
LR	Long Range
LSP	Light strand promoter
M1	early population of macrophages
M2	second population of macrophages
MACS	Magnetic-activated cell sorting
mATPase	myosin ATPase
MFF	mitochondrial fission factor
MFN1	mitofusin 1
MFN2	mitofusin 2
MHC / MyHC	Myosin Heavy Chain
MiD	mitochondrial dynamics protein
MLC	Myosin Light Chain
MPCs	myogenic precursor cells
MQ	Milli-Q
Mrf 4	Myogenic regulatory factor 4
MRFs	myogenic regulatory factors
mtDNA	mitochondrial DNA
mTORC	Mechanistic Target of Rapamycin
mtSSB	mitochondrial single-strand binding protein
MuSC(s)	Muscle satellite cell(s)
Myf5	Myogenic Factor 5
MyoD	Myogenic determinant 1
Na_2HPO_4	disodium hydrogen phosphate
NaCl	Sodium Chloride
NAD^+	Nicotinamide adenine dinucleotide
NADH	Nicotinamide adenine dinucleotide (NAD) + hydrogen (H)
NaOH	Sodium hydroxide
NBT	Nitroblue tetrazolium
NCR	non-coding region
nDNA / nucDNA	nuclear DNA
NRF1	nuclear respiratory factor 1
NRF2	nuclear respiratory factor 2
O_2	Oxygen
OH (OriH)	origin of the heavy strand DNA replication
OL (OriL)	origin of the light strand DNA replication
OM	Outer Membrane
OPA1	optic atrophy protein 1
OXPHOS	oxidative phosphorylation
Pax3	Paired homeo box 3

Pax7	Paired Homeo Box7
PBS	Phosphate Buffered Saline
PCR	Polymerase chain reaction
PEI	Polyethylenimine
PEO	Progressive external ophthalmoplegia
PFA	Paraformaldehyde
PGC1	PPARgamma coactivator-1
PINK	phosphate and tensin homolog (PTEN) - induced putative kinase
POLG	DNA polymerase gamma
POLRMT	DNA-dependent RNA polymerase
PRC	PGC1 related coactivators
PTEN	phosphate and tensin homolog
PVDF	polyvinylidene difluoride
QD	Quadriceps
RITOLS	ribonucleotide incorporation throughout the lagging strand
RNS	Reactive Nitrogen Species
ROIs	regions of interest
ROS	reactive oxygen species
ROX	residual oxygen consumption
RT	Room temperature
SBMA	spinal and bulbar muscular atrophy
SDH	Succinate dehydrogenase
SDS-PAGE	Sodium dodecyl-sulphate polyacrylamide gel electrophoresis
SkM	Skeletal muscle
SS	subsarcolemmal
TA	M. tibialis anterior
TAE	Tris-acetate-EDTA
TBST	Tris Buffered Saline, 0.1% Tween20
TCA cycle	Tricarboxylic Acid cycle
TFAM	Transcription Factor A mitochondrial
TFB2M	mitochondrial transcription factor B2
TnC	Troponin C
TNFα	tumour necrosis factor alpha
TnI	Troponin I
TnT	Troponin T
TOR	target of Rapamycin
tRNAs	transfer RNAs
$\Delta G^{\circ\prime}$	Gibbs free energy